Universität Hamburg

DER FORSCHUNG | DER LEHRE | DER BILDUNG

Development of non-nucleotide ADPR antagonists for inhibition of TRPM2

Dissertation for the Acquisition of a Doctoral Degree (Dr. rer.nat.)
at the Department of Chemistry
Faculty of Mathematics, Informatics and Natural Sciences
University of Hamburg

Submitted by

Swati Balasaheb Ohol

September 2022

1st reviewer: Prof. Dr. Chris Meier

2nd reviewer: Prof. Dr. Dr. Andreas H. Guse

Date of the oral defense: 18/11/2022

This work was done from July 2019 to June 2022 at the Institute of Biochemistry and Molecular Cell Biology, University Medical Center Hamburg-Eppendorf (UKE) under the supervision of Dr. Ralf Fliegert and Prof. Dr. Dr. Andreas H. Guse.

TABLE OF CONTENTS

Table of contents 4
Abstract 6
Zusammenfassung 8
List of abbreviations 10
List of figures 13
List of tables 15
1 Introduction 16
1.1 TRP channel superfamily 16
1.2 TRPM2 channels 17
1.2.1 TRPM2 gene and expression 18
1.2.2 Overall structure of TRPM2 channels 20
1.2.3 TRPM2 channel activation mechanism 22
1.2.3.1 Activation by ADPR and 2'deoxy ADPR 22
1.2.3.2 Activation by Calcium ion 24
1.2.3.3 Activation by reactive oxygen species (ROS) 24
1.2.3.4 Activation by temperature 25
1.2.4 TRPM2 role in cancer 25
1.3 Computer-aided drug design (CADD) 27
2 Aim and Motivation 29
3 Materials and Methods 30
3.1 Materials 30
3.2 Compound handling 31
3.3 *In-silico*/computer-aided drug design of TRPM2 inhibitors 37
3.3.1 Computer-aided drug design using a homology model of the NudT9H domain of human TRPM2 based on the x-ray crystal structure of NudT9 37
3.3.2 Computer-aided drug design using cryo-EM structure of human TRPM2 38
3.4 Cell culture 42
3.4.1 Human embryonic kidney cells (HEK293) 42
3.4.2 Pancreatic cancer cells 42
3.5 RP-HPLC 44
3.6 Fura-2 calcium measurement 45
3.6.1 Principle 45
3.6.2 Procedure 46
3.7 Patch clamp recordings 47
3.7.1 Principle 47
3.7.2 Procedure 48

3.8 RT-PCR....49
3.8.1 Principle....49
3.8.2 Procedure....49
3.9 RT-qPCR....51
3.9.1 Principle....51
3.9.2 Procedure....51
3.10 Cancer cell proliferation....52
3.10.1 Principle....52
3.10.2 Procedure....53
4 Results....54
4.1 Results for the computer-aided drug design approach using homology model....54
4.1.1 Compounds purity check with RP-HPLC....56
4.1.2 Effect of compounds on ADPR-induced TRPM2 currents....56
4.1.3 Effect of compounds on H_2O_2-induced increase in $[Ca^{2+}]_i$....57
4.2 Results for the computer-aided drug design approach using actual cryo-EM structure of hTRPM2....62
4.2.1 Compounds purity check with RP-HPLC....64
4.2.2 Effect of compounds on H_2O_2-induced increase in $[Ca^{2+}]_i$....64
4.2.3 Effect of compounds on ADPR-induced TRPM2 currents....69
4.3 Expression level of TRPM2 in different Pancreatic cancer cell lines....70
4.3.1 Using RT-PCR....70
4.3.2 Quantification of TRPM2 expression using quantitative RT-PCR....71
4.4 Effect of inhibitors on MIA PaCa-2 cell proliferation rate....72
5 Discussion....75
6 List of Hazardous chemicals....86
7 References....90
Declaration on Oath....99
Acknowledgement....100

ABSTRACT

Transient receptor potential melastatin 2 (TRPM2) is a ligand-gated non-selective, Ca^{2+}-permeable cation channel, activated by ADPR and 2'-deoxy-ADPR. TRPM2 is upregulated in a number of human tumour entities including pancreatic cancers and can promote cancer cell proliferation, migration as well as resistance to chemotherapeutic agents. Therefore, TRPM2 could be considered an interesting novel target for pharmacological intervention in cancer progression. All currently available compounds/drugs that inhibit TRPM2 are either channel blockers that also affect some other related ion channels or nucleotide-derivatives that are inherently unstable in the biological fluids and hardly membrane permeant. Hence, this thesis work is focused on developing novel non-nucleotide TRPM2 specific inhibitors. Which in future might provide a foundation for the development of ADPR antagonists/TRPM2 inhibitors into anti-tumour agents particularly for the treatment of pancreatic cancer particularly pancreatic ductal adenocarcinoma (PDAC).

For developing the TRPM2 inhibitors, a computer-aided drug design (CADD) by using structure-based drug design approach (SBDD) was performed. First attempt was made with SBDD using a homology model of the nucleotide binding NudT9-H domain of human TRPM2. Which resulted in a total 12 compounds and those compounds were tested *in vitro* for their potential to inhibit activation of TRPM2 by ADPR but they did not show complete inhibition of TRPM2 activation. Then in late 2019, Juan Du et al published the actual human TRPM2 (hTRPM2) cryo-EM structure. Therefore, another attempt of computer-aided drug design was made. This time it was based on this cryo-EM TRPM2 structure and used molecular dynamics (MD) simulations to refine the structure before performing the molecular docking. Then the compounds from this CADD were also checked *in vitro.* First, Fura-2 calcium measurements as a primary screening for membrane permeant compounds were performed and the impact of compounds on TRPM2 mediated calcium concentration by measuring the free cytosolic calcium concentration ($[Ca^{2+}]_i$) was checked. Six out of 13 compounds did show at least partial or nearly full inhibition of TRPM2 activation mediated increase in $[Ca^{2+}]_i$ in a concentration dependent manner. After checking the compounds on intact cells in Fura-2 calcium measurement experiments these six compounds were tested directly onto the target by using whole cell patch clamp technique by measuring the TRPM2 current in response to ADPR. All six compounds showed significant reduction in ADPR induced TRPM2 current. After this, the effect of these compounds on tumour cells was checked to confirm if the pharmacological inhibition observed during patch clamp and Fura-2 calcium measurement experiments has an impact on cancer cell proliferation and migration. Therefore, the RT-PCR and RT-qPCR

experiments were performed to check the expression level of hTRPM2 in different pancreatic cancer cell lines and select one particular cell line with higher level of hTRPM2. The selected one was used for checking the impact of these compounds on cancer cell proliferation and migration. None of the compounds showed significant effect on rate of cancer cell proliferation but one showed impact on rate of proliferation of TRPM2 overexpressing HEK293 cells.

As proliferation is not the only aspect of PDAC cells that could be affected by TRPM2 inhibition, hence it would be worthwhile to look into migration, clone formation and apoptosis. Nevertheless, in future these novel TRPM2 inhibitors could be used to study and understand better the physiological and pathological functions of the human TRPM2 channel and develop therapeutics to treat diseases associated with it.

ZUSAMMENFASSUNG

Das transiente Rezeptorpotential Melastatin 2 (TRPM2) ist ein ligandengesteuerter, nicht selektiver, Ca^{2+}-permeabler Kationenkanal, der durch ADPR und 2'-Desoxy-ADPR aktiviert wird. TRPM2 ist in einer Reihe von menschlichen Tumoren, einschließlich Bauchspeicheldrüsenkrebs, hochreguliert und kann die Proliferation von Krebszellen, die Migration sowie die Resistenz gegen Chemotherapeutika fördern. Daher könnte TRPM2 als ein interessantes neuartiges Ziel für die pharmakologische Intervention bei der Krebsprogression angesehen werden. Alle derzeit verfügbaren Verbindungen / Medikamente, die TRPM2 hemmen, sind entweder Kanalblocker, die auch einige andere verwandte Ionenkanäle beeinflussen, oder Nukleotidderivate, die in den biologischen Flüssigkeiten inhärent instabil und kaum membranpermeant sind. Daher konzentriert sich diese Arbeit auf die Entwicklung neuartiger nicht-nukleotid-TRPM2-spezifischer Inhibitoren. Dies könnte in Zukunft eine Grundlage für die Entwicklung von ADPR-Antagonisten/TRPM2-Inhibitoren zu Antitumormitteln insbesondere zur Behandlung von Bauchspeicheldrüsenkrebs, insbesondere des pankreatischen duktalen Adenokarzinoms (PDAC), bilden.

Für die Entwicklung der TRPM2-Inhibitoren wurde ein Computer-Aided Drug Design (CADD) unter Verwendung eines strukturbasierten Drug Design Ansatzes (SBDD) durchgeführt. Der erste Versuch wurde mit SBDD unter Verwendung eines Homologiemodells der Nukleotidbindung NudT9-H-Domäne von humanem TRPM2 unternommen. Dies führte zu insgesamt 12 Verbindungen und diese Verbindungen wurden in vitro auf ihr Potenzial getestet, die Aktivierung von TRPM2 durch ADPR zu hemmen, aber sie zeigten keine vollständige Hemmung der TRPM2-Aktivierung. Ende 2019 veröffentlichten Juan Du et al. dann die tatsächliche menschliche TRPM2 (hTRPM2) Kryo-EM-Struktur. Daher wurde ein weiterer Versuch des computergestützten Drogendesigns unternommen. Diesmal basierte es auf dieser Kryo-EM TRPM2-Struktur und verwendete Molekulardynamik (MD) - Simulationen, um die Struktur zu verfeinern, bevor das molekulare Andocken durchgeführt wurde. Dann wurden auch die Verbindungen aus dieser CADD in vitro überprüft. Zunächst wurden Fura-2-Calciummessungen als primäres Screening auf membranpermete Verbindungen durchgeführt und der Einfluss von Verbindungen auf die TRPM2-vermittelte Calciumkonzentration durch Messung der freien zytosolischen Calciumkonzentration ($[Ca^{2+}]_i$) überprüft. Sechs von 13 Verbindungen zeigten eine zumindest teilweise oder fast vollständige Hemmung der TRPM2-Aktivierung vermittelten Erhöhung von $[Ca^{2+}]_i$ in einer konzentrationsabhängigen Weise. Nach der Überprüfung der Verbindungen an intakten Zellen in Fura-2-Calcium-Messexperimenten wurden diese sechs Verbindungen direkt auf das Ziel

getestet, indem die Ganzzell-Patch-Clamp-Technik verwendet wurde, indem der TRPM2-Strom als Reaktion auf ADPR gemessen wurde. Alle sechs Verbindungen zeigten eine signifikante Verringerung des ADPR-induzierten TRPM2-Stroms. Danach wurde die Wirkung dieser Verbindungen auf Tumorzellen überprüft, um zu bestätigen, ob die pharmakologische Hemmung, die während der Patch-Clamp- und Fura-2-Calcium-Messexperimente beobachtet wurde, einen Einfluss auf die Proliferation und Migration von Krebszellen hat. Daher wurden die RT-PCR- und RT-qPCR-Experimente durchgeführt, um das Expressionsniveau von hTRPM2 in verschiedenen Bauchspeicheldrüsenkrebs-Zelllinien zu überprüfen und eine bestimmte Zelllinie mit einem höheren hTRPM2-Spiegel auszuwählen. Die ausgewählte wurde verwendet, um den Einfluss dieser Verbindungen auf die Proliferation und Migration von Krebszellen zu überprüfen. Keine der Verbindungen zeigte eine signifikante Wirkung auf die Proliferation von Krebszellen, aber eine zeigte Auswirkungen auf die Proliferationsrate von TRPM2-überexprimierenden HEK293-Zellen.

Da die Proliferation nicht der einzige Aspekt von PDAC-Zellen ist, der von der TRPM2-Hemmung betroffen sein könnte, lohnt es sich, Migration, Klonbildung und Apoptose zu untersuchen. Dennoch könnten diese neuartigen TRPM2-Inhibitoren in Zukunft verwendet werden, um die physiologischen und pathologischen Funktionen des menschlichen TRPM2-Kanals zu untersuchen und besser zu verstehen und Therapeutika zur Behandlung der damit verbundenen Krankheiten zu entwickeln.

LIST OF ABBREVIATIONS

Å	Angstrom
%	Percentage
°C	Celsius degree
μg	Microgram
μL	Microlitre
μM	Micromolar
aa	Amino acid
2APB	2-Aminoethyl-diphenylborinate
AMP	Adenosine monophosphate
ACA	N-(p-amylcinnamoyl) anthranilic acid
BAPTA	(1, 2-bis (o-aminophenoxy) ethane- N, N, N', N'-tetra acetic acid)
BSA	Bovine serum albumin
Ca^{2+}	Calcium
$[Ca^{2+}]_i$	Cytosolic calcium concentration
ADP	Adenosine 5'-diphosphate
ADPR	Adenosine diphosphate ribose
cADPR	Cyclic adenosine diphosphate ribose
CO_2	Carbon dioxide
CD38	Cluster of differentiation 38
CCR	Coiled coil region
Cryo-EM	Cryogenic electron microscopy
CytNudT9	Cytosolic NudT9
DNA	Deoxyribonucleic acid
DNAse	Deoxyribonuclease
2'-deoxy-ADPR	2'-Deoxy 5'-diphosporibose
e.g.	Example
DAG	Diacylglycerol
DMSO	Dimethyl sulfoxide
EDTA	Ethylenediaminetetraacetic acid
ECS	Extracellular solution
em	Emission
ex	Excitation

FBS	Fetal bovine serum
FFA	Flufenamic acid
g	Gram
HCl	Hydrochloric Acid
HEPES	4-(2-hydroxyethyl)-1-piperazineethanesulfonic acid
H_2O_2	Hydrogen peroxide
IV	Current-voltage
ICS	Intracellular solution
IL-8	Interleukin-8
KCl	Potassium chloride
kDa	Kilo dalton
M	Molar
mA	Milliampere
mg	Milligram
MAPK	Mitogen-activated protein kinases
$MgCl_2$	Magnesium chloride
$MgSO_4$	Magnesium sulphate
mL	Millilitre
mM	Millimolar
Na^+	Sodium ion
NAD	Nicotinamide adenosine 5'-dinucleotide
NMR	Nuclear Magnetic Resonance spectroscopy
NudT9-H	Nudix (Nucleoside Diphosphate Linked Moiety X)-Type Motif 9
NMDG	N-Methyl-D-glucamin
ng	Nanogram
nm	Nanometer
nM	Nanomolar
pH	Power of hydrogen
PCR	Polymerase chain reaction
qPCR	Quantitative polymerase chain reaction
RT-PCR	Reverse transcriptase polymerase chain reaction
PARP	Poly(ADPR) polymerase
PARG	Poly(ADPR) glycohydrolase
PK	Pharmacokinetic

PVDF	Polyvinylidene Fluoride
RNA	Ribonucleic acid
RNAse	Ribonuclease
TRPA	Transient receptor potential ankyrin
TRPC	Transient receptor potential canonical
TRPM2	Transient receptor potential channel, subfamily melastatin, member 2
TRPML	Transient receptor potential mucolipin
TRPP	Transient receptor potential polycystin
TRP	Transient receptor potential channels
TRPV	Transient receptor potential vanilloid
TAE	Tris-acetate-ethylenediaminetetraacetic acid
qPCR	Quantitative polymerase chain reaction
siRNA	Small interfering RNA
V	Voltage
v/v	Volume/volume
w/v	Weight/volume

LIST OF FIGURES

Figure 1: Branching diagram of TRP channels....17
Figure 2: TRP superfamily classification and further TRPM2 subdivision....18
Figure 3: Schematic depiction of the human TRPM2 gene isoforms....19
Figure 4: Structural representation of human TRPM2 in the Apo form (closed state)....21
Figure 5: Different pathways of TRPM2 channel activation....22
Figure 6: Molecular mechanisms of TRPM2 in PDAC cell proliferation and tumorigenesis.27
Figure 7: Structures of compounds selected from computer-aided drug design using homology model....34
Figure 8: Structures of compounds selected from computer-aided drug design using cryo-EM structure of hTRPM2....36
Figure 9: Schematic representation of the workflow for the structure-based drug design using homology model....38
Figure 10: Standard protocol for the MD simulations in GROMACS....39
Figure 11: Steps taken for Molecular dynamics simulation....41
Figure 12 Principle behind Fura-2 calcium measurement....45
Figure 13: Principle of Patch clamp technique....47
Figure 14: Evaluation of compounds selected from molecular docking....55
Figure 15: Effect of compounds selected from drug design using homology model on the activation of TRPM2 by ADPR....57
Figure 16: Effect of potential ADPR antagonist on the H_2O_2-stimulated Ca^{2+} signal in Fura-2 loaded TRPM2 expressing HEK293 cells....61
Figure 17: Schematic representation of the docking process....63
Figure 18: Measurement of Fura-2 loaded HEK293 cells for compounds selected from computer-aided drug design based on cryo-EM structure with their concentration-response curves....68
Figure 19: Effect of compounds selected from drug design using hTRPM2 cryo-EM structure on the activation of TRPM2 by ADPR....70
Figure 20: Analysis of expression of TRPM2 in human PDAC cell lines by RT-PCR....71
Figure 21: Bar plot showing gene expression levels of hTRPM2, measured by RT-qPCR....72
Figure 22: Bar graph showing impact of TRPM2 inhibitors on MIA PaCa-2 cell proliferation rate....73

Figure 23: Bar graph showing impact of TRPM2 inhibitors on TRPM2 overexpressing HEK293 cell proliferation rate.....74
Figure 24: Fura-2 calcium measurement results for compound 05, 10, 11 and 12.....83
Figure 25: HPLC experiment results for compound 12 over the period.....83
Figure 26: Concentration-response curve for compound 12.....84
Figure 27: Summary of results from calcium measurement and patch clamp experiments 85

LIST OF TABLES

Table 1: TRPM2 cryo-EM structure details with their specific ligands and resolution 21
Table 2: EC_{50} values of ADPR for different cell types 23
Table 3: TRPM2 Role in Human Cancer 26
Table 4: Buffer compositions with concentrations and pH 31
Table 5: Stock solution preparation for all of the compounds 32
Table 6: Origin information and details of the pancreatic cell lines 42
Table 7: Detailed composition of culture media 43
Table 8: Summarized Chromatographic parameters 44
Table 9: Gradient elution program for HPLC analysis 44
Table 10: Composition of Master-mix for one-step RT-PCR 50
Table 11: Composition of 2X reverse transcription mix 51
Table 12: Thermocycler conditions for reverse transcription 52
Table 13: Percentage purity values for compounds selected from drug design using homology model 56
Table 14: Percentage purity values for compounds selected from drug design using cryo-EM structure 64

1 INTRODUCTION

1.1 TRP CHANNEL SUPERFAMILY

Calcium signalling plays a role in various cellular mechanisms as well as pathological conditions. This is the reason why the channels involved in the regulation of calcium could also be considered as an important therapeutic target and TRP (transient receptor potential) channels come under that category. The very first time the TRP channels were investigated by Cosens and Manning. This group was working with *Drosophila melanogaster*, a species of fruit fly and during one study, they observed that a mutation in this species behaved differently upon exposure to continuous light in comparison to the wild type. The mutant species became blind over a shorter duration showing a transient effect while the effect on the wild type was quite sustained. Upon further investigation they figured out the source responsible for this mutation and named it as trp (transient receptor potential) locus of the Drosophila genome (Cosens and Manning, 1969), and then in late 80s Montell and Rubin sequenced the gene and concluded based on the protein sequence that the product of the gene is a channel (Montell and Rubin, 1989). Then upon further studies when several orthologues in vertebrates especially humans were identified they referred this mutant protein as the superfamily of ion channels (Nilius and Owsianik, 2011).

All these TRP channels form tetramers either homo- or hetero-tetramer. In addition, they all show some structural similarities with regard to the different domains they are made up of which are: a transmembrane domain, cytoplasmic N- and C- terminal regions, a pore-forming region between fifth and sixth transmembrane helix (Clapham, 2003).

Members of this TRP superfamily are present in the cells of all the living forms including vertebrates, invertebrates and yeast except in prokaryote. This superfamily has 29 members. As shown in the following figure 1, on a broader scale, this TRP superfamily consists of seven subfamilies: TRPC (canonical), TRPM (melastatin), TRPV (vanilloid), TRPP (polycystin), TRPA (ankyrin), TRPML (mucolipin), and TRPN (NOMPC-like). TRP channels are not voltage-gated but some of them show some sensitivity to membrane-potential (like TRPM4). Mostly these TRP channels are non-selective cation channels but some of them are highly calcium ion (Ca^{2+}) selective and some are magnesium ion (Mg^{2+}), potassium (K^{+}) and sodium ion (Na^{+}) permeable. Because of this these channels could also serve as a gatekeeper for the transport of Ca^{2+}, K^{+} ,Na^{+} and Mg^{2+} (Nilius and Owsianik, 2011).

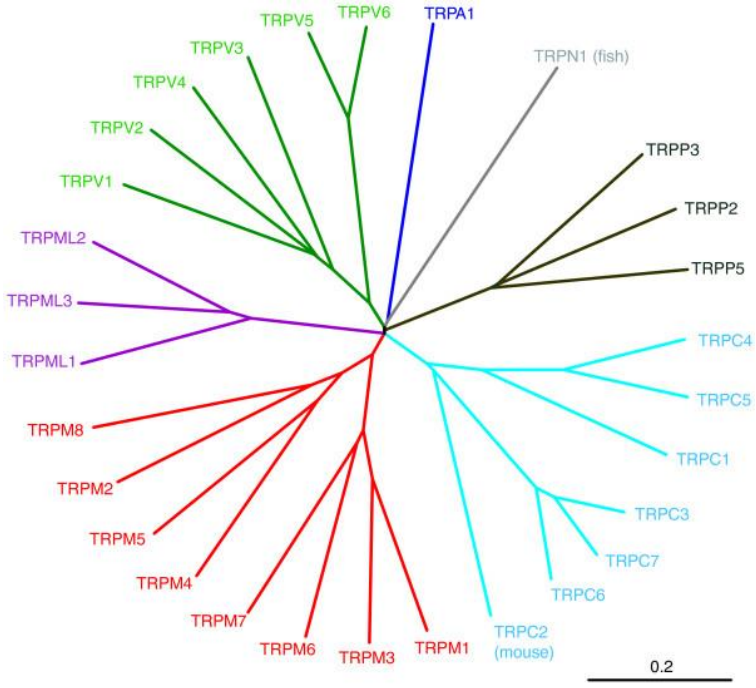

Figure 1: Branching diagram of TRP channels

This figure 1 shows the grouped division of all the seven members of TRP channel superfamily. This classification is based on the amino acid residue sequence similarity with each other. This figure is taken from (Nilius and Owsianik, 2011).

1.2 TRPM2 CHANNELS

The studies performed in this thesis are focused on exploring the TRPM2 channel (transient receptor potential cation channel, melastatin subfamily member 2).

As shown in the figure 2 the TRP-melastatin subfamily (TRPM) has eight members and is grouped into four pairs as follows: TRPM1/TRPM3, TRPM6/TRPM7, TRPM2/TRPM8 and TRPM4/TRPM5. And this classification is based on the degree of similarity of their amino acid sequences with each other (Voets et al., 2005).

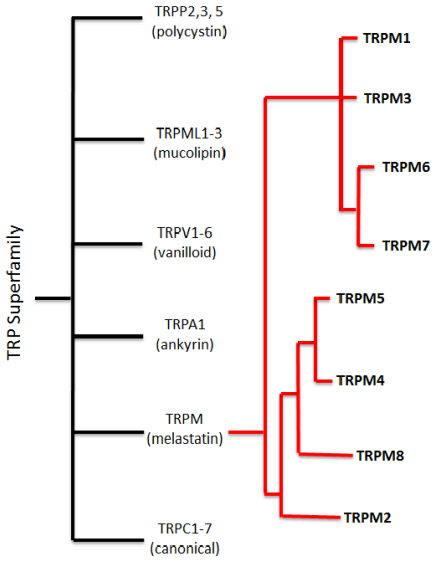

Figure 2: TRP superfamily classification and further TRPM2 subdivision

As shown in the figure 2 the TRP superfamily has in total 28 (excluding TRPN1) members, which on a broader scale are divided into total six subfamilies. In addition, this TRPM subfamily is further grouped into four pairs as is shown here and this division is based on the protein sequence similarities. This image is adopted from (Voets et al., 2005).

1.2.1 TRPM2 gene and expression

The chromosomal region 21q22.3 is exactly where the human TRPM2 (hTRPM2) gene is present and the gene is made up of 32 exons. (Nagamine et al., 1998). The TRPM2 genes were cloned from human (Nagamine et al., 1998), mouse (Okada et al., 1999) and rat (Kraft et al., 2004) and in the meantime also from *Nematostella vectensis*, zebra fish (*Danio rerio*) and from a number of other organisms as well. The full-length human TRPM2 protein comprises of total 1503 amino acid residues with a molecular weight of approximately 170kDa (Nagamine et al., 1998). While the mouse TRPM2 protein has 1506 (Uemura et al., 2005) and the rat TRPM2 protein have 1508 amino acid residues (Hill et al., 2006).

In general, the human TRPM2 has total seven isoforms which are shown in figure 3 and explained as follows (Belrose and Jackson, 2018, Uemura et al., 2005):

- The full-length long form (TRPM2-L) has 1503 amino acid residues and contains all the domains, which are the melastatin homology region (MHR), transmembrane domain, coiled-coil region (CCR) and the NudT9-H domain (figure 3).
- The TRPM2-ΔN having all the domains like the full-length form but the amino acid residues from 538 to 557 (20 amino acid residues) are missing.
- The TRPM2-ΔC that also has all the domains but the deletion of amino acid residue from 1292 to 1325 (34 amino acid residues are missing).
- The TRPM2-ΔNΔC splice variant with the deletions similar as both the TRPM2-ΔN and TRPM2-ΔC meaning deletions of amino acid residues from 538 to 557 as well as from 1292 to 1325, which accounts for total 54 amino acid residues missing.
- A splice variant found in the striatum and was called as striatum short form of TRPM2 (SSF-TRPM2). This splice variant has the first 214 amino acid residues missing but has all the remaining domains present.
- The TRPM2-S splice variant is a short form (amino acid residues missing from 846 to 1503) and consists of the homology region and the S1 and S2 helices from the transmembrane domain.
- The TRPM2-TE, which only has the NudT9-H domain meaning the amino acids from 1 to 1236 are missing (Belrose and Jackson, 2018, Uemura et al., 2005).

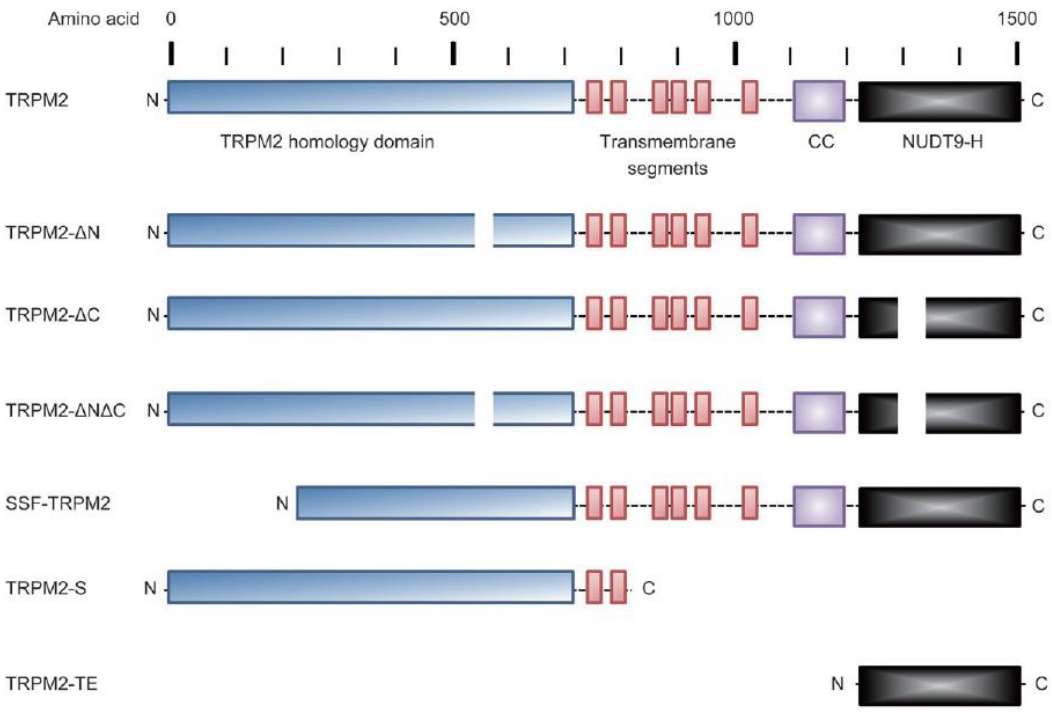

Figure 3: Schematic depiction of the human TRPM2 gene isoforms

The figure shows the human TRPM2 gene along with its different isoforms. It has a full-length form along with some other splice variants. The full-length TRPM2 form (first one from the top) has 1503 amino acid residues and contains all the domains namely starting from left, the homology region, transmembrane domains, coiled-coil region and the NudT9-H domain. Then comes the TRPM2 ΔN with the deletion of 20 amino acid residues starting from 538 to 557. The TRPM2 ΔC splice variant with the amino acid residues missing from 1292 to 1325. Then there is the slice variant TRPM2 ΔNΔC, which has amino acid residues missing from 538 to 577 as well as from 1292 to 1325. Then the SSF-TRPM2 splice variant which was found in striatum hence named as short striatum form of TRPM2 (SSF-TRPM2). Last two in the figure are the TRPM2-S and TRPM2-TE splice variants. Of these two, the TRPM2-S has amino acid residues missing from 846 to 1503 (consists of homology region and S1 and S2 helices from transmembrane domain). Then the TRPM2-TE splice variant only contains the NudT9-H domain. This figure is adopted from (Belrose and Jackson, 2018).

TRPM2 is extensively expressed in the central nervous system (CNS), particularly in microglia, striatum, hippocampus, cerebral cortex, as well as in thalamus (Nagamine et al., 1998, Kraft et al., 2004, Fonfria et al., 2006, Lipski et al., 2006).

The TRPM2 mRNA and protein are also expressed in some other types of cells. Which namely are: cells in the salivary glands (Liu et al., 2013), pancreatic β-cells (Uchida and Tominaga, 2011), neutrophil granulocytes (Heiner et al., 2003), microglia (Fonfria et al., 2006), monocyte cells (Yamamoto et al., 2008) and endothelial cells (Hecquet et al., 2008, p. 2). Moreover, TRPM2 channels have also been expressed in some other cells and their functional expression has been confirmed using fluorescent calcium imaging as well as patch clamp recordings. These cells are: peritoneal macrophages (Kashio et al., 2012), hippocampal neurons (Olah et al., 2009), DRG neurons (Nazıroğlu et al., 2011) and T-lymphocytes (Beck et al., 2006).

1.2.2 Overall structure of TRPM2 channels

Structurally the TRPM2 channel is unique compared to all the other TRP channels, as at the C-terminal side it possesses the NudT9-H domain, which is the distinctive feature of this channel. This NudT9-H domain has 39% similarity (Shen et al., 2003) and 50% homology (Perraud et al., 2001) with the enzyme ADPR pyrophosphatase NudT9 hence has been termed "NudT9-H domain" where 'H' stands for homologous. As already mentioned the TRP channels are homo or hetero-tetramers and TRPM2 is a homo-tetramer and it has approximate dimension of 150 Å by 100 Å by 100Å (figure 4B). Being the homo-tetramer all its monomeric units contains same domains and as shown in the (figure 4A), these are the melastatin homology region (MHR) in the N-terminus immediately followed by the transmembrane domain (TM) and then at the C-terminal end the unique NudT9-H domain. In more detail, the TRPM homology region is made up of MHR1/2, MHR3 and MHR4 domains, then the transmembrane region consisting of the S1-S4 voltage sensor-like domain (VSLD) and the pore region in between the helix 5 and 6. This transmembrane domain is again attached with the TRP helices H1 and H2, a rib helix and a pole helix (Wang et al., 2018). Then in the end, there is the unique NudT9-H domain at the C-terminus. In addition to this NudT9-H domain, the N-terminus also contains an IQ-like motif, which could probably offers itself as a binding site for the calmodulin (CaM) (Tong et al., 2006).

As it is demonstrated in the figure 4D, the whole TRPM2 structure is arranged in a three-tier domain layout. In which the top tier incorporates pre-S1 helix, the transmembrane domain and the TRP helices. The middle tier has MHR4 and the rib helix while the MHR1/2/3, the pole helix and NudT9-H are part of the bottom tier which is the most intracellular tier (Wang et al., 2018).

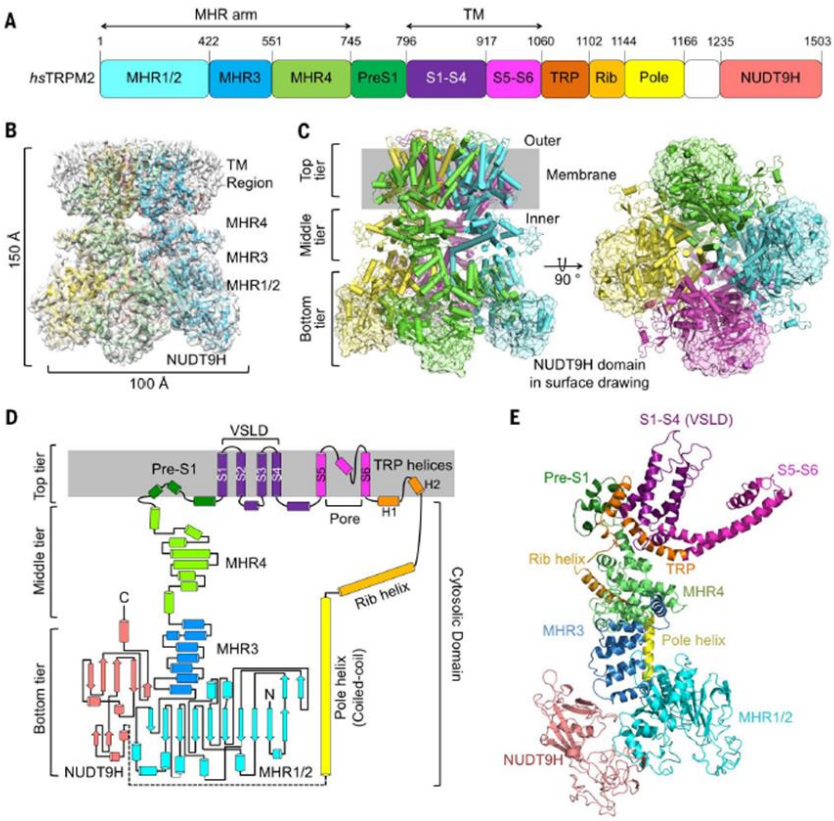

Figure 4: Structural representation of human TRPM2 in the Apo form (closed state)

The figure 4 (A) shows the TRPM2 structural layout with all the domains and at the top there is the entire amino acid residue numbers written. Then in figure 4 (B), the vertical image of the 3D cryo-EM model of TRPM2 along with its dimensions is shown. The figure 4 (C) presents the ribbon illustration of the TRPM2 in vertical and horizontal view with its each monomeric unit in different colours and the NudT9-H domain in transparent shade. Then figure 4 (D) represents the structural layout divided into three tiers. In addition, figure 4 (E) is just the ribbon diagram of a single monomeric unit. This figure is taken from (Wang et al., 2018).

So far, there have been many approaches tried for solving the structure of TRPM2 channel like x-ray crystallographic and Nuclear Magnetic Resonance spectroscopic (NMR) techniques. However, due to the inability of TRPM2 to crystallize, x-ray crystallographic technique could not be used as well as because of its big size (170 kDa), using NMR technique was not feasible as it could not be used for proteins more than 30 kDa. Hence, for resolving the TRPM2 structures cryogenic electronic microscopic technique (cryo-EM) was used. Some of the details of the cryo-EM structures of TRPM2 with their specific ligands have been enlisted in the following table 1.

Table 1: TRPM2 cryo-EM structure details with their specific ligands and resolution

Species	Ligand	Resolution(Å)	PDB Codes	Reference
Homo sapiens **(hTRPM2)**	Apo	3.3	6PUO	(Huang et al., 2019)
	ADPR	4.4	6PUR	
	ADPR/Ca^{2+}	3.7	6PUS	
	8-Br-cADPR/Ca^{2+}	3.7	6PUU	

	Apo	3.6	6MIX	(Wang et al., 2018)
	ADPR	6.1	6MIZ	
	ADPR/Ca^{2+}	6.4	6MJ2	
Danio rerio	Apo, C4	4.3	6PKV	(Yin et al., 2019)
	Apo, C2	4.5	6PKW	
	Ca^{2+}	3.8	6D73	
	ADPR/Ca^{2+}	4.2	6PKX	
Nematostella vectensis	Ca^{2+}	3.0	6CO7	(Zhang et al., 2018)

1.2.3 TRPM2 channel activation mechanism

There are different pathways through which the activation of TRPM2 channel could take place. Which are mentioned as follows as well as the overall mechanism of TRPM2 activation is shown in the following figure 5.

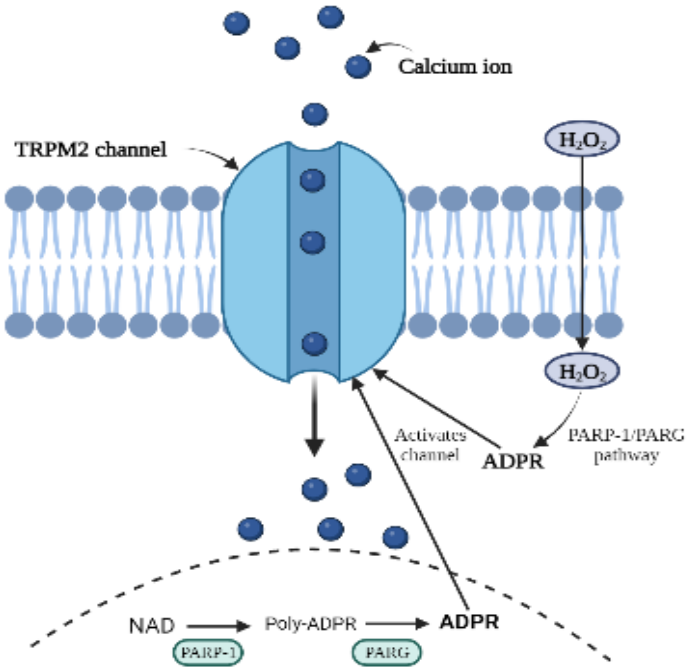

Figure 5: Different pathways of TRPM2 channel activation

This figure shows different pathways of ADPR-mediated TRPM2 activation. Upon cell or oxidative stress, there is production of NAD^+, which leads to generation of ADPR via the PARP-1/PARG pathway. In addition, reactive oxygen species (ROS) like H_2O_2 indirectly are converted into ADPR via DNA damage caused due to PARP-1/PARG pathway. This ADPR then binds to the unique NudT9-H domain of human TRPM2 channel and leads to activation of the channel and increase in the free cytosolic calcium concentration ($[Ca^{2+}]_i$). This figure was created in Biorender.com based on the figure from (Sumoza-Toledo and Penner, 2011).

1.2.3.1 Activation by ADPR and 2'deoxy ADPR

ADPR by acting as a TRPM2 channel activator/agonist is the key gating molecule required for the TRPM2 channel activation. By using an ADPR concentration between 300 to 500 µM the TRPM2 channel could be fully activated. This activation by ADPR occurs in a concentration

dependent manner and is different for different type of cells. These cells cover the wide range for the EC_{50} values between 1 to 90 μM (Sumoza-Toledo et al., 2011). Following is the table 2 for the different EC_{50} values for different cell types.

Table 2: EC_{50} values of ADPR for different cell types

Cell type	EC_{50} value (μM)	Calcium Concentration used (nM)	Reference
TRPM2 expressing HEK293	12	Un-buffered	(Kolisek et al., 2005)
Human neutrophils	1.1	Un-buffered	(Lange et al., 2008)
Jurkat T cells	7	200	(Beck et al., 2006)

As per the hypothesis based on some prior studies, under cellular or oxidative stress ADPR can be released inside the cells from mitochondria or in the nucleus, via PARP-1/PARG pathway. In mitochondria, the NAD^+ nucleosidase (NADase) is activated by reactive oxygen species (ROS) which hydrolyses NAD^+ to ADPR and nicotinamide (Perraud et al., 2005, Dölle et al., 2013). Whereas in nucleus, the poly (ADPR) polymerases (PARP-1) gets activated because of the reactive oxygen species (ROS)-induced DNA damage which results into PAR chain ultimately hydrolysed to ADPR by poly(ADPR) glycohydrolase (PARG) (Buelow et al., 2008). This ADPR from either the nucleus or the mitochondria, then probably gets into the cytosol by diffusion and binds to the NudT9-H domain of the TRPM2 channels.

Then there is one more endogenous TRPM2 channel activator called 2'-Deoxy 5'-diphosporibose (2'-deoxy-ADPR). This 2'-deoxy-ADPR is a superagonist of TRPM2 channel. Upon testing the agonistic effect of 2'-deoxy-ADPR using patch clamp experiments it showed 10.4 fold higher current as well as activated the channel at lower concentration compared to ADPR (Fliegert et al., 2017a).

The ADPR has two binding sites in the human TRPM2 channel: first, the classic NudT9-H binding domain and second the recently discovered MHR1/2. Along with these two, there is one more binding site in the transmembrane domain for binding of the Ca^{2+}. Therefore, in total there are three binding sites to be occupied for the activation of TRPM2 channel. The MHR1/2 is that binding site for ADPR, which is found in all the species and hence Huang *et al* called it as the primary binding site. The classic NudT9-H binding pocket apparently is not needed for the channel activation in invertebrates (nvTRPM2). The shape of these two ADPR binding sites is quite different from each other. The NudT9-H binding domain is very much wide and more relaxed while the MHR1/2 binding site is small and embedded into the N-terminal side. Because of these different shapes of the binding sites, the respective ADPR molecule also has to take the shape of these binding sites to fit into them. Meaning because of the broader shape of NudT9-H domain the ADPR molecule could fit in more relaxed while in case of the MHR1/2 domain the ADPR molecule has to bend into and form a compact U shape (Huang et al., 2019).

1.2.3.2 Activation by Calcium ion

Even though as mentioned earlier ADPR is the main molecule responsible for TRPM2 activation, there are some studies suggesting that presence of intracellular Ca^{2+} along with ADPR is necessary for full TRPM2 activation. Which means binding of Ca^{2+} along with the ADPR to the NudT9-H domain or MHR1/2 domain is required for the channel activation. Moreover, in absence of binding of these Ca^{2+} intracellularly, the channel remains inactive. Ca^{2+} acts as a cofactor for TRPM2 activation.

To prove this McHugh *et al* performed one study where they used BAPTA (1, 2-bis (o-aminophenoxy) ethane- N, N, N', N'-tetra acetic acid), which is a Ca^{2+}chelator. In the patch clamp experiment, they infused the cells with BAPTA and maintained the extracellular calcium concentration. Upon entering the cell BAPTA formed a complex with the intracellular calcium ions thereby lowering the free cytosolic calcium concentration ($[Ca^{2+}]_i$), which ultimately resulted in the reduced ADPR-mediated TRPM2 currents. Which suggests that intracellular calcium concentration is also required for the full activation of TRPM2 channel along with the extracellular calcium concentration. Also in whole-cell patch clamp recordings, it has been shown that there is an increase in ADPR-mediated TRPM2 currents in presence of intracellular Ca^{2+} and this increase happens in a concentration dependent manner (McHugh et al., 2003).

1.2.3.3 Activation by reactive oxygen species (ROS)

Hydrogen peroxide (H_2O_2), superoxide ion (•O2−) and hydroxyl radical (HO•) are the different types of reactive oxygen species (ROS). Normally these ROS are generated from the mitochondrial respiration and nicotinamide adenine dinucleotide phosphate (NADPH) oxidation hence have an important role in various cellular processes (Finkel and Holbrook, 2000).

So far, there are many studies showing the involvement of ROS particularly, H_2O_2 in the activation and function of TRPM2 channels. H_2O_2 cannot directly activate the TRPM2 channel but it activates the channel indirectly producing ADPR. Tóth and Csanády investigated this in 2010, where they performed inside-out patch clamp recordings using *Xenopus oocytes* heterogeneously expressing TRPM2. For this experiment, the patches were pulled out of the membrane and because of this, upon application of H_2O_2 there was no production of intracellular ADPR (in response to oxidative stress) which could activate the channel. Hence, it was proved that H_2O_2 directly cannot activate TRPM2 channel (Tóth and Csanády, 2010). Some other research groups using different other experimental techniques also further investigated this. With the help of Fura-2 calcium measurement experiments it has been proven that extracellular application of H_2O_2 on TRPM2 overexpressing HEK293 cells, indirectly

activates the channel and thereby resulting in an elevated $[Ca^{2+}]_i$. This happens in a concentration dependent manner showing an EC_{50} value of about 30 μM for H_2O_2 (Hara et al., 2002, Fonfria et al., 2005, Perraud et al., 2005).

Most of these studies showing activation of TRPM2 by H_2O_2 propose that being a reactive oxygen species (ROS), H_2O_2 induces this channel activation by stimulating the production of ADPR in the mitochondria and nucleus via PARP-1/PARG pathway (refer figure 5), as discussed above (see above 1.2.3.1 section of ADPR induced TRPM2 activation). Perraud *et al* have studied this relation between PARP-1 to hydrogen peroxide (H_2O_2) and their impact on TRPM2 activation extensively.

They could demonstrate the role of PARP-1 and intracellular ADPR by blocking H_2O_2-mediated TRPM2 activation using either a specific PARP-1 inhibitor (5[H]-phenanthridin-6-one, GPI16539) or overexpression of ADPR-hydrolysing NudT9-H (Perraud et al., 2005). This study clearly showed that if there were no ADPR accumulation the activation of TRPM2 by H_2O_2 would not happen.

1.2.3.4 Activation by temperature

TRPM2 channel is sensitive to temperature and is activated in response to heat (mostly more than 35°C). Different groups have studied this influence of temperature on TRPM2 activation but no one has shown this temperature-mediated channel activation in absence of ligand.

Of which Togashi *et al* performed Ca^{2+} imaging experiments using HEK293 cells expressing TRPM2 as well as pancreatic β-cells and insulinoma RIN-5F cells. In case of TRPM2 expressing HEK293 cells upon exposure to heat of about 40°C there was an increase in $[Ca^{2+}]_i$. While similar response of elevated $[Ca^{2+}]_i$ has also been observed in insulinoma RIN-5F cells and pancreatic β-cells (Togashi et al., 2006).

There was one more study performed using HEK293 cells also showed the similar increase in $[Ca^{2+}]_i$ in response to heat. In contrast to Togashi *et al* the authors used comparatively higher average threshold of heat of around 47°C (Kashio et al., 2012).

1.2.4 TRPM2 role in cancer

Calcium ions (Ca^{2+}) as being involved in numerous cellular processes are an important secondary messenger. Hence, any alterations in calcium signalling could lead to a number of pathological conditions including various types of human cancers. Due to this, the ion channels regulating calcium signalling play an important role in these pathological conditions. There are many ion channels regulating the transport of Ca^{2+} including TRP channels which regulates some of the calcium dependent processes (Gautier et al., 2019).

TRPM2 channels have shown to play an important role in a wide range of human cancers hence the studies performed in this thesis are focused on exploring the TRPM2 channels. Various types of human cancers including pancreatic cancer, breast cancer, prostate cancer, melanoma, leukaemia, and neuroblastoma have shown high expression of TRPM2. See table 3 for details on the TRPM2 role human cancers (Miller, 2019).

Table 3: TRPM2 Role in Human Cancer

Cancer type	Activity/function	Reference
Pancreatic Cancer	-Pancreatic cancer patients have shown shorter survival duration in case of high expression level of TRPM2	(Lin et al., 2018, Bauer et al., 2012)
Breast Cancer	-Breast cancer cells have shown decreased rate of proliferation upon TRPM2 inhibition	(Hopkins et al., 2015)
Prostate Cancer	-Prostate cancer cell proliferation is lowered after TRPM2 inhibition	(Zeng et al., 2010)
Gastric Cancer	-Gastric cancer cell proliferation has been impacted upon TRPM2 inhibition	(Almasi et al., 2018)
Neuroblastoma	-Inhibition of TRPM2 in Neuroblastoma has shown to downturn cancer cell viability and tumour growth in the xenografts	(Bao et al., 2016)
Lung Cancer	-In case of Lung cancer tumour size and patient survival was shown to be affected by high expression of TRPM2-AS	(Huang et al., 2017)
Squamous Cell Carcinoma	-Inhibition of TRPM2 in Squamous cell carcinoma have shown declined tumour viability	(Zhao et al., 2016)

Though this TRPM2 overexpression leads to different types of cancer but of these all, the work in this thesis has been done around finding the TRPM2 inhibitors to aid in the treatment of pancreatic cancer especially pancreatic ductal adeno carcinoma (PDAC). Pancreatic cancer affects pancreas, a digestive organ located in the upper abdomen. There are different types of pancreatic cancer but of them all PDAC is the most lethal as it accounts for 90% of all the pancreatic cancer cases and is at 4th position in the list of most frequent deathly cancers list worldwide (Adamska et al., 2017). There could be several mechanisms or pathways responsible for PDAC cells proliferation and overall tumorigenesis. However, interestingly TRPM2 activation mediated increase in Ca^{2+} has a role to play in the activation of MAPK pathway responsible for encouraging PDAC cell proliferation and tumorigenesis. Lin *et al* have tried to explain the role of TRPM2 in PDAC proliferation. As shown in figure 6 the activation of MAPK signalling pathway by TRPM2 activation happens in 2 ways:

1) Direct mechanism- As activation of TRPM2 channel leads to influx of Ca^{2+}, these Ca^{2+} could directly activate PKCα which is a member of the classical Protein Kinase C

(PKC). This PKCα then activates the MAPK pathway and thereby encouraging the proliferation and metastatic ability of PDAC cells (Lin et al., 2021).

2) Indirect mechanism- Increased Ca^{2+} level due to activation of TRPM2 leads to activation of phospholipase C (PLC). This PLC causes degradation of phospholipids resulting into production of diacylglycerol (DAG), which is a second messenger in cell. This increased DAG level triggers the activation of PKCε and PKCδ which ultimately activates MAPK pathway and supporting PDAC cells proliferation and tumorigenesis (Lin et al., 2021).

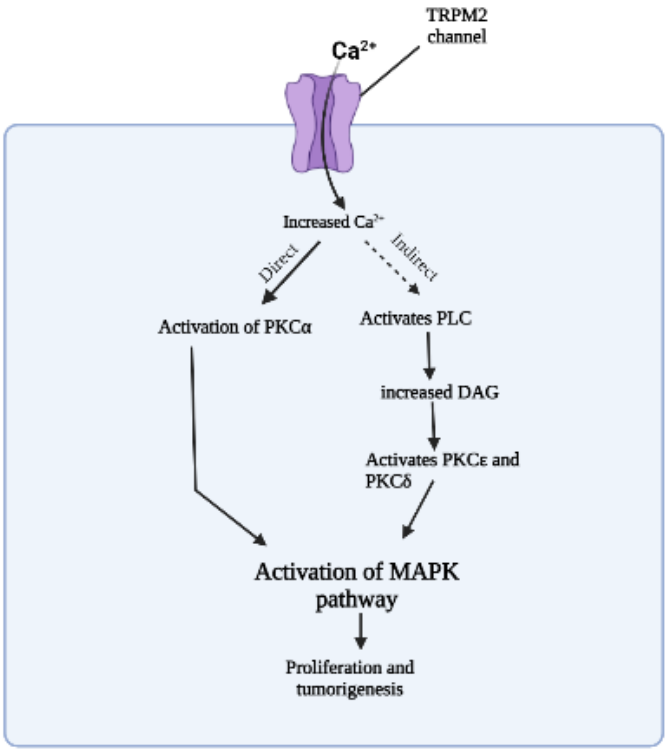

Figure 6: Molecular mechanisms of TRPM2 in PDAC cell proliferation and tumorigenesis

Activation of TRPM2 leads to an increase in Ca^{2+} influx into the pancreatic cancer cells. This could result in direct activation of PKCα leading to activation of MAPK pathway. In addition, this elevated Ca^{2+} levels could indirectly activate MAPK pathway by triggering the phospholipase C (PLC) to increase diacylglycerol (DAG) level leading to activation of PKCε and PKCδ that ultimately activates the MAPK pathway and then encouraging the PDAC cells ability to proliferate and metastasize. This figure is made using Biorender.com and is based on explanation from Lin et al., 2021.

1.3 COMPUTER-AIDED DRUG DESIGN (CADD)

In drug discovery, the next stage after drug target identification is the drug design and development. This drug design includes high throughput screening (HTS) or computer-aided drug design (CADD). In comparison to the other options, CADD provides high success rates of the hit compound identification hence used frequently these days. In general, there are two different methods for the computer aided drug design based on the information available about the target as well as the ligands structures.

1) Structure-based drug design (SBDD) could be applied in instances where the high-resolution structure of target protein is known and is available for use. The structure of the protein is mostly obtained from the protein data bank (PDB) database.
2) Ligand-based drug design (LBDD) is applied when there is no or very little information about the target protein structure available. So in this case the drug design is based on the knowledge of available inactive and active molecules or ligands (Katsila et al., 2016).

In this thesis for the development of novel TRPM2 inhibitors, instead of ligand-based drug design a structure-based drug design approach has been used. This approach was used because there is very little information available about the ligands/agonists of TRPM2 as well as there was first a homology model based structure of NudT9-H domain of human TRPM2 and then later on an actual cryo-EM structure of human TRPM2 was published.

Drug design using homology modelling is based on the principle that proteins with similar amino acid residue sequence have similar structures and hence could be used to predict the conformation of a target protein whose structure is not available. In this case, the quality of the homology model and ultimately the success of drug design depends on the percentage of similarity of the amino acid sequence. Generally, the amino acid similarity above 50% is considered to deliver a reliable homology model, which could be used for the structure-based drug design. However, the amino acid sequence similarity below 15% could lead to deceptive results and cannot be used to perform drug design (Hillisch et al., 2004).

Drug design using experimentally determined structures is the advanced approach of drug design. The 3D structure of target protein is the prerequisite for the structure-based drug design. And the x-ray crystallography, cryo-EM and NMR are the frequently used techniques for the target structure determination. Of these techniques, cryo-EM microscopy could be used when the target protein structure cannot be crystallized and has one more advantage of being able to study the protein in its native state. However, the most important drawback of this technique is that it results in a low resolution protein structure (Renaud et al., 2018).

2 AIM AND MOTIVATION

The main objective of this thesis is to develop non-nucleotide TRPM2 inhibitors that target the ADPR-binding NudT9-H domain unique to TRPM2 channels, making them more specific to TRPM2.channels. As this NudT9-H domain is the binding site for the ADPR molecules, each of the TRPM2 inhibitors have to compete with ADPR for the binding site. For this reason, these non-nucleotide TRPM2 inhibitors could also be called as "ADPR antagonists".

The required work can be broken down into three separate steps:

i. Identification of potential ADPR antagonists by computer-aided drug design.
ii. Testing (*in vitro*) of the potential TRPM2 inhibitors in a cell based assay and in whole-cell patch clamp experiments using human TRPM2 overexpressing HEK293 cells to check their potential to inhibit the activation of TRPM2.
iii. Assessment of the impact of these TRPM2 inhibitors on the pancreatic cancer cells with respect to their rate of proliferation.

3 MATERIALS AND METHODS

3.1 MATERIALS

- $CaCl_2$ (* $2H_2O$), (D)-glucose (* H_2O), KCl, $MgCl_2$ (* $6H_2O$), were purchased from Merck (Darmstadt, Germany).
- G418-disulfate salt, Dimethyl sulfoxide (DMSO), N-Methy-D-glucamin (NMDG) and EGTA (Ethylene glycol-bis (2-amino-ethylether)-N, N, N', N'-tetra-acetic acid) were purchased from Merck, Sigma Aldrich, Germany.
- LiChroSolv methanol for HPLC was also purchased from Merck KGaA, Darmstadt, Germany, TRIzol was purchased from OCI Thermo Fischer, and Ethanol was purchased from OCI Sigma.
- Roti® GelStain Red (Carl Roth, Karlsruhe, Germany), 6X loading dye (Thermo Fisher Scientific, Waltham, Massachusetts, USA), GeneRuler DNA Ladder Mix (Thermo Fisher Scientific, Waltham, Massachusetts, USA), Agarose SeaKem® LE (Lonza, USA).
- Fura-2-AM was purchased from Calbiochem (Merck, EMD Millipore Corp., Billerica, MA USA).
- AgCl, NaCl, Triton X-100 and Tris were purchased from Sigma-Aldrich Co. (St. Louis, MO USA) or Sigma-Aldrich Chemie GmbH (Steinheim, D).
- HEPES was purchased from Carl Roth (Karlsruhe, D).
- DMEM (1X) + GlutaMAX™-I– Pyruvate + 4.5g/L D-Glucose, RPMI Medium 1640 (1X) + GlutaMAX™-I + 25 mM HEPES and PenStrep were purchased from Gibco (Life Technologies Corporation, Grand Island, NY USA), Trypsin-EDTA solution 10X was purchased from Sigma-Aldrich, US.
- FBS was purchased from Biochrom (Berlin, D).
- NaOH was purchased from J.T. Baker (Deventer, NL).
- Solutions: Unless noted otherwise, all buffers were sterile filtered with a 0.2 µm filter. Prepared buffers and stock solutions were stored at +5°C up to several months. Unless otherwise noted, all experiments were performed at room temperature (RT).
- Stock solutions: 1 M stock solutions of $CaCl_2$ and $MgCl_2$ were prepared, sterile filtered and stored at +5°C for preparing electrophysiological buffers. Fura-2AM: 1 mM in DMSO, 4.3 µl aliquots were stored at -20 °C for several months. Tris-EGTA:

4 M Tris and 300 mM EGTA in high-purity water, 1 mL aliquots were stored at -20 °C for several months. Triton X-100: 10 % (w/v) in high-purity water; 1 mL aliquots were stored at -20 °C for several months.

- The compounds selected from structure-based drug design based on the homology model were purchased from Mcule (Mcule, Inc. 535 Everett Ave #410 Palo Alto, CA 94301 USA) ("Mcule"). And the ones selected from of the structure-based drug design using cryo-EM structures were purchased from Molport (MolPort, SIA Lacplesa street 41 Riga, LV1011 Latvia) ("Molport-Compound Sourcing, Selling and Purchasing Platform").
- Buffer compositions:

Table 4: Buffer compositions with concentrations and pH

Solutions	NaCl	KCl	NMDG	$MgCl_2$	$CaCl_2$	Glucose	HEPES	EGTA	pH
ECS Ca^{2+} buffer	140 mM	5 mM	---	1 mM	1.8 mM	10 mM	15 mM	---	7.40 using NaOH
Intracellular solution (ICS)	8 mM	120 mM	---	1 mM	5.6 mM	---	10 mM	10 mM	7.20 using KOH
Extracellular solution (ECS)	---	5 mM	140 mM	3.3 mM	1 mM	5 mM	10 mM	---	7.40 using HCl

3.2 COMPOUND HANDLING

In this thesis, based on the computer-aided drug design (CADD), total 25 compounds were purchased from different suppliers and taken care of while testing them on the cells for their respective efficacies. The table 5 shows the details about the compounds purchased with their stock concentrations, molecular weights and the amount in which they were received. The compounds were purchased from two ready-to-use drug discovery platforms, which are Mcule ("Mcule") and Molport ("Molport-Compound Sourcing, Selling and Purchasing Platform,"). After receiving the compounds, as per the solubility information provided in their respective certificates of analysis (COA) the stock solutions were prepared in dimethyl sulfoxide (DMSO). The compounds were prepared in different stock solution concentrations from 10 to 50 mM. Then some stability studies were performed to decide upon the storage conditions for the compounds in DMSO as well as in the intracellular solution. The stability studies included the freeze thaw cycles, room temperature condition as well as keeping at 5-7°C in refrigerator.

And the results from these studies showed that the compounds were degrading when frozen or prepared and kept (at 5°C or RT) in intracellular solution a day before the experiment. As the compounds were crystalline in nature keeping them in freezer could recrystallize or precipitate them out hence the compounds were kept in a dry and well-ventilated place. Once a compound crystallizes out from solvent (DMSO), it will not easily re-dissolve and as freeze thaw cycles increases the probability of crystallization, the compounds were not frozen. Rather samples for test were freshly prepared just an hour prior to the experiments and were not used for more than 4 hours after preparation.

Table 5: Stock solution preparation for all of the compounds

Name	Mass (mg)	Molecular weight (g/mol)	Final stock solution concentration (mM)
Compounds selected from computer aided drug design using homology model structure			
Compound A01	5.2	406.43	10
Compound A02	5.1	336.31	10
Compound A03	5.1	323.35	10
Compound A04	5.1	412.47	10
Compound A05	5.1	354.31	10
Compound A06	5.1	408.43	10
Compound A07	5.1	477.44	10
Compound A08	5.3	341.27	10
Compound B01	5.2	288.26	10
Compound B02	5.2	422.43	10
Compound B03	5.1	350.33	10
Compound B04	5.1	318.35	10
Compounds selected from computer aided drug design using actual hTRPM2 cryo-EM structure			
Compound 01	5.0	367.41	50
Compound 02	5.0	401.46	50
Compound 03	5.0	372.38	50
Compound 04	5.0	369.37	50
Compound 05	3.0	464.53	50
Compound 06	5.0	381.38	50
Compound 07	5.0	392.38	50
Compound 08	5.0	454.50	30
Compound 09	5.0	363.45	50
Compound 10	5.0	464.53	10
Compound 11	3.0	392.44	50
Compound 12	3.0	424.42	50
Compound 13	3.0	383.46	10

Compounds structures:

Compounds selected from computer-aided drug design using homology model-

Compound A01

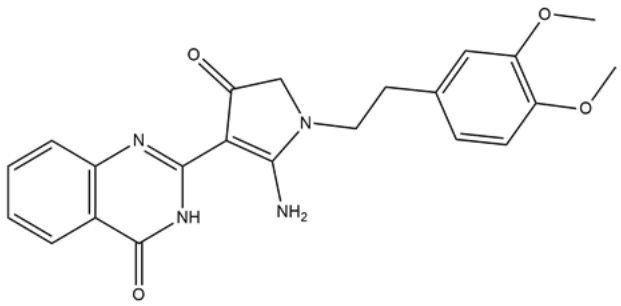

Compound A02

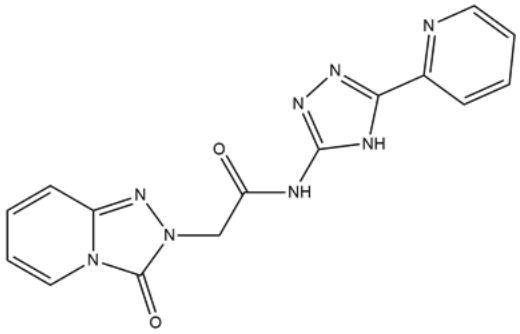

Compound A03

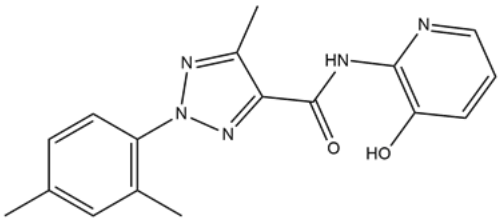

Compound A04

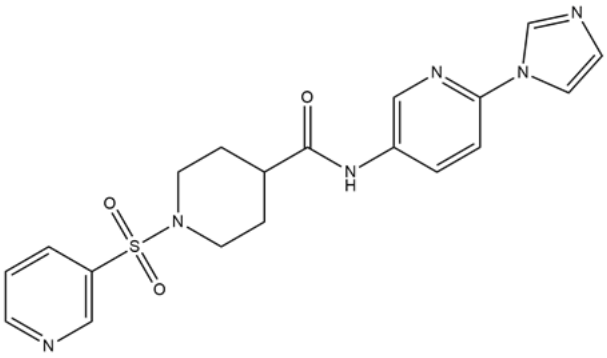

Compound A05

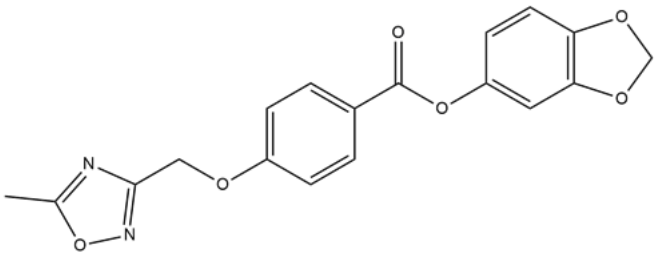

Compound A06

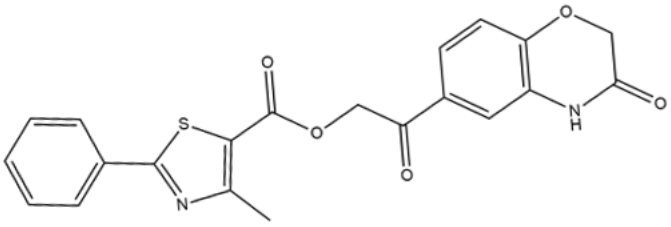

Compound A07

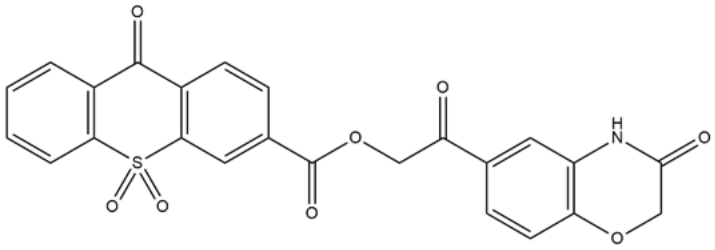

Compound A08

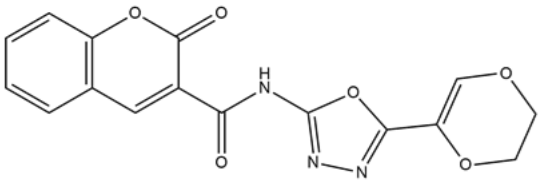

Compound B01

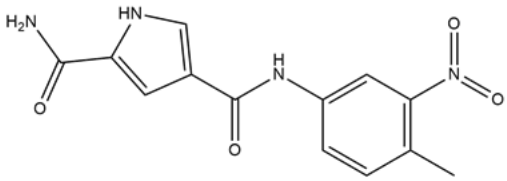

Compound B02

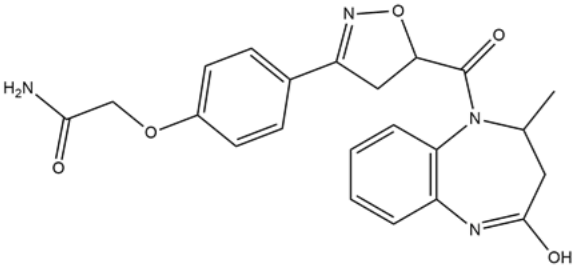

Compound B03

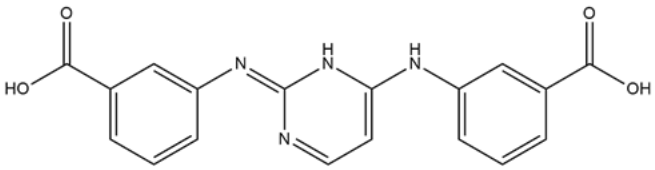

Compound B04

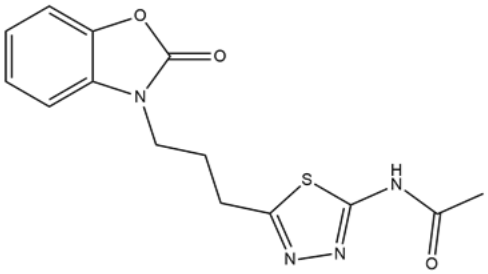

Figure 7: Structures of compounds selected from computer-aided drug design using homology model

Compounds selected from computer-aided drug design using cryo-EM structure of hTRPM2-

Compound 01

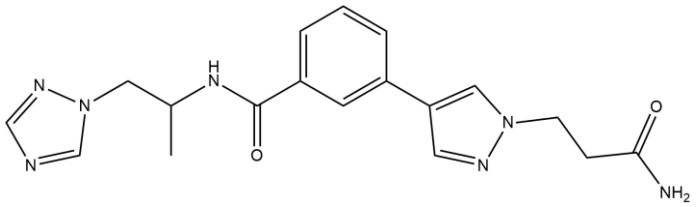

Compound 02

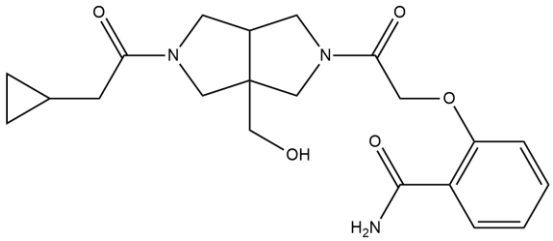

Compound 03

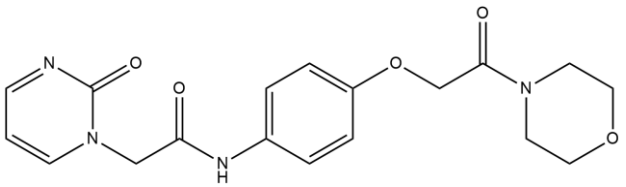

Compound 04

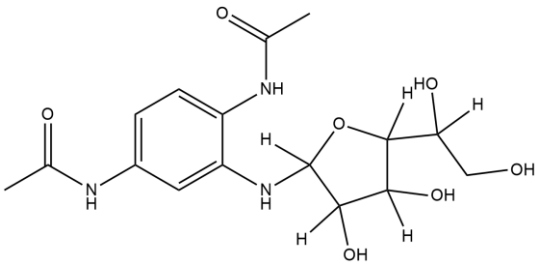

Compound 05

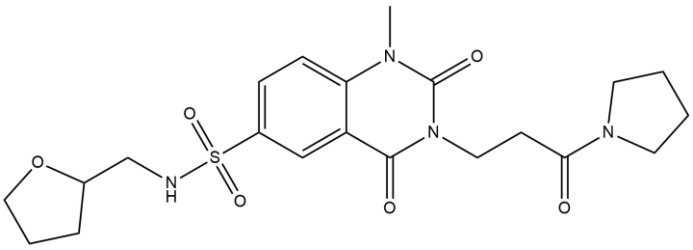

Compound 06

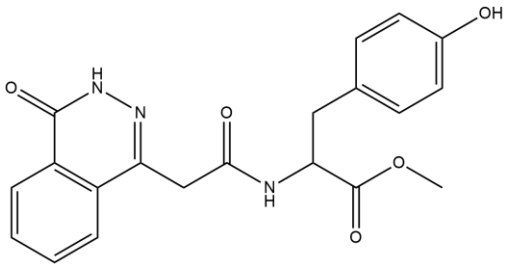

Compound 07

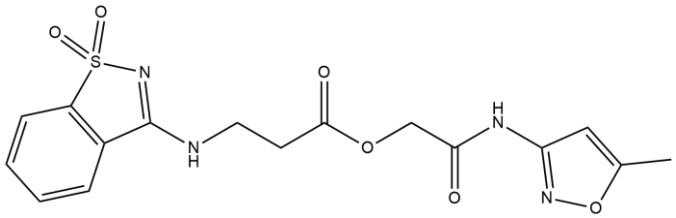

Compound 08

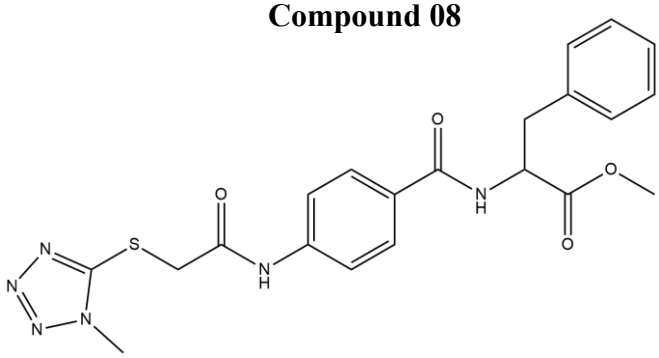

Compound 09

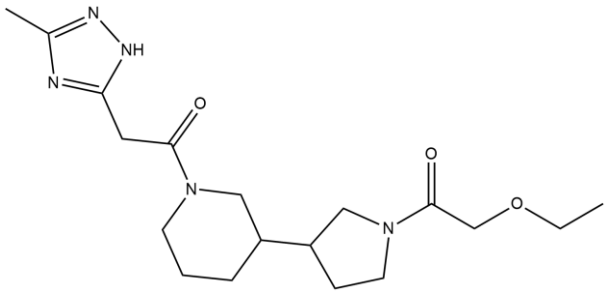

Compound 10

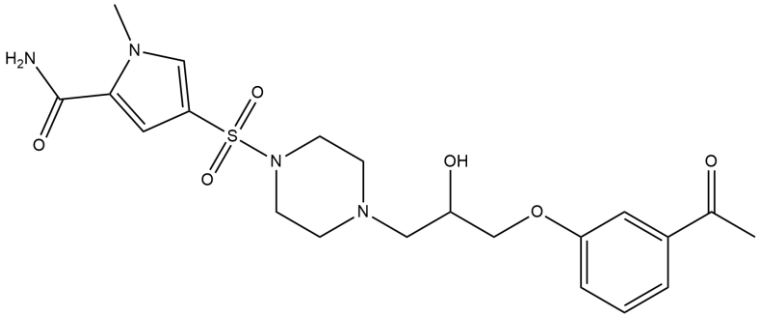

Compound 11

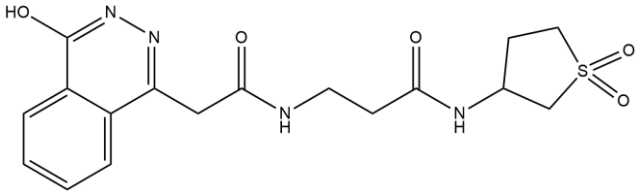

Compound 12

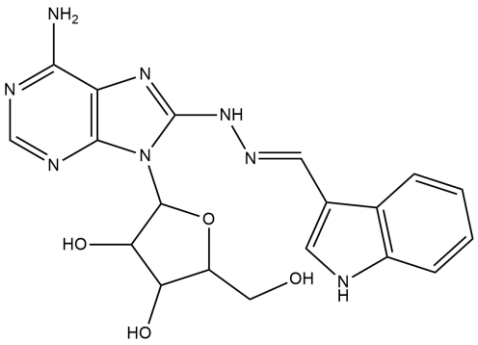

Compound 13

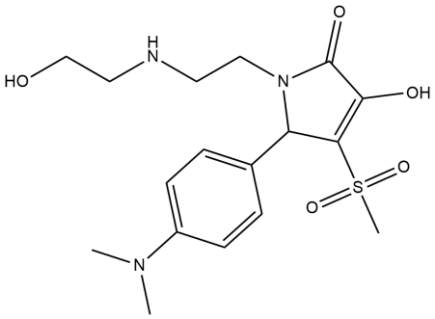

Figure 8: Structures of compounds selected from computer-aided drug design using cryo-EM structure of hTRPM2

3.3 *IN-SILICO*/COMPUTER-AIDED DRUG DESIGN OF TRPM2 INHIBITORS

3.3.1 Computer-aided drug design using a homology model of the NudT9H domain of human TRPM2 based on the x-ray crystal structure of NudT9

The first attempt of computer-aided drug design (CADD) for the development of TRPM2 inhibitors targeting NudT9-H domain was performed using an homology model of NudT9-H domain (Fliegert et al., 2017b) based on the x-ray crystal structure of NudT9 (Shen et al., 2003). The structure-based virtual screen workflow option available in Mcule was used to perform the *in-silico* screening for the hit/compound identification. The Mcule purchasable (in-stock) collection was used along with some basic physicochemical parameter filters. The basic property filters applied for selection were Molecular weight. - 150 to 450 Daltons, clogP-between- 0.4 to 5.6, Rotatable bonds- 10, chiral centers-3, H-bond donor-5, H-bond acceptor-8, PSA- 70 to 140, Molar refractivity- 160-480 so basically Lipinski's Rule of 5 violations and a minimum of eight heavy atoms and one ring, a maximum of three halogen atoms and components with 1 to 15 nitrogen or oxygen atoms. For the ligand preparation, the ligand library used was initially containing around 200,000 compounds. Then upon applying the diversity selection filter criteria with the similarity threshold of 0.85 the maximum number of compounds were 20,000. After this, the structure-based virtual screening was run and for docking the Autodock Vina option was used (Trott and Olson, 2010). For this docking, the NudT9-H homology model was used as a starting point. This NudT9-H homology model was built in the Sybyl software from Tripos. Due to its high sequence homology (50%) to the NudT9-H domain of TRPM2, the mitochondrial enzyme NudT9 crystal structure was used as a reference for building the homology model. Hence, for building this homology model (Fliegert et al., 2017b) the most of the sequence was adopted from the NudT9 crystal structure available (PBD: 1QVJ) (Shen et al., 2003). Then the option for docking (Vina) was selected in Mcule and for this the homology model crystal structure was uploaded to Mcule and the amino acids Y1349 (Tyrosine 1349) was placed as a centre for the docking process. The top-1000 compounds were retained and further evaluated in Schrödinger's Maestro ("Schrödinger maestro"). Figure 9 shows a detailed schematic representation of the approach to structure-based drug design and the docking process.

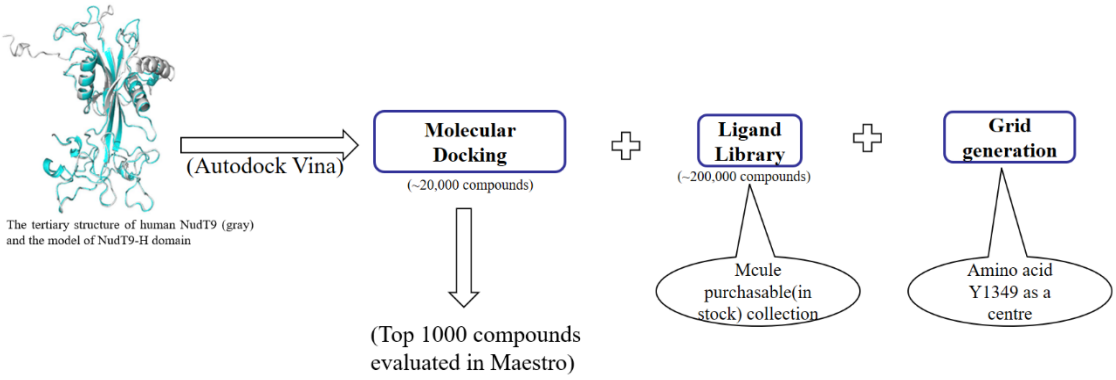

Figure 9: Schematic representation of the workflow for the structure-based drug design using homology model
Homology model crystal structure (1QVJ) was used as a starting point of the structure-based drug design approach. Then the homology model crystal structure was uploaded to Mcule in the docking (Vina) option for the further docking process and the Mcule ligand library was used for screening. Tyrosine 1349 (Y1349) was used as a docking centre. Based on the docking score, top 1000 compounds were selected and checked for their ligand conformation, binding pose and ligand-receptor interaction in Maestro.

3.3.2 Computer-aided drug design using cryo-EM structure of human TRPM2

As a second approach to computer-aided drug design, the cryo-EM structures of human TRPM2 published in 2019 were used for the structure-based drug design approach (Huang et al., 2019). Human TRPM2 structures derived from cryo-EM maps were downloaded from the protein data bank (PDB) 6PUO and 6PUS. Here two cryo-EM structures were considered, apo state and ADPR and calcium bound state. 6PUO corresponds to the protein in the Apo state and 6PUS is the ADPR and calcium-bound conformation. For computer aided drug design, x-ray crystal structures are usually preferred because of their higher resolution. However, no x-ray crystal structure of TRPM2 or partial structures of isolated nucleotide binding domains were available at that time. In comparison to x-ray structures, the cryo-EM structures offer only a relatively poor resolution of 3.3Å for 6PUO and 3.7Å for 6PUS. Therefore, for the refinement of the structures and to obtain improved receptor structures for docking, MD simulation was performed. In the case of 6PUO, a MD simulation was performed to refine the complete structure. On the other hand, to preserve the active site (NudT9-H domain) conformation upon ADPR binding for the docking virtual screening, 6PUS was only refined through energy minimization. Since in the cryo-EM TRPM2 structures some loops have not been resolved and were thus missing in the PDB-files, which were: from aa (G)6 to aa(K)55-1st loop, aa (H)582 to aa(G)613-2nd loop, aa(Q)981 to aa(A)1019-3rd loop and aa(P)1166 to aa(P)1234-4th loop. After filling in the missing loops, the system was simplified by removing the transmembrane region (TM) of TRPM2 (from pre S1 helix till after the S6 helix: aa733 to aa1099) and considering for the simulation the N- and C- terminus of each TRPM2 chain as separate proteins. Simultaneously, to simulate a region of the protein in a membrane-like environment and the remaining protein in water adds a large degree of complexity to the simulations that

was not needed since the binding pocket of the TRMP2 channel is located in the cytosol. Thus, for a short refinement simulation it was decided to work solely with the cytosolic region of TRPM2. For this purpose, MODELLER was used ("MODELLER," Webb and Sali, 2016). This is a stand-alone software mostly used for homology modelling of protein three-dimensional structures. After filling in the missing loops and removing the transmembrane region (TM) the input structure was ready. The complete MD simulation was performed on GROMACS, which is an open source software (www.gromacs.org). It is a MD package designed for simulations of proteins, lipids and nucleic acids and it works on a unix like operating systems e.g. Linux. GROMACS needs several steps to set up an input file for the simulation. The steps can be seen in following flowchart.("Exercise: Atomistic Simulation of Biomolecular function, Part 1," 2022).

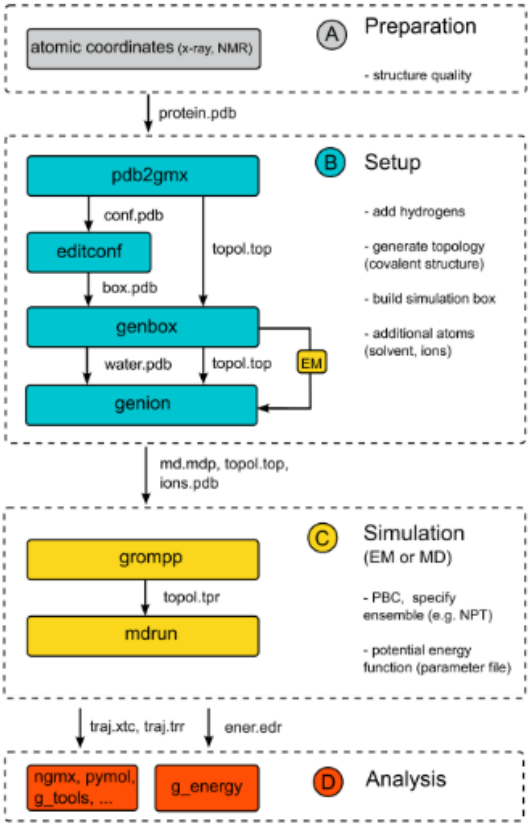

Figure 10: Standard protocol for the MD simulations in GROMACS

The figure shows the standard protocol with individual steps followed during the MD simulations on a protein. First is the preparation of the structure which involves getting the initial structure of the protein from Protein Data Bank (PDB). Then the setup happens in GROMACS where the structure is prepared for the simulation by adding hydrogens, solvent and ions, generating the required topology file and building the simulation box. Then comes the starting of the energy minimization run followed by the MD simulation run. After the completion of the MD simulation run the results are analysed. This figure is adopted from ("Exercise: Atomistic Simulation of Biomolecular function, Part 1," 2022).

As soon as the input structures were ready, they needed to be prepared for simulation. For this, a topology file was generated. While doing this the program asked for a force field and the broadly applicable and extensively tested in proteins OPLS-AA force field (Jorgensen and Tirado-Rives., 1988) was selected. Now the simulation is *in vacuo* so water was added to it.

Before adding solvent, the size and shape of the simulation box had to be determined. Here a rhombic dodecahedron box was used. The shape of the solvent box has a huge impact on the computational work required for the simulation. The simplest box is the cubic box, which results in large numbers of solvent molecules interacting only with each other (not with the protein). This demands an unnecessary extra computational power and therefore other box shapes that better fit the protein resulting in less solvent molecules were preferred, in this case such as the rhombic dodecahedron. Then water was added in the box to solvate the protein. The widely used 3-point TIP3P water model (Jorgensen et al., 1983) was used in this step. After adding solvent and ions to neutralize the negative charge of the protein, it is a solvated electroneutral system. If the simulation started now the added hydrogens and broken hydrogen bond network in water could generate large forces and lead to structure distortion so to remove any steric clashes or weird geometry a short energy minimization (EM) was ran. Energy minimization helped to relax the protein structure.

Now it is a well-defined system in terms of solvent, orientation, and geometry so an equilibration run was performed. In this equilibration run, all the heavy protein atoms (non H-atoms) are restrained to their starting positions while the water is relaxing around the structure. It is similar to energy minimization but for the MD simulations, the temperature and pressure with the v- rescale and Berendsen weak coupling algorithms were also controlled. This algorithm by rescaling the particle velocities helps in achieving a controlled temperature for simulations (Berendsen et al., 1984). Then finally, the production simulation run was started. Here 10 ns production MD simulation run was performed. This could determine how long simulation would run, in this case it took 7 days. Figure 11 shows a schematic representation of the procedure followed.

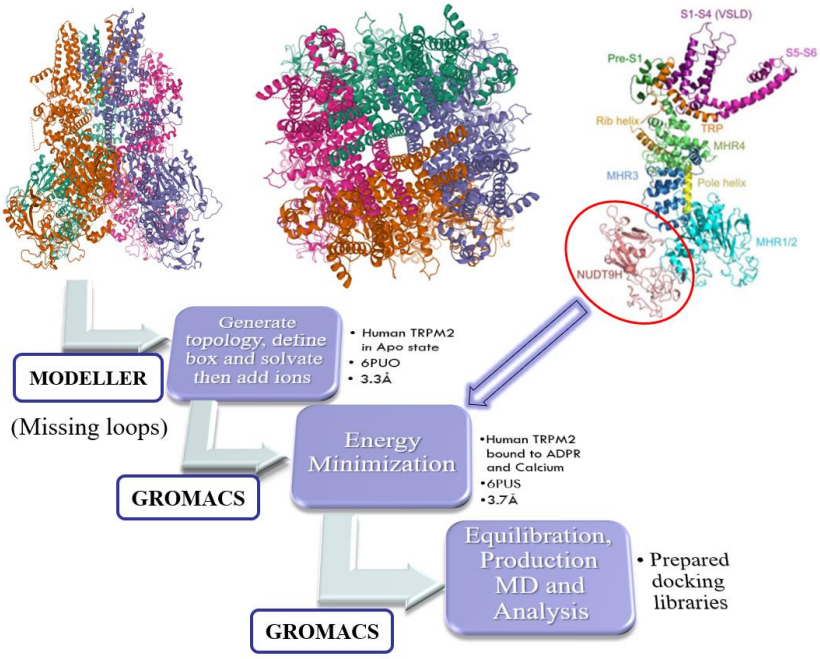

Figure 11: Steps taken for Molecular dynamics simulation

This figure shows the various steps taken during the molecular dynamics simulations. On top starting from extreme *right* it is the vertical representation of the TRPM2 cryo-EM structure (PDB: 6PUO) and in middle the top view of the same structure. To the extreme *left* there is the monomeric unit with the NudT9-H domain encircled red. After taking the 6PUO structure from the RCSB PDB, the missing loops were filled in using MODELLER. Then the input 6PUO structure was put into GROMACS where the topology files generated, the simulation box was added and system was solvated. After this, the energy minimization run was started for both the 6PUO structure as well for the NudT9-H domain from 6PUS structure. Then for both the structures equilibration and production MD, simulation run was started and then analyzed in VMD while preparing the docking libraries.

In order to extract the most representative binding site conformation for the docking virtual screening, the trajectories of the heavy protein atoms were clustered. The clustering was performed by grouping the simulation frames in terms of the RMSD of atomic positions. After the simulation, the analysis was done using the software Visual Molecular Dynamics (VMD) (https://www.ks.uiuc.edu/Research/vmd/), VMD can be used to view and analyze the results of MD simulations. After this, the molecular docking was performed on the two selected grids from this molecular dynamics simulation.

3.4 CELL CULTURE

3.4.1 Human embryonic kidney cells (HEK293)

Clonal HEK293 cell lines overexpressing human TRPM2 (HEK293 TRPM2 #23 and HEK293 TRPM2 #24) were used in this study for the Fura-2 calcium measurement (HEK293 TRPM2 #23) and the patch clamp (HEK293 TRPM2 #24) experiments. Generation of these HEK293 cells overexpressing human TRPM2 is described in (Fliegert et al., 2007). The Dulbecco's Modified Eagle Medium (DMEM) containing GlutaMAX™-I and 4.5g/L D-Glucose supplemented with 10% fetal bovine serum (FBS) and 1% penicillin/streptomycin was used for the culture of these cells. The detailed composition of the medium is mentioned in the following table 7. Cells were cultured in a cell culture flasks with a growth area of 25cm^2 (Sarstedt) for adherent cells at 37°C in a humidified atmosphere (incubator) holding 5% CO_2. For passage, cells were first washed with 3 mL of Dulbecco's phosphate buffered saline (DPBS) without Ca^{2+} and Mg^{2+}. Then 2 mL of trypsin was added onto the cells to detach them from culture flasks. Then to stop this trypsin digest, after approximately 2 minutes 8 mL of the pre-warmed culture medium was added to the cells. And in this 8 mL medium the detached cells were re-suspended gently. Finally, for a 1 to 10 dilution 1 mL of this cell suspension was transferred to a new flask containing 7 mL of pre-warmed fresh medium and for a 1 to 20 dilution 0.5- mL of cell suspension to a new flask containing 7.5 mL of pre-warmed fresh medium. Then to this 160 µL of the antibiotic G418 was added to the medium. The concentration of G418 solution was 200 µg/mL. Then cells were transferred to the incubator. Then again upon reaching 80% confluency, these cells were passaged which is every 3 days at a dilution of 1 to 10 or sometimes 1 to 20.

3.4.2 Pancreatic cancer cells

The pancreatic cell lines were received from the Institute of Anatomy, UKE (PANC-1, SU 86.86, BxPC-3 and T3M4) and the University Hospital Bonn (UKB) (MIA PaCa-2). The information about the origin of these cell lines is given in the following table 6.

Table 6: Origin information and details of the pancreatic cell lines

Cell line	Patient (M/F)	Derived from	Disease	Reference
MIA PaCa-2	Male	Pancreas	PDAC	(Barton et al., 1991)
PANC-1	Male	Pancreatic duct	PDAC	(Lieber et al., 1975)

T3M4	Male	Metastatic site lymph node	PDAC	(Okabe et al., 1983)
SU 86.86	Female	Metastatic site liver	PDAC	(Drucker et al., 1988)
Bx-PC-3	Female	Pancreas	PDAC	(Tan et al., 1986)

For the maintenance of all these pancreatic cancer cell lines except MIA PaCa-2, Roswell Park Memorial Institute (RPMI)-1640 media containing GlutaMAX™-I and 25 mM HEPES supplemented with 10% fetal bovine serum (FBS) and 1% penicillin/streptomycin was used for all the cells. In case of MIA PaCa-2, Dulbecco's Modified Eagle Medium (DMEM) prepared as mentioned in section 3.3.1 was used. The details of the culture media used are enlisted in table 7. The different pancreatic cell lines were also cultivated in T25 cell culture flasks for adherent cells. All cell lines were passaged differently on different days upon reaching approximately 70% confluency. Considering the proliferation rate, T3M4 and SU 86.86 cells grew at the highest rate and needed subculturing every 2 days, while Bx PC-3 cells were the slowest so was passaged every 4 days and the MIA PaCa-2 and PANC-1 cells were passaged every 2-3 days.

Table 7: Detailed composition of culture media

Cell Type	Culture Media
HEK293 TRPM2 #24 and HEK293 TRPM2 #23	DMEM containing GlutaMAX™ and D-glucose supplemented with 10% (v/v) FBS, 100 U/mL penicillin and 100 µg/mL streptomycin
MIA PaCa-2	DMEM containing GlutaMAX™ and D-glucose supplemented with 10% (v/v) FBS, 100 U/mL penicillin and 100 µg/mL streptomycin
T3M4	RPMI-1640 containing GlutaMAX™ and 25 mM HEPES supplemented with 10% (v/v) FBS, 100 U/mL penicillin and 100 µg/mL streptomycin
SU 86.86	RPMI-1640 containing GlutaMAX™ and 25 mM HEPES supplemented with 10% (v/v) FBS, 100 U/mL penicillin and 100 µg/mL streptomycin
BxPC-3	RPMI-1640 containing GlutaMAX™ and 25 mM HEPES supplemented with 10% (v/v) FBS, 100 U/mL penicillin and 100 µg/mL streptomycin
PANC-1	RPMI-1640 containing GlutaMAX™ and 25 mM HEPES supplemented with 10% (v/v) FBS, 100 U/mL penicillin and 100 µg/mL streptomycin

3.5 RP-HPLC

The potential TRPM2 inhibitors selected from both the approaches of computer-aided drug design were purchased from commercial vendors (Mcule and Molport). As a first check of the purity and integrity, these compounds were analysed by reverse phase HPLC (RP-HPLC) on a 1200 series system (Agilent Technologies). The chromatographic parameters are described in the table 8. The compounds were run on a 250 mm x 10 mm C8, 5-µm column (Phenomenex Luna) equipped with a 10 mm x 10 mm guard cartridge containing a C8 ODS filter element (Phenomenex) at a column temperature of 20°C and with a flow rate of 1.0 mL/min. The mobile phase consisted of buffer A: 20 mM KH_2PO_4 pH 6.0 and buffer B: 90% methanol in buffer A and a gradient elution was used. The gradient elution conditions were as shown in the following table 9. All compounds contained aromatic ring systems and could thus be detected by the UV/Vis detector due to their absorbance at 260 nm. Peaks were integrated with ChemStation Software (Rev. C.01.05; Agilent Technologies).

Table 8: Summarized Chromatographic parameters

Chromatographic Parameters	
HPLC system	Agilent
Column	C8 Luna Phenomenex
Method of elution	Gradient
Detector	UV-Vis detector
Mobile phase	Methanol phosphate buffer pH 6.0 (80:20 v/v)
System temperature	20°C
Auto sampler temperature	8°C
Flow rate	1.0 mL/min
Run time	40 minutes

Table 9: Gradient elution program for HPLC analysis

Time (min)	Methanol %	Buffer %	Flow mL/min	Pressure bar
0	80	20	1	270
3	80	20	1	270
20	0	100	1	270
25	0	100	1	270
30	80	20	1	270
40	80	20	1	270

3.6 FURA-2 CALCIUM MEASUREMENT

3.6.1 Principle

In this study Fura-2 calcium measurement experiments were performed to check the effect of compounds on the TRPM2 channel activation triggered by oxidative stress caused by reactive oxygen species particularly hydrogen peroxide (H_2O_2). Please refer to the section 1.2.3.3 for the mechanism behind activation of TRPM2 channel by hydrogen peroxide (H_2O_2). These Fura-2 calcium measurement experiments were performed using a Fura-2AM (Fura-2-acetoxymethyl ester) dye, which is a membrane permeable derivative of Fura-2. Upon incubating the cells for around 30 minutes in a water bath with Fura-2AM, it penetrates the cell membrane and after entering into the cell, it is converted into the free Fura-2. This process of conversion of Fura-2AM into Fura-2, removal of this acetoxymethyl group is carried out by esterases present in the cytosol. This free Fura-2 then forms a complex with the free Ca^{2+} resulting in a change of the fluorescence (Grynkiewicz et al., 1985). The diagrammatic representation for this can be seen in the following figure 12. During experiments, 340 nm and 380 nm excitation wavelengths were set into the programme, and the fluorescent emission intensities at 510 nm were measured. Then from this, the free cytosolic calcium concentration ($[Ca^{2+}]_i$) was estimated, and the increase in $[Ca^{2+}]_i$ was calculated as a measure of the channel activation.

This cellular assay helped in determining whether the compounds are sufficiently membrane permeant to inhibit TRPM2 in intact cells.

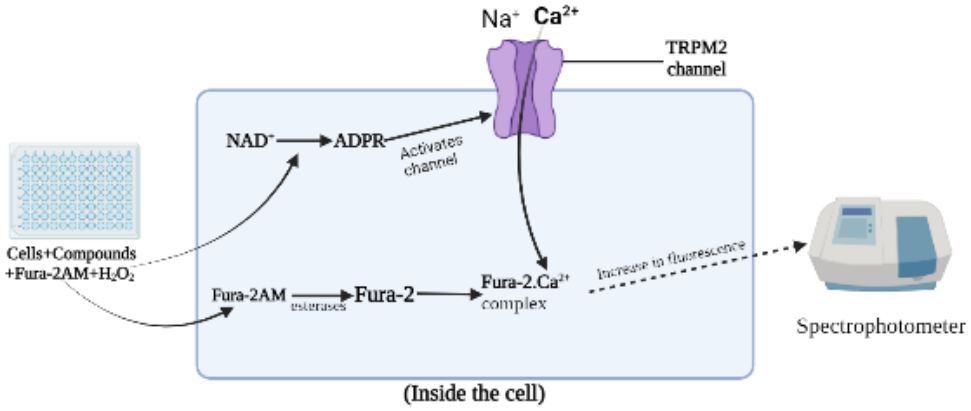

Figure 12 Principle behind Fura-2 calcium measurement

The figure 12 is the diagrammatic representation of principle behind Fura-2 calcium measurement experiments. From the right it could be seen that addition of hydrogen peroxide (H_2O_2) leads to indirect production of ADPR, which binds to the NudT9-H domain of TRPM2 and activates the channel. This activation of the channel causes influx of calcium into the cell. Fura-2 AM on entering the cell gets converted to Fura-2 which then forms a complex with the calcium present and this complex gives rise to the increase in fluorescence intensity demonstrating activation of channel. This figure is created in BioRender.com.

3.6.2 Procedure

For performing these Fura-2 calcium measurement experiments, a microplate reader (Tecan INFINITE M FLEX, Germany) was used. These experiments were performed using HEK293 TRPM2 #23 cells expressing human TRPM2. Cells were first detached using trypsin, re-suspended into pre-warmed medium, centrifuged, and then re-suspended in extracellular solution (ECS) calcium buffer. The composition of the extracellular (ECS) calcium buffer is mentioned in section 3.1 in the table 4. Then incubated with final concentration of 4 µM of Fura-2AM for about 30 minutes in a water bath at 37°C. Then the cells were washed with buffer twice to remove excess of Fura-2AM entrapped into the cells and re-suspended in ECS buffer. After this, they were dispensed in a black 96 well plate in which already different concentrations of potential TRPM2 inhibitors were added. Then this 96 well plate was kept into the microplate reader at room temperature for 20 minutes so that the cells are incubated with the potential TRPM2 inhibitors. Then the run was started and TRPM2-dependent calcium signals were stimulated by addition of a final concentration of 1 mM hydrogen peroxide (H_2O_2) after three minutes. The fluorescence of the indicator dye at 510 nm after excitation of 340 nm and 380 nm was measured every 15 seconds. The ratio of fluorescence intensities after excitation at 340 nm and 380 nm was calculated as a measure of the Ca^{2+} signal. In case of the first round of compounds, the ratio was used to construct the concertation-response curve. In case of the second round of compounds two additional conditions (Triton X-100 for R_{max} and Triton X-100/EGTA for R_{min}) were included for calibration purposes and the Ca^{2+} concentration was calculated from the ratio using following equation. The change in the Ca^{2+}-concentration was then used for construction of the concentration-response curves.

The equation used was:

$$[Ca^{2+}]_i = = K_d * \frac{R-Rmin}{Rmax-R} * \frac{F(380)max}{F(380)min}$$

$[Ca^{2+}]_i$ is the free cytosolic Ca^{2+} concentration. K_d refers to the dissociation constant which is 224 nM. R is the ratio of fluorescence at an excitation of 340 nm F (340) nm divided by fluorescence at an excitation of 380 nm F (380). $R = \frac{F340}{F380}$. R_{min} and R_{max} are the minimal and maximal ratio, respectively, which were obtained using 1 % (w/v) Triton X-100 and EGTA/Tris.

For preparation of samples, the initial stock solutions were prepared in DMSO. The final dilution step was done in ECS-buffer to maintain a DMSO concentration 0.1% over the whole range of concentrations of the test compound. This is required to avoid any artifacts due to effects of higher DMSO concentrations on the cells. For negative control, only ECS buffer with

0.1 % of DMSO was added in the wells and for positive control 0.1% DMSO + at 3 minutes final concentration of 1 mM hydrogen peroxide (H_2O_2) was added.

3.7 PATCH CLAMP RECORDINGS

3.7.1 Principle

After checking the impact of potential TRPM2 inhibitors on TRPM2 activation by H_2O_2 on intact cells in Fura-2 calcium measurements, their impact directly onto the target was assessed with the help of patch clamp recordings. This technique is used for the electrophysiological measurements of currents through ion channels in the cell membranes. In this technique a glass pipette filled with test sample in intracellular solution is tightly attached onto the cell membrane patch making a 'gigaseal' and then isolating the membrane patch electrically, allowing the continuous flow of current in the form of ions from the electrode in the pipette to the bath electrode. And as the ions cannot pass the lipid bilayer of the cell, the current only flows through the ion channels in the membrane (which is then measured). The diagrammatic representation of this is shown in the figure 13. The composition of the intracellular solution is mentioned in section 3.1 in the table 4. An electrode is present inside the glass pipette, which records the currents flowing through the channel in this patch as this electrode is directly connected to the amplifier. The electrode does not only record the current but its purpose is also to control the application of the potential. In this thesis, for the patch clamp experiments the whole-cell (WC) configuration was used. In the configuration, the voltage was held constant allowing to monitor the ADPR-induced TRPM2 currents.

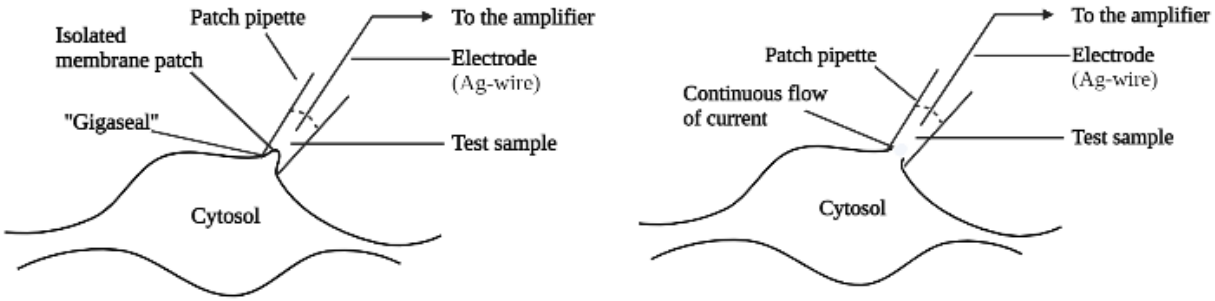

Figure 13: Principle of Patch clamp technique

This diagrammatic representation shows the principle behind patch clamp technique. A patch pipette containing the test sample in intracellular solution is tightly attached to the membrane called 'Gigaseal', shown in the left side figure. Then this patch is isolated by applying a suction pulse and allowing the continuous flow of test solution into the cell cytosol, creating a whole-cell mode configuration. Then the flow of current is measured by the electrode present in the pipette solution and connected to the amplifier. This figure is created in BioRender.com.

3.7.2 Procedure

For performing these patch clamp experiments a manual patch clamp set up was used and the electrophysiological signals were recorded in a whole-cell configuration mode. The experiments were performed using HEK293 TRPM2 #24 cells expressing human TRPM2 and cells were plated on 35 mm dishes a day before the start of these experiments. For filling in the test sample containing potential TRPM2 inhibitors patch pipettes having 1.5-mm-diameter, made from borosilicate glass capillaries were used (GB150T-8P Science Products GmbH, Hofheim). On the experiment day, these patch pipettes were pulled and fire polished using a pipette puller (Flaming/Brown micropipette puller P-97, Sutter instruments Co, Novato, CA USA) to a desired resistance which for these experiments was between 1.5-3MΩ. Then the dishes were placed on the stage of an inverted microscope (Axiovert 100, Carl Zeiss Microscopy GmbH, Jena, Germany) and the second electrode was put into the extracellular solution (ECS). The composition of the extracellular solution is mentioned in section 3.1 in the table 4. After this, every day prior to the starting of the experiment the intracellular electrode (made up of Ag-wire) was gently cleaned with the sandpaper and coated with melted AgCl. Then this intracellular electrode was connected to a HEKA EPC-10 amplifier (HEKA Elektronik Dr. Schulze GmbH, Lambrecht, Germany) with the help of a pipette holder. The pipette holder was connected via tubing and a three-way valve to a 1 mL syringe attached to ease in blowing air into the tube and ultimately into the pipette. Through this syringe, a positive pressure was applied by blowing air into it by mouth before dipping of the pipette tip into the dish containing extracellular solution (ECS). The pipettes were filled with only intracellular solution (for negative control sample) or the intracellular solution containing either 100 µM ADPR (for positive control sample) or 100 µM ADPR and 10 µM or 100 µM of one of the potential TRPM2 inhibitors for testing them. Each solution contained 0.2% DMSO. The composition of the intracellular solution is mentioned in section 3.1 in the table 4. TRPM2 currents were recorded in voltage-clamp mode and the EPC-10 amplifier was combined with the Patch Master software (2.40, HEKA Electronic, Germany) for the experimental recording and data acquisition.

To get into the whole-cell configuration mode the positive pressure was removed (by opening the three-way valve) which led to formation of a gigaseal. Then after applying a small suction pulse and breaking-in into the cell this whole-cell mode was achieved leading to the continuous flow of current through the intracellular solution into the cell. After isolating the membrane patch, a holding potential of -50 mV was maintained and every 5 seconds the voltage ramps from -85 mV to +20 mV in 140 ms were applied. There was no additional current observed with the pipette filled with buffer but inclusion of ADPR in the pipette solution resulted in

development of a current with a characteristic curve, which is a typical ADPR-induced TRPM2 current. This maximum current readout at +15 mV was used as a measure of TRPM2 activation. Since both ADPR and the TRPM2 inhibitors were able to enter the cell in a whole-cell mode, this allowed observation of the effect of the compounds directly onto the target.

3.8 RT-PCR

3.8.1 Principle

There are multiple techniques used for the analysis of gene expression but here in this thesis first reverse transcription polymerase chain reaction (RT-PCR) technique was performed to check the expression of human TRPM2 (hTRPM2) in the different pancreatic cancer cell lines available in the lab. PCR is used for DNA amplification by generating million copies out of a particular DNA sequence. Which then used in the detection of particular gene expression *in vitro* by RT-PCR. It uses RNA as a template. However, as in normal PCR reaction DNA polymerase makes copies from a DNA template as it can only copy DNA not RNA, so first this RNA is converted into the DNA by the enzyme reverse transcriptase. Since reverse transcriptase used this RNA as a template, the sequence of that new DNA molecule is complementary to the RNA hence called cDNA. Then by DNA polymerase, this single stranded cDNA is converted into the double-stranded DNA and is used as a template. Since the starting point was copying RNA into DNA using reverse transcription, it is called 'reverse transcription PCR'. This complete reaction can be performed in two ways as a one-step or a two-step RT-PCR. In this study, one-step RT PCR was used in which the cDNA production and PCR reaction was performed in a single reaction using a common reaction buffer.

3.8.2 Procedure

The RNA was extracted from the T3M4, PANC-1, MIA PaCa-2, BxPC-3, SU 86.86 and HEK293 overexpressing TRPM2 cells according to the protocol provided in the RNeasy RNA extraction kit. The QIAshredder spin column was used for shredding of DNA. The QIAGEN RNase-Free DNase kit was used for on-column digestion of residual DNA during RNA purification. The primers used for this RT-PCR were 5'-CGGAGGAGTATGAGCACAGAG-3' and 5'-AAGTCCACCATGAGCACGTAG-3'.

For PCR, briefly, first, the concentrations of the RNA preparations were measured by determining the OD using photometry at 260 nm and 280 nm (two independent RNA preparations were used for this experiment). Then the RNA templates were diluted to 500 ng

in a 5 µl volume of master reaction mix, the composition is mentioned in the table 10 below. The Hot Star *Taq* polymerase included in the one-step PCR-Kit requires a heat activation step of 15 min at 95°C, which also inactivates the reverse transcriptase enzyme. The Mastercycler (Eppendorf, KME 2021) was pre-heated to 50°C before placing samples in it. The amplification protocol for PCR was set as follows: 95°C for 15 minutes (hot start of *Taq* polymerase), followed by 39 cycles of amplification steps (94°C for 30 seconds, 55°C for 30 seconds, 72°C for 60 seconds), and a final extension at 72°C for 10 minutes. The PCR products were analyzed on an agarose gel (2%) and visualized under UV light after staining with Roti®-Safe GelStain Red dye, 2.5 µL per 50 mL gel (Carl Roth, Karlsruhe, Germany)

Table 10: Composition of Master-mix for one-step RT-PCR

Component for master reaction mix	Final concentration
QIAGEN One step-RT-PCR buffer, 5X	1X,2.5 mM Mg^{2+}
dNTP mix(10 mM each)	400 µM of each dNTP
Primer A	0.6 µM
Primer B	0.6 µM
QIAGEN One step-RT-PCR Enzyme mix	2 µl
RNase-free water	To make up the required volume

Agarose gel electrophoresis:

For separation of the DNA fragments in this study, Agarose Gel Electrophoresis was used. For this TAE buffer of the following composition was prepared , TAE Buffer: 40 mM Tris base, 1.14% v/v glacial acetic acid, 0.1 mM ethylenediaminetetraacetic acid (EDTA), pH 8.0, and then the Agarose gel: 2% w/v electrophoresis grade Agarose was prepared in this TAE buffer. The mixture was heated in a microwave until the agarose was completely dissolved and then this mixture was allowed to cool to ~60°C. Then 0.5 µg/mL of the Roti® GelStain Red dye was added to this at warm temperature, gel mixture before casting so as to visualize the DNA fragments in the gel. Then this gel was poured into the cast stand with a gel comb and kept at room temperature until the gel is solidified. Prior to this, the DNA samples were diluted to the desired concentration using Milli-Q water and commercial 6X loading buffer. The solidified pre-cast agarose gel was placed in an electrophoresis apparatus, which was then filled with the TAE buffer. Then the DNA samples were loaded into the gel pockets alongside a size marker for comparison and this DNA samples were separated by size by gel electrophoresis (Casting system compact S, Bimetra, Germany). Then Electrophoresis was performed by applying a constant voltage of 120V for 30 minutes or until adequately resolved using horizontal electrophoresis system using power source (Bio-Rad Laboratories Inc., Hercules California,

USA). Finally, the gel was visualized and documented using Gel Doc trans-illuminator 2000 (BioRad). (Bio-Rad, Hercules California, USA).

3.9 RT-qPCR

3.9.1 Principle

Quantitative reverse transcription PCR (RT-qPCR) is the real-time polymerase chain reaction used to amplify and concurrently quantify a targeted DNA molecule and thereby the mRNA transcribed from the gene (in this case hTRPM2). In this reaction to determine the mRNA, a RT step is required. This follows the same principle of PCR as described above, only difference is the amplified DNA is detected and simultaneously quantified in real time. There are two variants of this technique: 1. SYBR Green and 2. TaqMan Probe. In this study TaqMan assay (TaqMan Universal Master Mix II, no UNG, OCI Thermo Fisher) was used for this RT-qPCR as it is considered a gold standard.

3.9.2 Procedure

RNA isolation for all the six cell lines (T3M4, PANC-1, MIA PaCa-2, BxPC-3, SU 86.86 and HEK293 overexpressing TRPM2 cells) was done by first detaching the cells using TRIzol and then this suspension of cells with TRIzol was mixed with chloroform in 1:5 ratio then this mixture was centrifuged at 13,000 RPM for 15 minutes at 4°C. Then the supernatant was discarded and to the pellet 70 % ethanol was added and stored at –20°C. For reverse transcription, High capacity cDNA reverse transcription kit with RNase inhibitor (OCI Thermo Fisher) was used. To synthesize single stranded cDNA from total RNA, first the 2X reverse transcription mix was prepared as shown the following table 11.

Table 11: Composition of 2X reverse transcription mix

Component	Volume
10X RT buffer	2.0 µL
25X dNTP mix	0.8 µL
10X RT random primers	2.0 µL
MultiScribe™ Reverse Transcriptase	1.0 µL
RNase Inhibitor	1.0 µL
Nuclease-free water	3.2 µL

After mixing these all ingredients together around a 10 µL of RT master mix is ready. This all RT mix preparation was done on ice. Then cDNA RT reaction was prepared by pipetting first

10 µL of 2X RT master mix into each well of 96-well reaction plate and to this 10 µL of RNA sample was added. Gently this plate was centrifuged to avoid any air bubble plus for proper mixing. Until the thermocycler was ready for loading this plate it was placed on ice. Then the thermocycler conditions for reverse transcription were set as described in the table 12.

Table 12: Thermocycler conditions for reverse transcription

Parameter	Step 1	Step 2	Step 3	Step 4
Temperature (°C)	25	37	85	4
Time	10 minutes	120 minutes	5 minutes	∞

Then after setting the reaction volume to 20 µL, the reactions were loaded into the thermal cycler and the reverse transcription run was started. Then the total yield of the cDNA from the reverse transcription was determined using quantitative PCR. TaqMan® Gene Expression Assays were used to evaluate the yield of cDNA conversion. And the TRPM2 gene was quantified in five of the pancreatic cancer cell lines. This TaqMan® Gene Expression Assay kits were purchased from ThermoFisher Scientific, Germany.

For this RT-qPCR experiment, a housekeeping gene was used as a reference gene and RT-qPCR was performed for that as well. Then the data for hTRPM2 gene was normalized to the housekeeping gene. Housekeeping gene used for this gene expression assay was the hypoxanthine phosporibosyltransferase 1 (HPRT1) gene. Moreover, both the TRPM2 gene and the HPRT1 gene were selected as FAM-MGB.

3.10 CANCER CELL PROLIFERATION

3.10.1 Principle

Uncontrolled proliferation of cells is one of the hallmarks of cancer and it has been shown that TRPM2 plays an essential role in cancer cell proliferation (Zeng et al., 2010) (see section. 1.2.4). To assess the impact of the selected TRPM2 inhibitors onto the pancreatic cancer cells, cancer cell proliferation assays were performed using IncuCyte® Zoom Live Cell Analysis technique. There are different methods used to assess the cancer cell proliferation to name a few: Cell counting using Trypan blue, Colorimetric tests (MTT, MTS, XTT and crystal violet), Fluorometric tests (Almar blue and propidium iodide) and Luminometric tests (ATP measurement and real-time assay). However, in this study IncyCyte technique was used, as it is a non-invasive kinetic measurement of cell growth. This cell growth measurement is based on the cell confluence. The cell confluence was scanned and captured every 2 hours until the cells reach the 100% confluency. Moreover, measuring the cell confluence to determine cell

growth is considered a valid approach because for the analysis the values from the middle point from the exponential growth curve are being considered. Hence, this technique gives an insight into real-time analysis of the cells confluence. In addition to this, measurement of proliferation rate by this technique also tells about the cell morphology as we could see the cells during the analysis, which facilitates understanding of the systematic differences between the different treatments and conditions (Artymovich et al).

3.10.2 Procedure

Proliferation assays were run in 96- well microplates. Pancreatic cancer cell line, MIA PaCa-2 was used for these experiments and treated as described in section 3.4.2. For one set of experiments, TRPM2 overexpressing HEK293 cells were also used and were treated as mentioned in section 3.4.1. Cells were seeded in technical replicates in a density of 1500 cells/well (MIA PaCa-2 cells) and 2000 cells/well (TRPM2 overexpressing HEK293 cells) into a 96 well flat bottom cell culture plate (Thermo Scientific Nunclon^{TM} Delta Surface, Denmark). Then the cells were kept in an incubator at 37°C, 5% CO_2 and were allowed to settle down overnight. The next day, different concentrations of the top six selected TRPM2 inhibitors were prepared in pre-warmed culture medium (used as solvent). Different concentrations (50 μM for HEK293 cells and 100 μM for MIA PaCa-2 cells), in four technical replicates were prepared for these six selected TRPM2 inhibitors. Then these freshly prepared different concentrations of TRPM2 inhibitors and a positive control containing only DMSO (0.4%) in the solvent (culture media) were added into the wells. Then immediately the plate was placed into the IncuCyte® Zoom Live Cell Analysis System (Essen Bioscience, Ann Arbor, MI, USA). After placing, the plate into the IncuCyte® the plate map was prepared and loaded into the software with the identification details like cell type, cell count, passage number and different conditions used. In addition, every time the confluence mask was prepared as the cell morphology is different for different cell type. Then after preparing the confluence mask, it was loaded and the analysis was started. Then the cell confluence was measured every 2 hours and recorded. Analysis of data was done based on cell confluence using the IncuCyte® Zoom Software. Statistical analysis of acquired data was carried out using GraphPad Prism 9.1 (GraphPad Software Inc., San Diego, CA, USA).

4 RESULTS

For the development of non-nucleotide TRPM2 inhibitors, the computer-aided drug design (CADD) approach was used and the selected compounds from the structure-based drug design were tested *in vitro* for their inhibitory effect. As soon as the compounds were received, they were checked for their purity with the help of RP-HPLC. Then the compounds were tested for their efficacy (effect on TRPM2 activation) using Fura-2 calcium measurements and patch clamp recordings. Therefore, this results section has been divided into four parts. First part contains the results for the testing of compounds selected from CADD using homology model approach, second part comprises of the result for the compounds selected from the CADD using cryo-EM structure of actual hTRPM2 while the third part has the result for the hTRPM2 gene expression assays. In addition, the last part includes the proliferation assay results for the top six TRPM2 inhibitors using PDAC cell line (MIA PaCa-2) as well as TRPM2 overexpressing HEK293 cells.

4.1 RESULTS FOR THE COMPUTER-AIDED DRUG DESIGN APPROACH USING HOMOLOGY MODEL

After performing the docking process on the homology model structure (explained in the methods section 3.3.1) the top 1000 compounds selected from based on docking score were retained and evaluated in Schrödinger's Maestro. As shown in the figure 14 this evaluation was mostly based on their position in the active site as well as their interaction pattern with NudT9-H followed by the consideration of physicochemical properties of the compounds. The selection of evaluation parameters was based on the prior findings from the literature regarding how the ADPR binds with the NudT9-H domain. As the potential TRPM2 inhibitors, have to compete with ADPR molecule for the ADPR binding site to be specific for the TRPM2 channel. Mainly three parameters were checked in case of binding into the NudT9-H pocket, which were ligand conformation, binding pose and ligand receptor-interactions. In case of ligand conformation, in what shape the molecule is fitting into the binding pocket is observed. As NudT9-H domain being a more wide and relaxed binding pocket it allows the ADPR to sit in a saddle like conformation (Huang et al., 2019). So the compounds were also checked if they take similar conformation and there is not more strain on the molecule. Then the binding pose of the molecules is checked if it is taking the similar binding pose as that of the ADPR. This was confirmed by checking the different amino acid residues the molecule is interacting with in the pocket. As in case of ADPR it has been shown that the terminal ribose of ADPR forms

H-bonds with the Arg 1433 and Tyr 1349 from the NudT9-H domain (Fliegert et al., 2017b). So this was checked if the compounds also forms bonds with these amino acid residues. Then different interactions between the compound and the binding domain were checked as the protein holds the molecule through different interactions. These reactions could be H-bonding, pi-pi interactions, pi-cation interactions, salt bridges or lipophilic interactions. However, mostly focus was given on finding the compounds with H-bonding, as amongst all these other interactions they are the strongest. And for instance if the compound is forming any other weak interaction while the ADPR is forming H-bonding with the binding site then obviously these type of interactions would make the compounds less competitive compared to the ADPR for the binding domain.

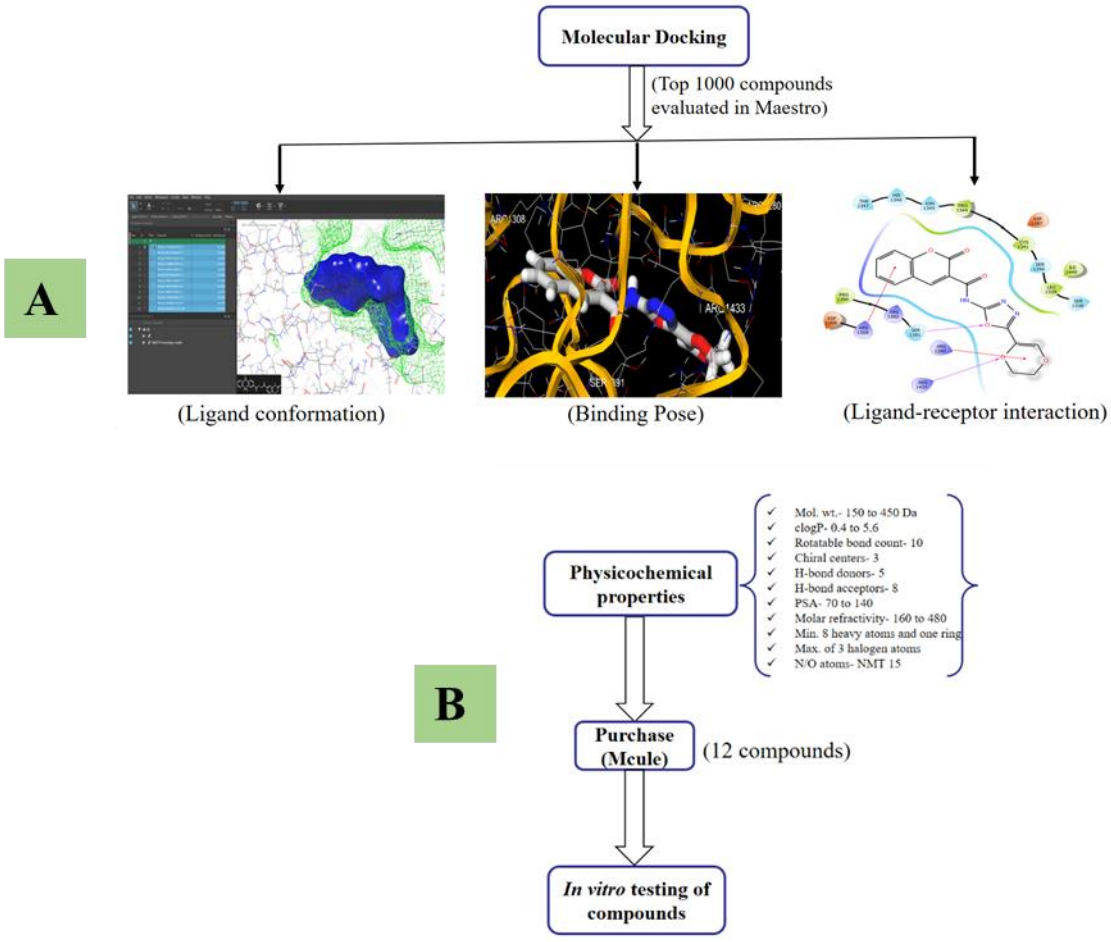

Figure 14: Evaluation of compounds selected from molecular docking

This figure shows the different steps taken in the process of evaluation of the top 1000 compounds selected from molecular docking performed on homology model structure. The part A of the figure shows the screenshots of different evaluation parameters checked in Maestro for compound A08. Then part B of figure shows the further evaluation of compounds based on their physicochemical properties and then selection of best 12 compounds based on these all evaluation parameters.

Furthermore, under consideration of their chemical properties based on Lipinski's Rule of five (Lipinski, 2004) the most promising 50 compounds were selected and out of them 12

compounds were purchased from Mcule for further analysis based on their structural diversity with regard to each other.

4.1.1 Compounds purity check with RP-HPLC

The purity check analysis for all the compounds was performed in our lab using RP-HPLC hence the integrity of the compounds was confirmed. The compounds selected from structure-based drug design using homology model were received from Mcule and as mentioned in the table 13 these compounds had percentage purity range from 92 to 99%.

In total 12 compounds were purchased from Mcule. Compounds were kept at room temperature in their native form (crystalline powder form) when they arrived. Then different concentration stock solutions were prepared in DMSO and the compounds were stored at room temperature in the DMSO. Within first few weeks, the purity of the each compounds was checked using RP-HPLC.

To assess the purity of the compounds the peak area of the main peak was divided by the total peak area that is addition of peak areas of all the impurities as well as the compound. In these experiments, it was assumed that the extinction coefficient at 260 nm is the same for all the compounds and their respective impurities as all the compounds were checked at a constant wavelength of 260 nm.

Table 13: Percentage purity values for compounds selected from drug design using homology model

Compound	**A01**	**A03**	**A04**	**A06**	**A07**	**A08**	**B01**	**B02**	**B03**	**B04**
Purity [%]	97	97	97	94	92	98	93	98	96	99

Table 13**.** Compounds selected from structure based drug design using homology model (purchased from Mcule) were analyzed by RP-HPLC using a C8 column at a flow rate of 1.0 mL/min with a linear gradient from phosphate buffer to methanol)

While most of the compounds showed one major peak, the compounds A02 and A05, we purchased from Mcule were excluded from further analysis because they showed multiple peaks. In case of compound A02 the supplier confirmed, that the preparation is degraded or contaminated and refunded. Otherwise, all the remaining compounds were in good condition.

4.1.2 Effect of compounds on ADPR-induced TRPM2 currents

After checking the purity of the compounds, all of these compounds were tested using whole-cell patch clamp recordings for their effect directly on target. As in this technique, both the ADPR control and the compounds were applied via the patch pipette directly onto the target

hence permeability of the compounds was not a limiting step and compounds were tested for their effect on activation of the channel by ADPR.

The electrophysiological study results demonstrated that two of the 12 compounds (compound A07 and B04) selected from computer aided drug design based on homology model did show partial inhibition of ADPR-induced hTRPM2 currents at 10 µM concentration. As it could be seen in, figure 15 that infusion of the TRPM2 expressing HEK293 cells with 100 µM ADPR results in a maximum outward current of approximately 1 nA. Co-infusion of most of the compounds (with 10 µM concentration) selected from computer aided drug design based on homology model did not significantly reduce this current. Co-infusion of compound A07 and compound B04 led to a weak but significant reduction in net outward current when compared to the ADPR control and showed 62% (compound A07) and 69% (compound B04) inhibition of net outward current evoked by ADPR.

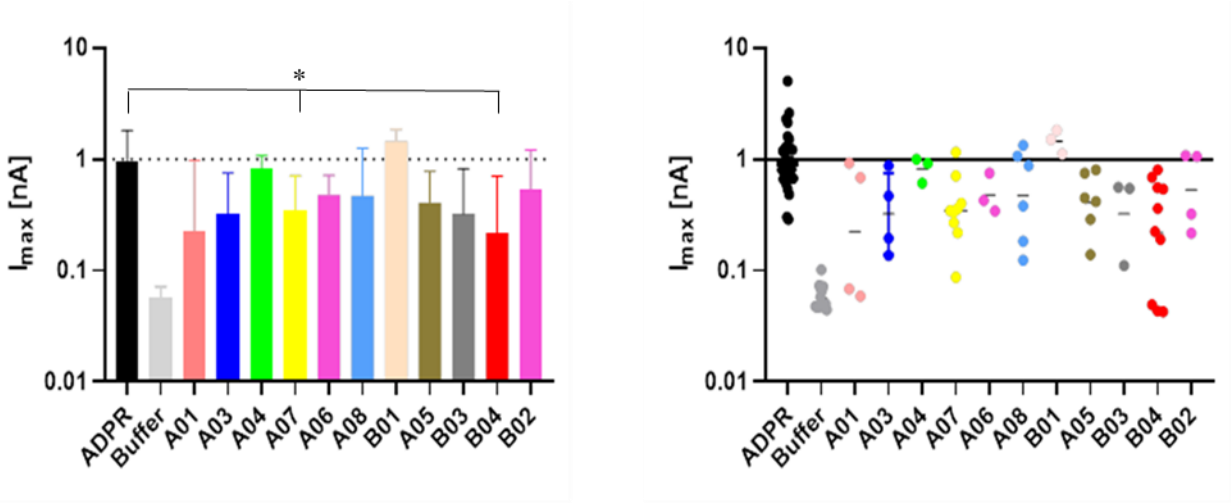

Figure 15: Effect of compounds selected from drug design using homology model on the activation of TRPM2 by ADPR

Maximum outward currents were measured at +15 mV. The pipette solution contained either 100µM ADPR (control) or test solution (10µM compound + 100µM ADPR). Since the distribution of currents is normally positively skewed, the data were plotted on a log-scale. Data points are represented as mean +/- SEM. Log transformed data were tested by one-way ANOVA (followed by post-hoc t-test with Bonferroni correction, the asterisks indicate adjusted *p<0.05 against ADPR control). Data analysis was carried out in Prism (8.4.3, GraphPad Prism Software Inc., USA) and Microsoft Excel 2016 (Microsoft Corporation, Redmond, WA USA).

4.1.3 Effect of compounds on H_2O_2-induced increase in $[Ca^{2+}]_i$

Since TRPM2 channel is a Ca^{2+} permeable channel and activation of channel results in an increase in calcium influx, fluorometric Ca^{2+} measurements were performed to check the effect of potential TRPM2 inhibitors on increase in Ca^{2+} influx because of activation of TRPM2. As it has been discussed earlier in section 1.2.3, the indirect effect (via activating PARP-1/PARG mechanism) of H_2O_2 on activating the TRPM2 channel by oxidative stress and thereby

increasing the free cytosolic calcium concentration ($[Ca^{2+}]_i$). This Fura-2 calcium measurement using H_2O_2 was performed to monitor the changes in the $[Ca^{2+}]_i$ as a measure of channel activation.

For compounds selected from structure-based drug design based on homology model cells were loaded with Fura-2, incubated with compounds and then fluorescence intensity was measured after three minutes of H_2O_2 addition. Then after excitation at 340/380, the ratio of fluorescence intensities was calculated to monitor the changes in the intracellular Ca^{2+} concentration and thereby determining the effect of potential TRPM2 inhibitors on TRPM2 channel activation. Furthermore, dilution of stock solutions were made using DMSO to get different compound concentrations. This ensured that the DMSO was added in same volume and concentration in every measurement. This was done to exclude off-target effects, which might arise from different DMSO concentrations. Cells were pre-incubated (for 20 minutes in the microplate reader) with different concentrations of the compounds before addition of the H_2O_2. In the unstimulated cells, the Ca^{2+} concentration should not increase during the experiment. Therefore, this condition serves as negative control and defines the lower limit. In the figure 16, the different concentrations were highlighted using different colours for better distinction. The addition of H_2O_2 to the HEK293 cells overexpressing hTRPM2, activated the channel and resulting in the highest amount of intracellular calcium so defines the upper limit and hence that is the positive control for these experiments. Then the cells without addition of H_2O_2 did not activate the TRPM2 channel hence that is the lower limit and is considered as the negative control.

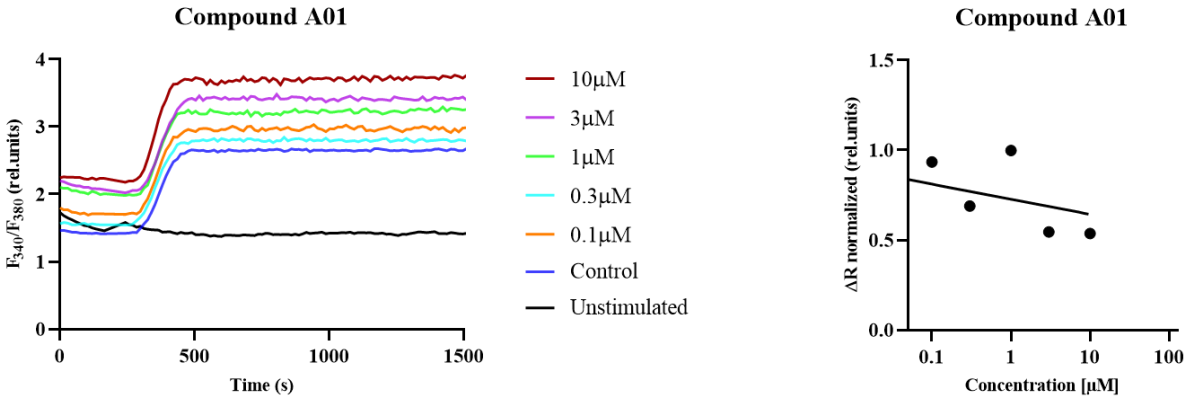

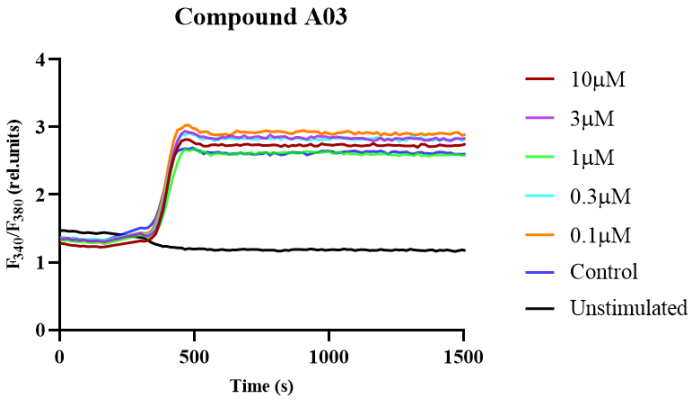
Compound A03
F340/F380 (rel.units)
Time (s)
10µM
3µM
1µM
0.3µM
0.1µM
Control
Unstimulated

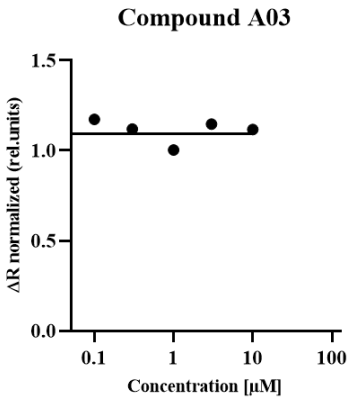
Compound A03
ΔR normalized (rel.units)
Concentration [µM]

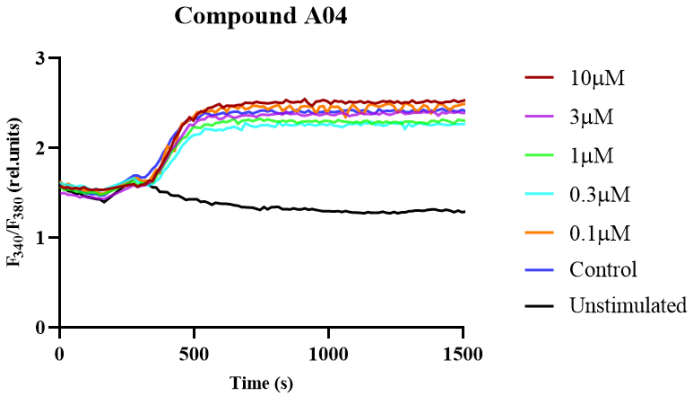
Compound A04
F340/F380 (rel.units)
Time (s)
10µM
3µM
1µM
0.3µM
0.1µM
Control
Unstimulated

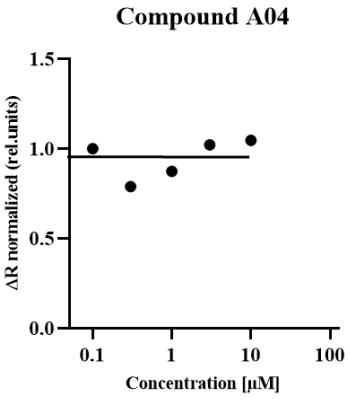
Compound A04
ΔR normalized (rel.units)
Concentration [µM]

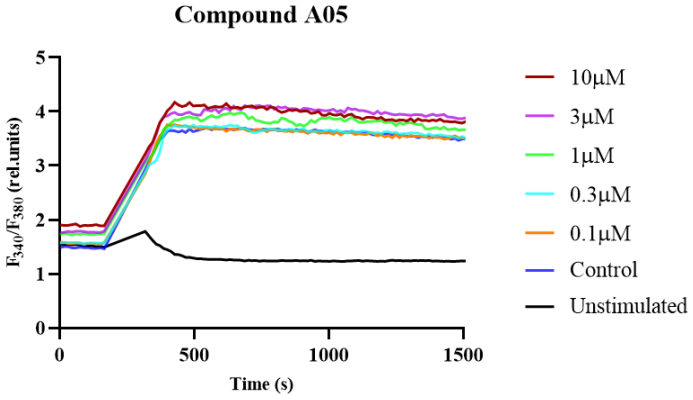
Compound A05
F340/F380 (rel.units)
Time (s)
10µM
3µM
1µM
0.3µM
0.1µM
Control
Unstimulated

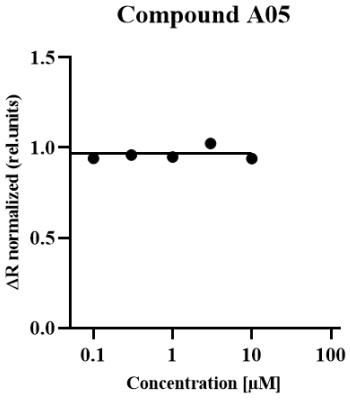
Compound A05
ΔR normalized (rel.units)
Concentration [µM]

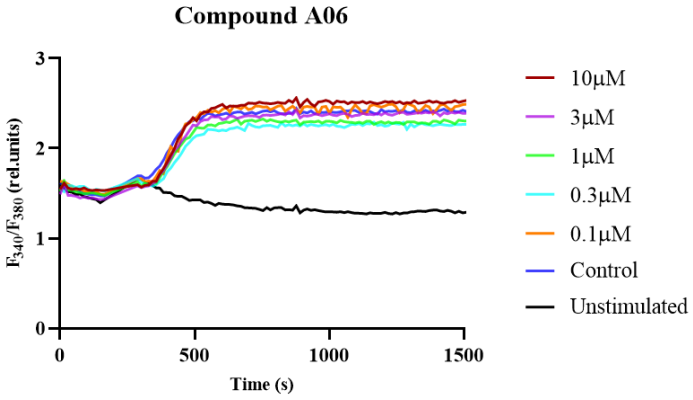
Compound A06
F340/F380 (rel.units)
Time (s)
10µM
3µM
1µM
0.3µM
0.1µM
Control
Unstimulated

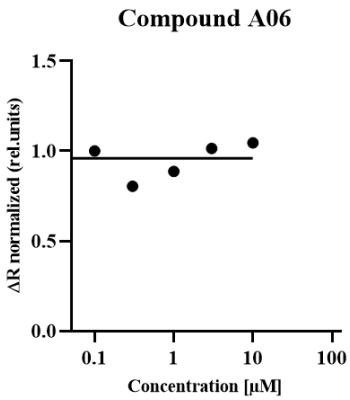
Compound A06
ΔR normalized (rel.units)
Concentration [µM]

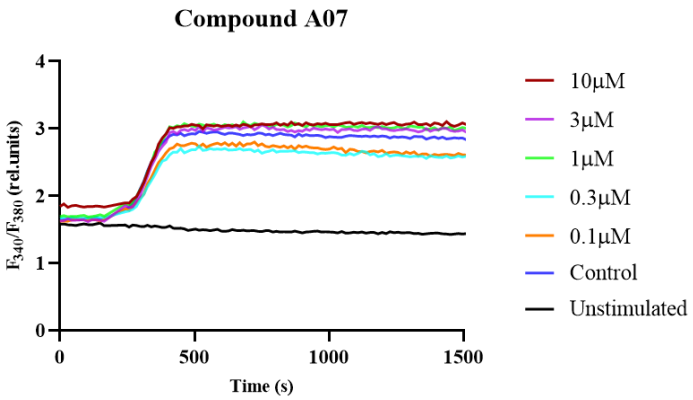
Compound A07
F340/F380 (rel.units)
Time (s)
10µM
3µM
1µM
0.3µM
0.1µM
Control
Unstimulated

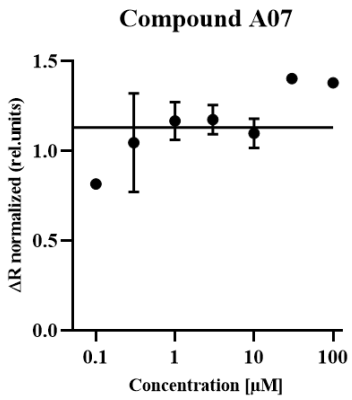
Compound A07
ΔR normalized (rel.units)
Concentration [µM]

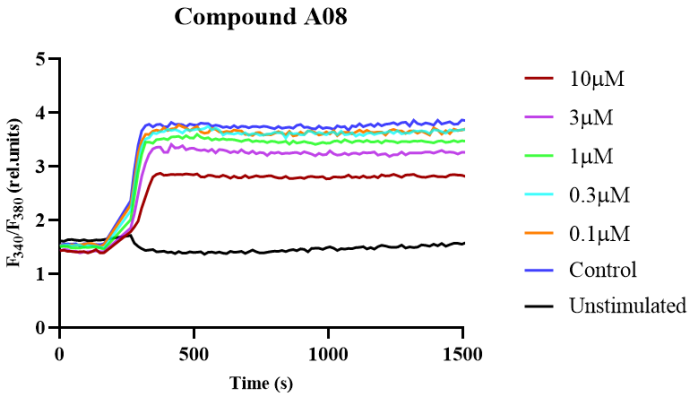
Compound A08
F340/F380 (rel.units)
Time (s)
10µM
3µM
1µM
0.3µM
0.1µM
Control
Unstimulated

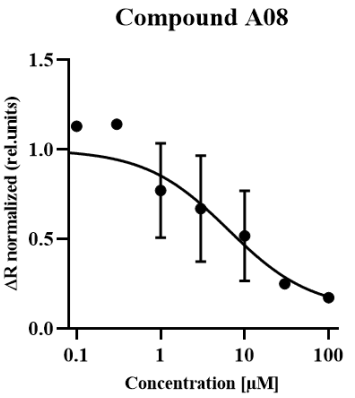
Compound A08
ΔR normalized (rel.units)
Concentration [µM]

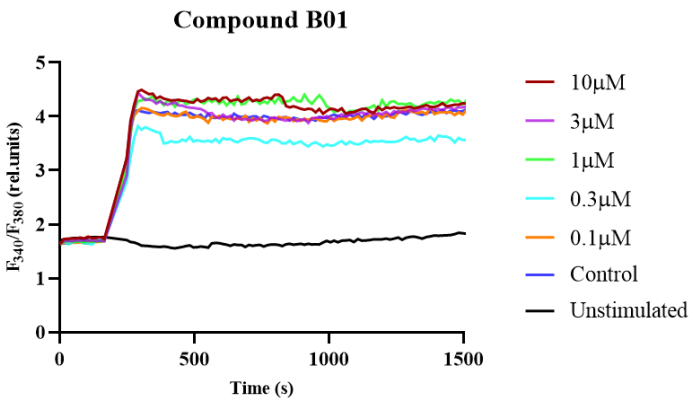
Compound B01
F340/F380 (rel.units)
Time (s)
10µM
3µM
1µM
0.3µM
0.1µM
Control
Unstimulated

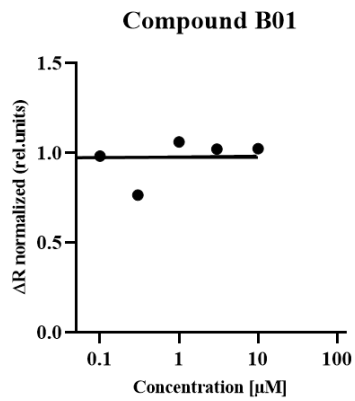
Compound B01
ΔR normalized (rel.units)
Concentration [µM]

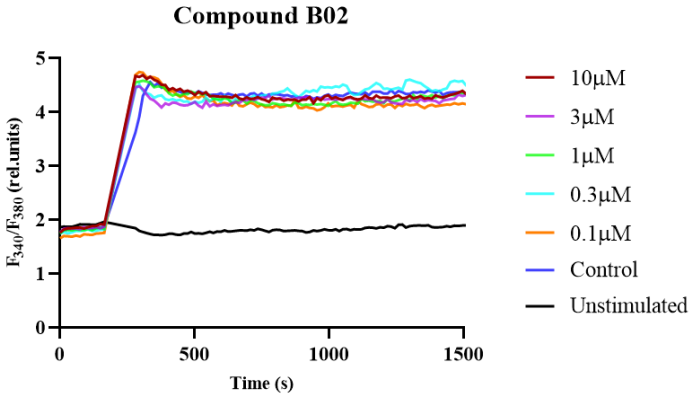
Compound B02
F340/F380 (rel.units)
Time (s)
10µM
3µM
1µM
0.3µM
0.1µM
Control
Unstimulated

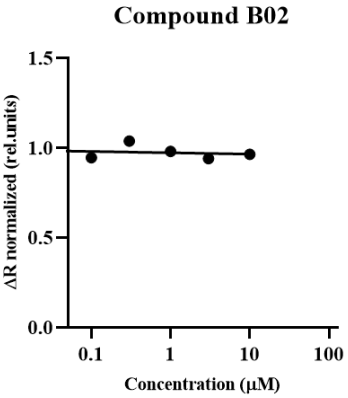
Compound B02
ΔR normalized (rel.units)
Concentration (µM)

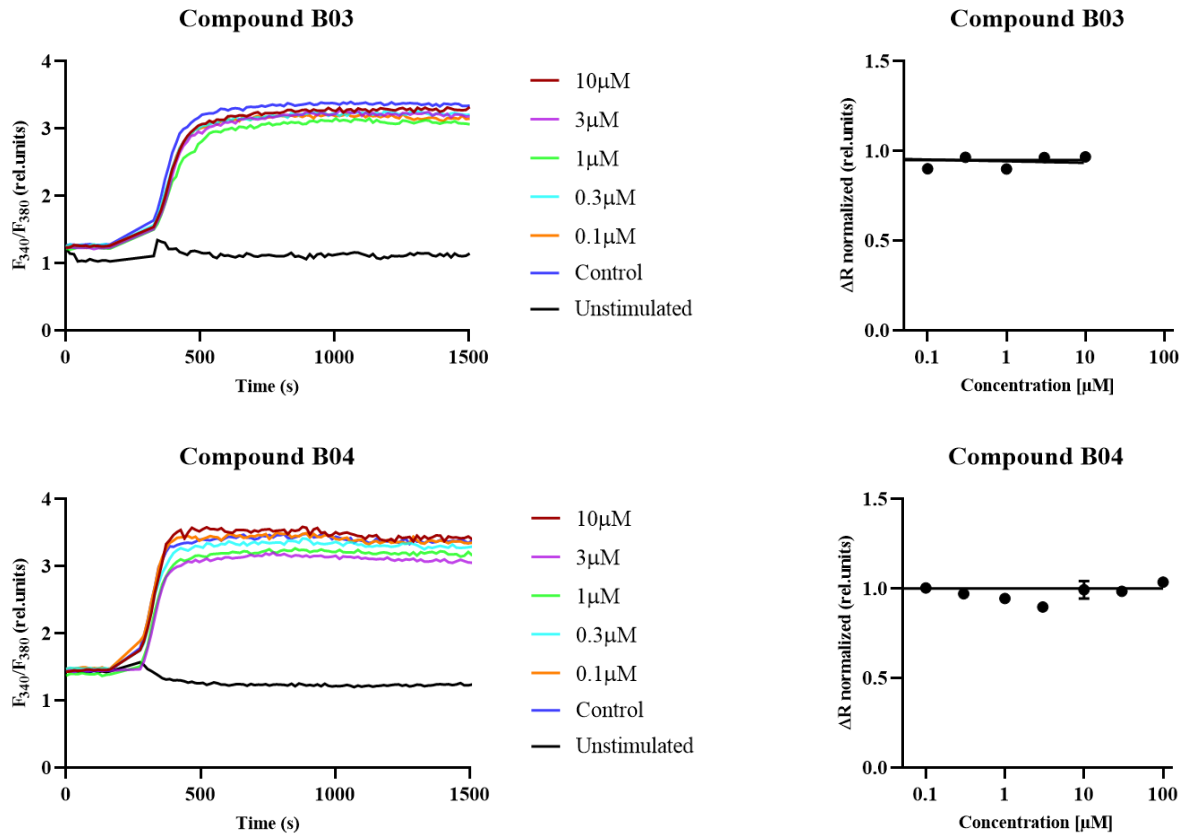

Figure 16: Effect of potential ADPR antagonist on the H_2O_2-stimulated Ca^{2+} signal in Fura-2 loaded TRPM2 expressing HEK293 cells

Changes in the Ratio F_{340}/F_{380} reflect changes in the intracellular Ca^{2+}-concentration. Three min after start of the recording cells were stimulated by addition of a final conc. of 1 mM H_2O_2. This results in intracellular production of ADPR and activation of TRPM2. After addition of H_2O_2, there is this plateau-like increase in fluorescence intensity ratio 340/380. The differently coloured lines show recordings from cells pre-incubated (for 20 minutes) with different concentrations of all the compounds. The increase in the ratio was calculated as measure of channel activation and plotted against the different concentrations of the compounds as shown in these figures. For the concentration-response curves, the initial ratio was subtracted and data normalized to the positive (w/o compound) and negative control (w/o compound and w/o hydrogen peroxide). Data points are represented as mean +/- SEM. Data analysis was performed in Microsoft Excel 2016 (Microsoft Corporation, Redmond, WA USA) as well as GraphPad Prism 8.4.3 (GraphPad Prism Software Inc., USA).

The results in figure 16 shows that in case of compound A01, A03, A04, A05, A06, A07, B01, B02, B03 and B04 there is no concentration dependent decrease in the fluorescence intensity ratio (F_{340}/F_{380}) in presence of compounds. This could mean that the compounds either do not inhibit the TRPM2 channel or may be are not even able to permeate through the cell membrane. From these calcium measurement results concentration-response curves were constructed to check the impact of compounds on TRPM2 activation mediated calcium signal, which are also shown besides the calcium tracings. Initial ratio was subtracted and data normalized to positive and negative control.

These results show that the compounds selected from structure-based drug design using homology model except compound A08 did not show concentration dependent inhibition of TRPM2 channel activation mediated calcium signal. Only compound A08 did show concentration dependent decrease in the fluorescence intensity ratio F_{340}/F_{380} and a sigmoidal

curve showing good inhibition of calcium signal caused by activation of hTRPM2 with an IC_{50} of around 6 μM (figure 16). However, as seen previously with the patch clamp experiment this compound A08 did not show inhibition of ADPR-induced TRPM2 current hence this could mean that the inhibition it showed with this calcium signal in the Fura-2 calcium measurements is unlikely due to the competitive inhibition of binding of ADPR to the intracellular NudT9-H domain of TRPM2. A possible explanation would be that it acts as an antioxidant and thus reduces the effect of H_2O_2. Moreover, on comparing this calcium measurements results with previous patch clamp experiments in case of compound A07 and B04 it could be concluded from the fact that they can inhibit the channel but did not show a reduction in the Ca^{2+} signal which means these compounds are not membrane permeant. Fura-2 calcium measurements even after showing partial inhibition of ADPR-induced TRPM2 currents.

4.2 RESULTS FOR THE COMPUTER-AIDED DRUG DESIGN APPROACH USING ACTUAL CRYO-EM STRUCTURE OF HTRPM2

After performing the molecular dynamic simulations on the structures, the docking was performed for these structures. As already mentioned in the procedure section 3.3.2 two cryo-EM structures (PDB: 6PUO and 6PUS) were used for this structure-based drug design approach. Therefore, after analyzing the results from the MD simulations, there were two grids for docking: 6PUO and 6PUS. For 6PUO, the frame selected from MD simulation, the library used was HTS (High throughput screening) library of 30,000 compounds, which became 100,000 after ligand preparation in Maestro, as after ligand preparation, different isomers of the same compound will be considered as a different entity/compound. In case of the isolated NudT9-H domain (6PUS structure), first a similarity search as well as substructure search was performed on different small libraries collected online (Mcule, ZINC, Innovamol, NCI and MedChemexpress) and prepared a set of compounds for further docking. In similarity search the structure of ADPR was used as a reference while substructure search was performed using different permutation combinations including terminal ribose, pyrophosphate group and adenosine moiety. This means substructure search was performed based on ADPR structure like removing pyrophosphate group from the ADPR structure and preparing the similarity search library or removing the adenine moiety and so on. Initially a high throughput virtual screening (HTVS) precision docking using Maestro was performed for 6PUO because it allows for a fast screening of a large number of compounds (2 seconds per compound). The best 3000 compounds were selected based on their docking score and re-docked with SP (standard

precision) docking, which resulted in around 2700 compounds. In case of 6PUS virtual screening was done by SP docking (10 seconds per compound) and resulted in additional 3500 compounds. From virtual docking using both grids a total of 6200 compounds were obtained, those were further evaluated manually for ligand receptor-interaction, fit in the pocket, ligand strain and physicochemical properties. Based on this evaluation, the best 85 compounds from the 6PUO grid and the best 40 compounds from the 6PUS grid were selected for extra precision (XP) docking. XP docking is a more powerful, harder function as it takes longer, so it could not be used to screen a large number of compounds. The Maestro manual recommends first running a SP-docking and then taking 10-30% of the final poses and re-docking them using XP-docking. The detailed docking procedure is outlined in the following figure. 17.

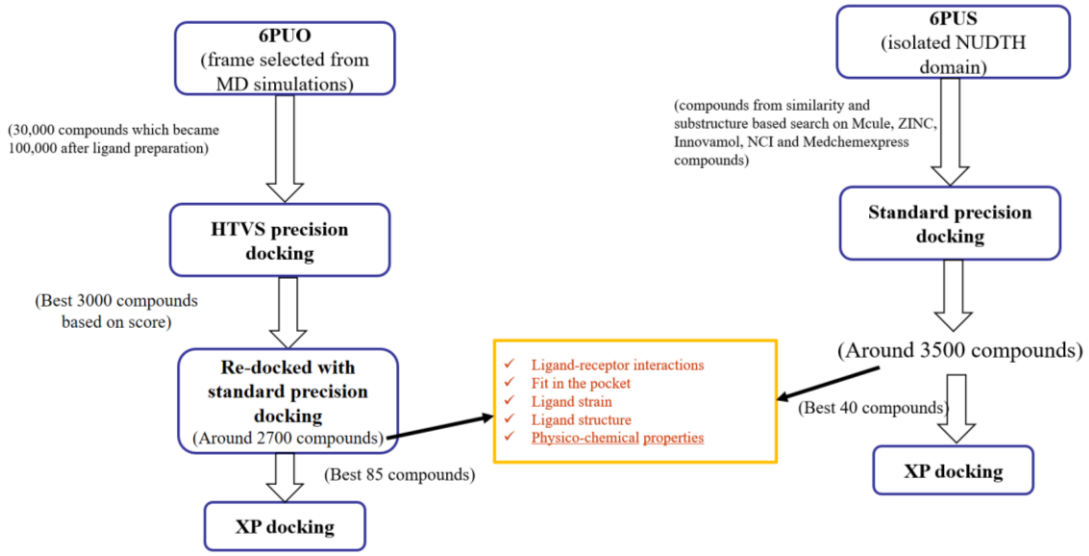

Figure 17: Schematic representation of the docking process

This figure shows the docking steps taken on the MD simulated and energy minimized structural grids. Different dockings were performed on two different grids. In case of 6PUO, first HTVS precision docking was run followed by standard precision docking then after checking the output compounds for their different necessary properties (written in yellow text) again the XP docking was performed on them. In case of 6PUS, directly the standard precision docking was performed then the output compounds were checked for the same properties as the others and then the XP docking was performed.

From this set of 125 compounds, 13 compounds were selected based on their ligand-receptor interactions, docking score, ligand strain, fit in the pocket, ligand structure and physicochemical properties evaluation (explained in section 4.1) and then purchased from Molport. This time the utmost care was taken to check the logP values for all the compounds as in the previous lot of compounds from homology model based drug design the compounds were having low logP values, which made them sparingly soluble in DMSO. Moreover, because of this they could not be used in higher concentrations in the patch clamp experiments for testing their effect onto the target as well as might be the reason why they did not show good inhibition in calcium measurements.

4.2.1 Compounds purity check with RP-HPLC

Same as the previous lot of compounds the purity check analysis for all these compounds was also performed in our lab using RP-HPLC confirming the integrity of the compounds. All of these compounds selected from computer aided drug design using cryo-EM structure of hTRPM2 were purchased from Molport and the percentage purity values for all of them (table 14).

In total 13 compounds were purchased from Molport. Compounds were kept at room temperature in their native form (crystalline powder form) when they received then different concentration stock solutions were prepared in DMSO and the compounds were stored at room temperature in the DMSO. Within first few weeks, the purity of the each compounds was checked using RP-HPLC.

To assess the purity of the compounds the same procedure was followed as previous (section 4.1.1) by dividing the peak area of the main peak by the total peak area (peak area of compound + peak area of all the impurities).

Table 14: Percentage purity values for compounds selected from drug design using cryo-EM structure

Compound	C01	C02	C03	C04	C05	C06	C07	C08	C10	C11	C12	C13
Purity [%]	98	68	90	90	98	92	87	93	95	97	54	97

Table.14. Compounds selected from computer aided drug design using cryo-EM structure (purchased from Molport) were analyzed by RP-HPLC. The analysis was done using a C8 column at a flow rate of 1.0 mL/min with a linear gradient from phosphate buffer to methanol.

Compound 12 did show degradation after few weeks that was visible in its calcium measurement results hence was excluded from further studies. Also compound 08 did precipitate out but it happened very in the end means at the time of proliferation experiments till then it was in good condition.

4.2.2 Effect of compounds on H_2O_2-induced increase in $[Ca^{2+}]_i$

The Fura-2 calcium measurement experiments were performed as a primary screening tool for the compounds selected from the second attempt of drug design approach. The same procedure of Fura-2 calcium measurement experiments was followed also for the compounds selected from computer aided drug design based on cryo-EM structure, only change was that in case of results calculation, instead of the ratio F_{340}/F_{380}, the direct $[Ca^{2+}]_i$ was calculated using the equation described by (Grynkiewicz et al., 1985), explained in the section 3.6.2.

However, the compounds selected from structure-based drug design based on molecular dynamics simulated hTRPM2 cryo-EM structure did show a concentration dependent inhibition of TRPM2 activation mediated calcium signal indicating significant inhibition of activation of hTRPM2 channel. The results as shown in the figure 18 indicate that there were some compounds, which did not show any inhibition those were compound 01, 07, and 13 and compounds like 05, 10, 11 and 12 showed inhibition during first weeks but failed to show inhibition after few weeks. Nevertheless, there were six compounds showing inhibition of the channel: compound 02, 03, 04, 06, 08 and 09. Besides the calcium tracings, there are the concentration-response curves for all of these compounds shown in the figure 18. Total six compounds showed sigmoidal curves with the IC_{50} values ranging from 1.8 to 4.7 µM. Compound 02, 03, 04, 06, 08 and 09 has IC_{50} values 3.6, 4.7, 2.5, 1.8, 3.8 and 4.3 µM respectively. And the percentage inhibition for these compounds were like compound 02 and 03 showed a partial inhibition of 63 % and 60% respectively while compound 04, 06, 08 and 09 showed around 89%, 85%, 81% and 82% of inhibition.

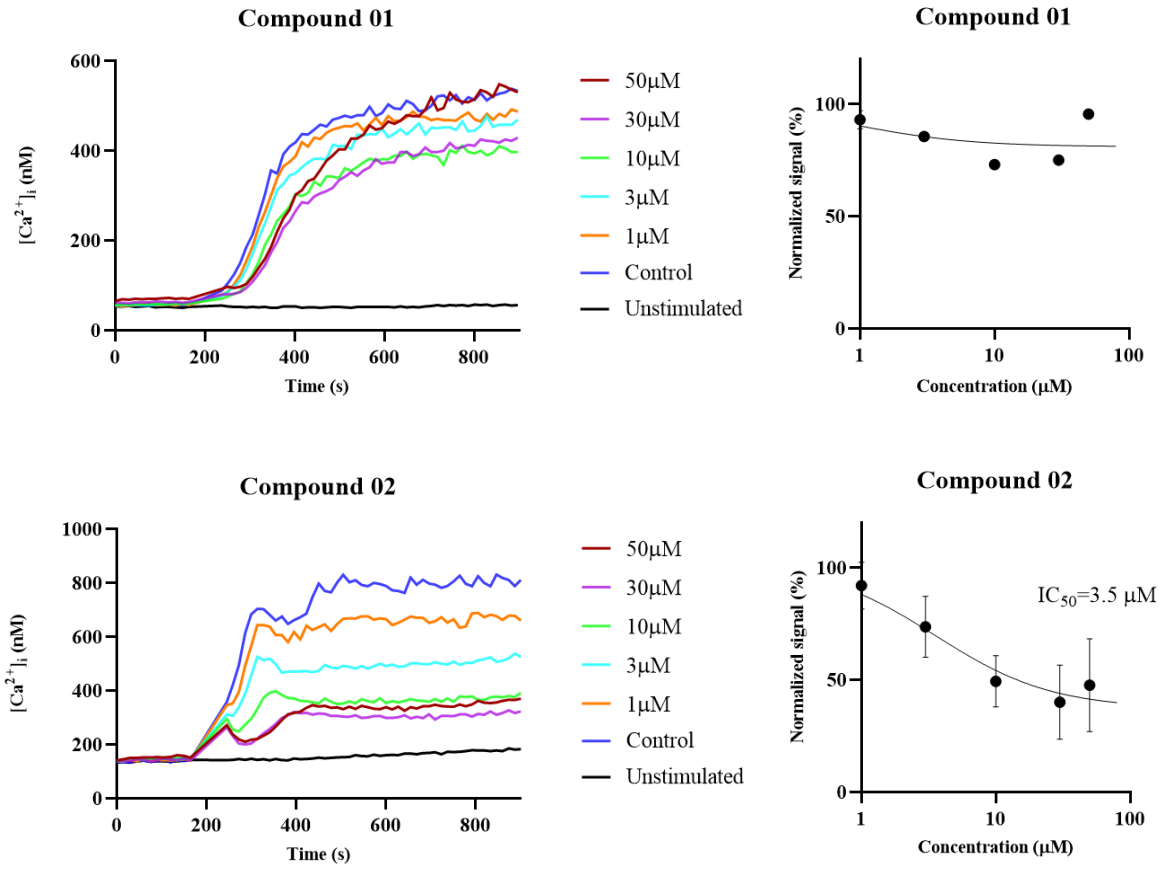

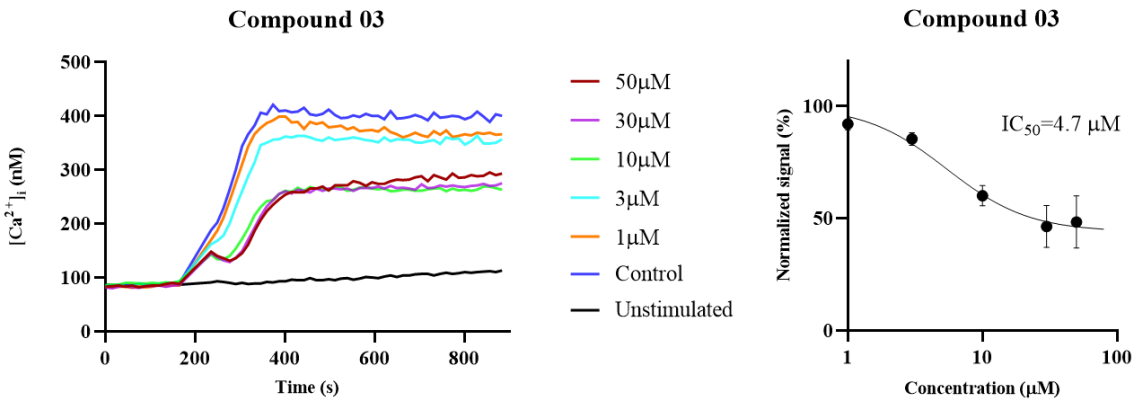
Compound 03
[Ca2+]i (nM)
Time (s)
50μM
30μM
10μM
3μM
1μM
Control
Unstimulated
Compound 03
Normalized signal (%)
IC50=4.7 μM
Concentration (μM)

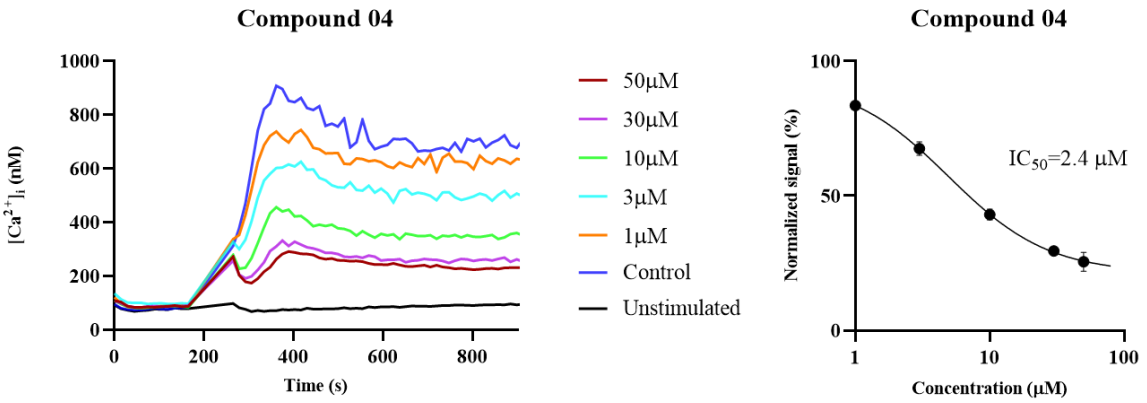
Compound 04
[Ca2+]i (nM)
Time (s)
50μM
30μM
10μM
3μM
1μM
Control
Unstimulated
Compound 04
Normalized signal (%)
IC50=2.4 μM
Concentration (μM)

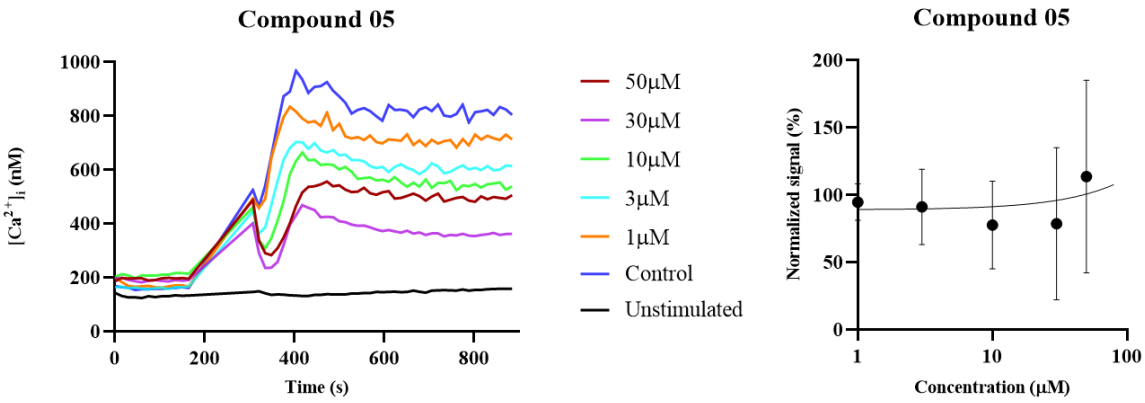
Compound 05
[Ca2+]i (nM)
Time (s)
50μM
30μM
10μM
3μM
1μM
Control
Unstimulated
Compound 05
Normalized signal (%)
Concentration (μM)

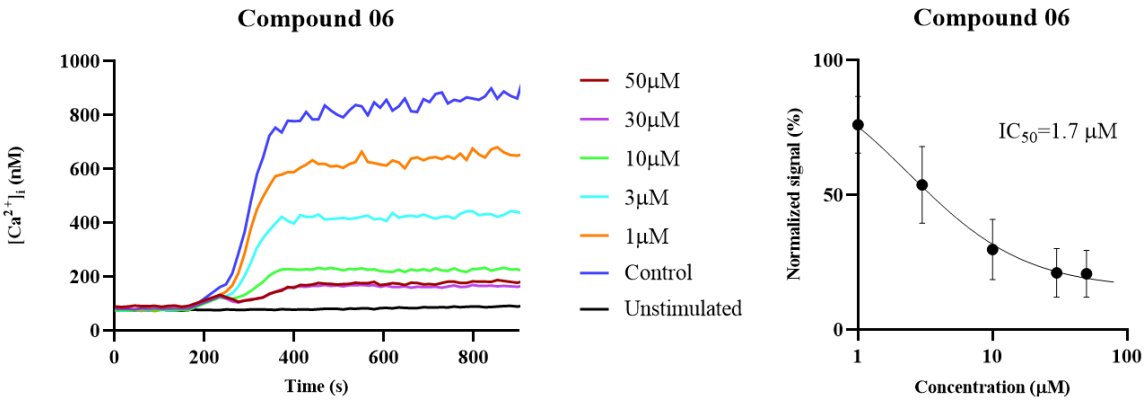
Compound 06
[Ca2+]i (nM)
Time (s)
50μM
30μM
10μM
3μM
1μM
Control
Unstimulated
Compound 06
Normalized signal (%)
IC50=1.7 μM
Concentration (μM)

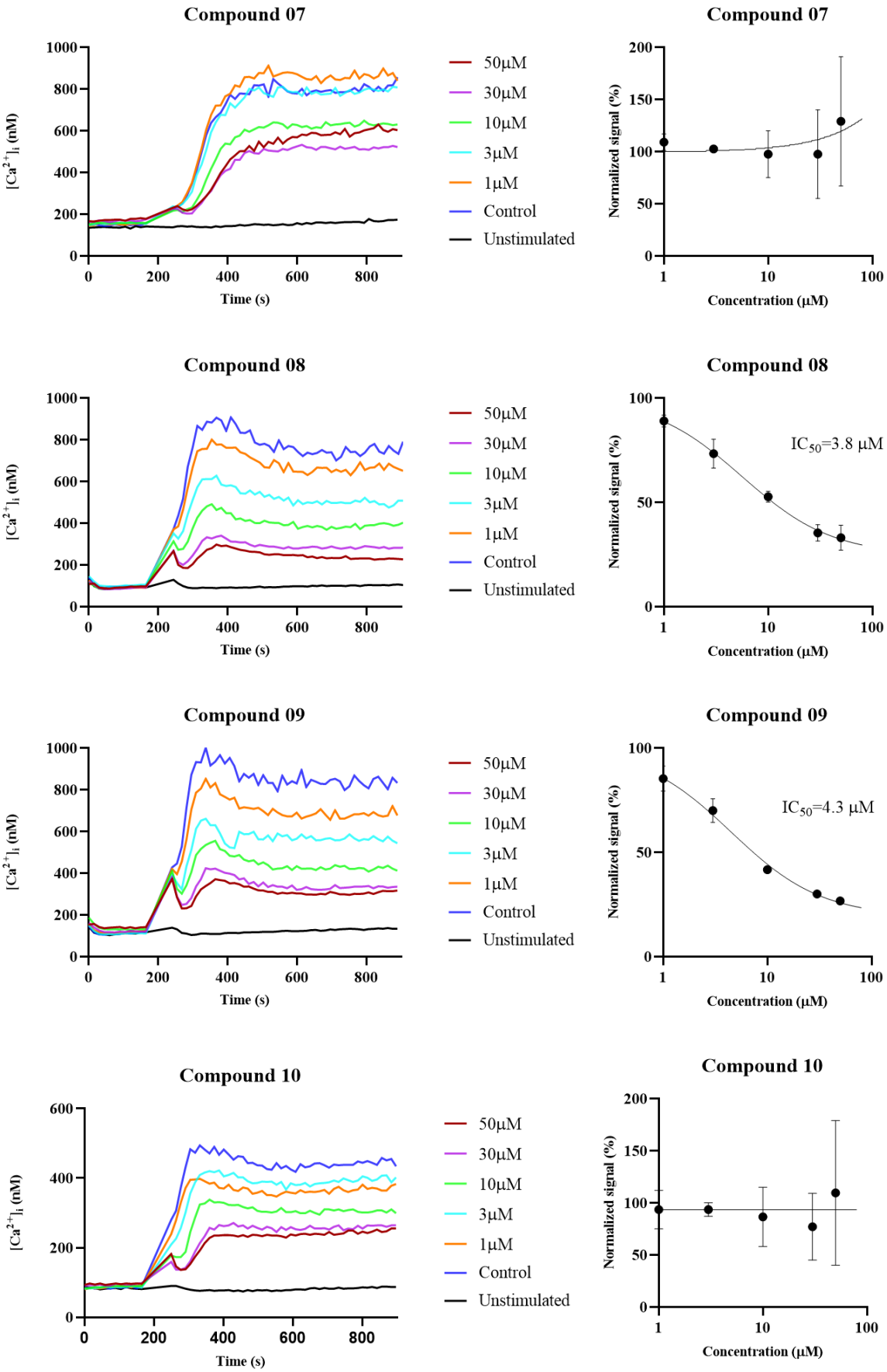
Compound 07
[Ca2+]i (nM)
Time (s)
50μM
30μM
10μM
3μM
1μM
Control
Unstimulated
Compound 07
Normalized signal (%)
Concentration (μM)
Compound 08
Compound 08
IC50=3.8 μM
Compound 09
Compound 09
IC50=4.3 μM
Compound 10
Compound 10

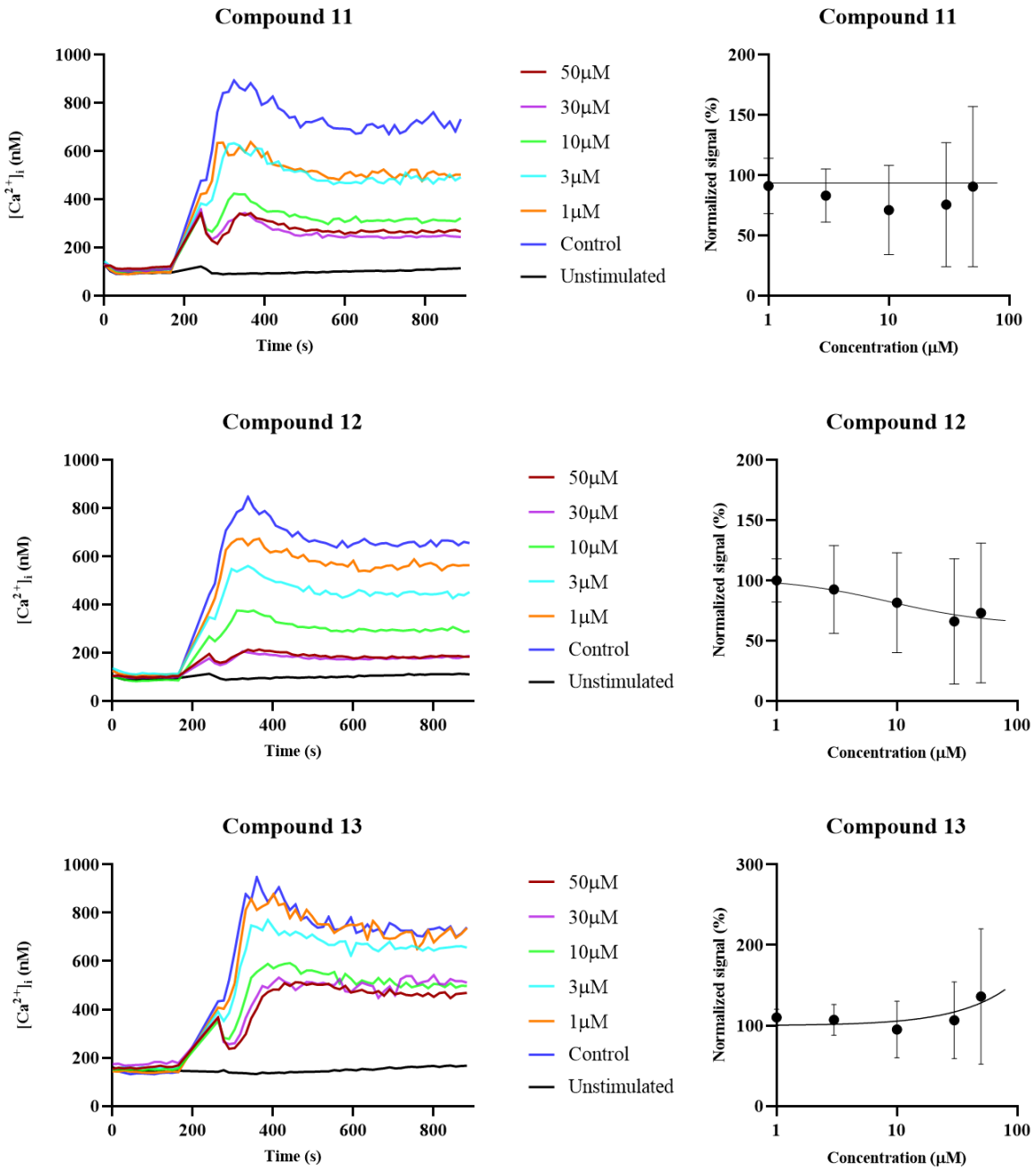

Figure 18: Measurement of Fura-2 loaded HEK293 cells for compounds selected from computer-aided drug design based on cryo-EM structure with their concentration-response curves

Three minutes after the start of the recording, the cells were stimulated by addition of 1.5 mM H_2O_2 that resulted in intracellular production of ADPR and thereby activation of the channel. After addition of H_2O_2, there is this plateau-like increase in Ca^{2+} concentration. Here the differently colored lines shows recordings from cells pre-incubated (for 20 minutes in microplate reader) with different concentration of compounds. The increase in free cytosolic calcium concentration after stimulation by H_2O_2 was considered as a channel activation. For the concentration-response curves, the basal Ca^{2+} concentration was subtracted and data was normalized to the positive (w/o compound) and negative control (w/o compound as well as hydrogen peroxide). Here some of the compounds did show a concentration dependent inhibition of TRPM2 dependent Ca^{2+} signal and have IC_{50} values below 5 µM. Data points are represented as mean +/- SEM. Data analysis was performed in Microsoft Excel 2016 (Microsoft Corporation, Redmond, WA USA) as well as GraphPad Prism 8.4.3 (GraphPad Prism Software Inc., USA).

The results for the calcium measurements of the compounds selected from computer-aided drug design based on cryo-EM hTRPM2 structure demonstrated that half of the compounds selected this time have shown concentration dependent an inhibition of the TRPM2 mediated

calcium signal in response to H_2O_2. As it could be seen in the figure 18 the compounds, which showed concentration dependent inhibition of TRPM2, were compound 02, 03, 04, 06, 08 and 09 and compounds that did not show inhibition at were compound 01,07 and 13. Moreover, the compounds 05, 10, 11 and 12 did show some inhibition in the beginning but after few weeks, they failed to show inhibition of TRPM2 activation mediated calcium signal (explained in detail in discussion section). Hence, these compounds were also excluded from further studies.

4.2.3 Effect of compounds on ADPR-induced TRPM2 currents

After testing the potential hTRPM2 inhibitors on intact cells using Fura-2 calcium measurements, the compounds were tested in patch clamp experiments with TRPM2 expressing HEK293 cells as well. Here the Fura-2 calcium measurement experiments were used as a primary screening for the compounds. This was done because in Fura-2 calcium measurements the hTRPM2 is activated indirectly upon application of H_2O_2 because of accumulation ADPR and as the downstream mechanism for this is via activation of PARP-1/PARG pathway, this could also lead to having false positive compounds, which are PARP-1 inhibitors and not specifically hTRPM2 inhibitors. Therefore, to eliminate this doubt, in addition to the Fura-2 calcium measurements the compounds were tested directly onto the target with the help of patch clamp experiments to validate the inhibitory activities of the potential hTRPM2 inhibitors observed during Fura-2 calcium measurements.

Based on the results of the Fura-2 calcium measurements only six compounds from structure-based drug design using hTRPM2 cryo-EM structure were tested using the patch clamp experiments. This was done because as the Fura-2 calcium measurement also gave an idea about membrane permeant compounds so it was wise to check only the membrane permeant compounds for their effect directly on target. Because if they could not permeate through the cell membrane they probably will not reach the target (NudT9-H domain binding site) which is intracellular in this case.

As can be seen in the figure 19, application of 100 µM ADPR into the TRPM2 expressing HEK293 cells via the patch pipette resulted in a maximum outward current of approximately 2.5 nA. Co-infusion of any of the six selected compounds from Ca^{2+} measurement experiment results did significantly reduce this ADPR-induced TRPM2 current. For these six compounds the fractional inhibition of TRPM2 current varied between 63% for compound 08 to 83% for compound 03 (figure 19).

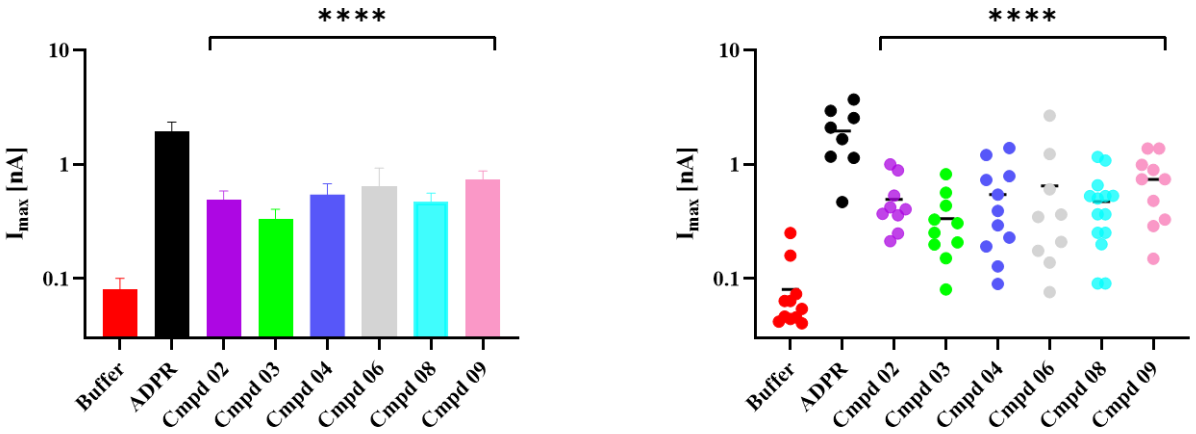

Figure 19: Effect of compounds selected from drug design using hTRPM2 cryo-EM structure on the activation of TRPM2 by ADPR

Maximum outward currents were measured at +15 mV. The pipette solution contained either 100µM ADPR (control) or test solution (100µM compound + 100µM ADPR). Since the distribution of currents is normally positively skewed, the data were plotted on a log-scale. Data points are represented as mean +/- SEM. Log transformed data were tested by one-way ANOVA (followed by post-hoc t-test with Bonferroni correction, the asterisks indicate adjusted ****p<0.0001 against ADPR control). Data analysis was done using Prism (8.4.3, GraphPad Prism Software Inc., USA) and Microsoft Excel 2016 (Microsoft Corporation, Redmond, WA USA).

4.3 Expression level of TRPM2 in different Pancreatic cancer cell lines

After checking the TRPM2 inhibitors using Fura-2 calcium measurement (to check effect on intact cells) and patch clamp recordings (to check effect on target), it was decided to check the impact of these TRPM2 inhibitors on pancreatic cancer cell proliferation. For this different pancreatic cell lines were checked for expression of human TRPM2 using RT-PCR and RT-qPCR.

4.3.1 Using RT-PCR

As discussed in section 1.2.4 that the expression of hTRPM2 is associated with many different pathological conditions including cancer so the studies in this thesis are mostly focused on developing specific TRPM2 inhibitors, which could be used in the treatment of pancreatic ductal adeno carcinoma (PDAC). Keeping this in mind, the different pancreatic cancer cell lines were studied for their expression level of hTRPM2. The different pancreatic cancer cell lines used were MIA PaCa-2, SU 86.86, PANC-1, Bx PC-3 and T3M4. These five different pancreatic cell lines were cultured and passaged (section 3.4.2). Then these all were checked for their expression of TRPM2 by performing RT-PCR using two independent RNA preparations. The figure 20 shows the results of RT-PCR experiment demonstrating the expression of hTRPM2 in these different pancreatic cancer cell lines. The expected amplicon for hTRPM2 has a size of 472bp. The positive control (HEK293 TRPM2 #24) clearly shows a

band running slightly below the 500 bp fragment in the Marker (100bp DNA ladder) whereas the water control did not show any band.

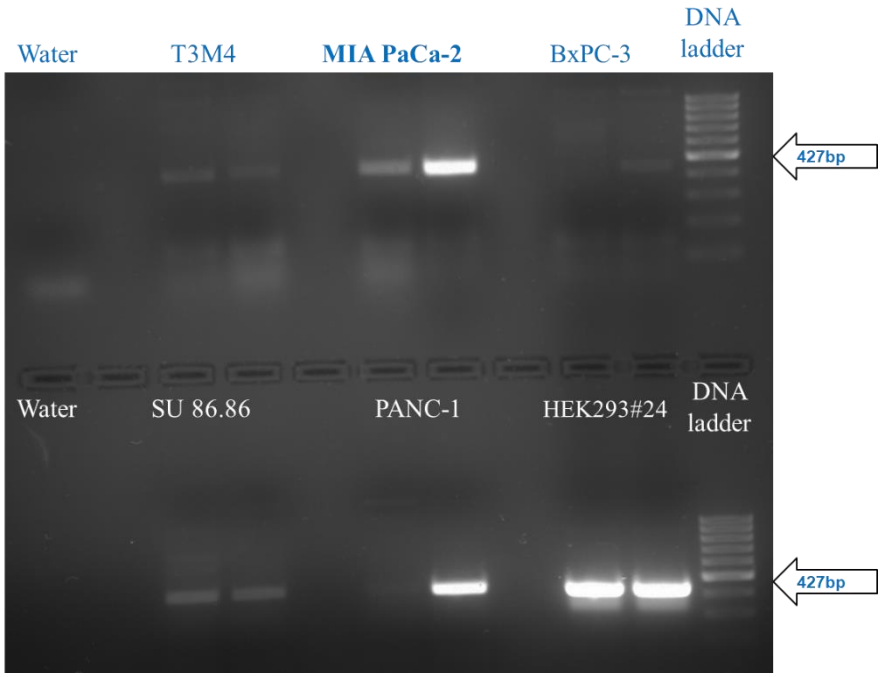

Figure 20: Analysis of expression of TRPM2 in human PDAC cell lines by RT-PCR
Starting with the top row, to the left most is the water sample-containing lane, then in the middle there are the lanes for T3M4 and MIA PaCa-2 cells sample and to the most right it is the BxPC-3 cells sample-containing lane. Then at the bottom row, to the left most is again the water sample-containing lane, then there are the lanes for the SU 86.86 and PANC-1 cells sample in the middle and then to the most right, it is the lane for the sample for HEK293 TRPM2 #24 cells. Then there is a lane for the DNA ladder.

The result showed that compared to other pancreatic cancer cell lines (SU 86.86, BxPC-3, and T3M4), MIA-PaCa-2 and PANC-1 did show a bright band at 427bp indicating and confirming the expression of hTRPM2. On the other hand, T3M4 and SU 86.86 did show very little expression of TRPM2 but BxPC-3 did show no expression of hTRPM2.

4.3.2 Quantification of TRPM2 expression using quantitative RT-PCR

Real time quantitative polymerase chain reaction (RT-qPCR), as being the most sensitive technique for mRNA detection and quantification was performed to quantify the expression of hTRPM2 in the different pancreatic cancer cell lines available. So after confirming the qualitative expression or presence of expression of TRPM2 in the five different pancreatic cancer cell lines, it was decided to check the level of expression or quantify the expression of hTRPM2 so that only one cell line could be taken forward for the further experiments.

The RT-qPCR results demonstrated that out of all these five different pancreatic cancer cell lines MIA PaCa-2 is the one showing comparatively high expression of hTRPM2. As it could

be seen from the figure 21 that the hTRPM2 overexpressing HEK293 cells have the highest level of hTRPM2, followed by the MIA PaCa-2 cells.

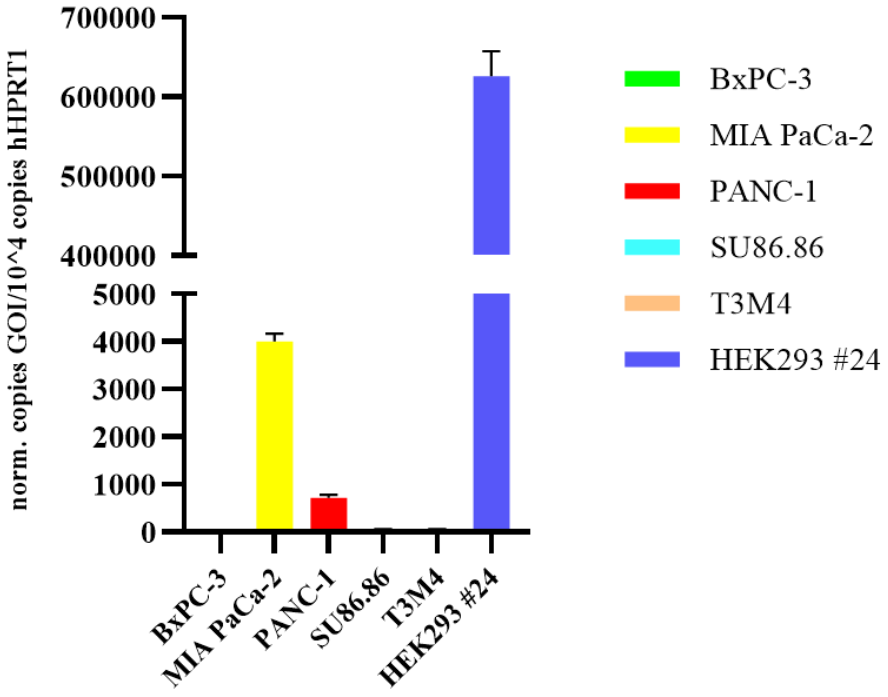

Figure 21: Bar plot showing gene expression levels of hTRPM2, measured by RT-qPCR
The hTRPM2 overexpressing HEK293 cells shows the highest amount of hTRPM2 followed by the MIA PaCa-2 and then very little expression in PANC-1 too. But not much in other cell lines. Data points are represented as mean +/- SEM. The data has been analysed using Microsoft excel and Prism (8.4.3, GraphPad Prism Software Inc., USA).

4.4 Effect of inhibitors on MIA PaCa-2 cell proliferation rate

As confirmed with the Fura-2 calcium measurement and the patch clamp experiments that the six compounds selected from computer-aided drug design based on molecular dynamics simulated hTRPM2 cryo-EM structure can pharmacologically inhibit the activation of TRPM2 channel. Therefore, these should be further investigated for their impact on cancer cell proliferation rate. For this IncuCyte® Zoom Live Cell imaging system was used.

This study was originated to evaluate the impact of the selected TRPM2 inhibitors on the pancreatic cancer cell line: MIA PaCa-2. This cell line was chosen for these experiments because it has shown to express higher amount of hTRPM2 compared to the other available pancreatic cell lines and this has been confirmed with the RT-PCR and RT-qPCR experiments performed earlier in this study.

Figure 22 shows the impact of TRPM2 inhibitors on the rate of proliferation of MIA PaCa-2 cell line.

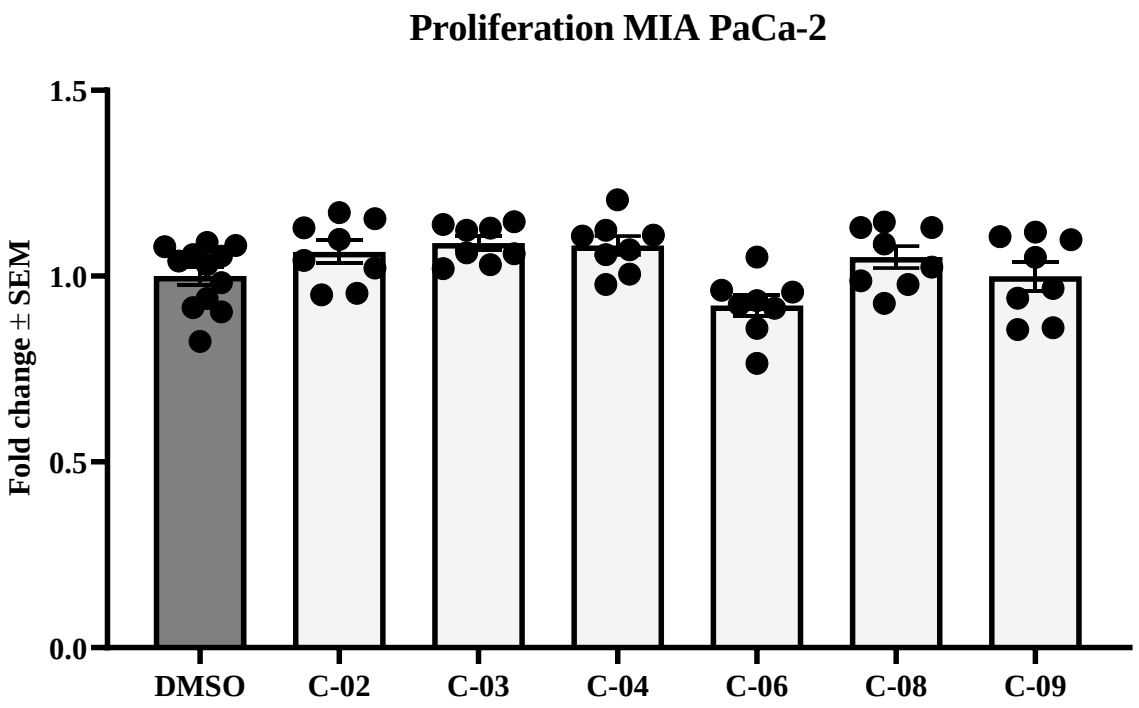

Figure 22: Bar graph showing impact of TRPM2 inhibitors on MIA PaCa-2 cell proliferation rate
The figure shows the impact of TRPM2 inhibitors on proliferation of the MIA PaCa-2 cells. For the experiment the cells were seeded in quadruplicates in a density of 1500 cells per well in a 96-well plate. The next day the TRPM2 inhibitors in a final concentration of 100 µM were added into each well except the control wells. Then plate transferred into the IncuCyte®Zoom Live Cell Analysis System and cell confluence was measured every two hours. For the analysis of the data, the values from one middle time point from the exponential growth phase were considered and normalized to the DMSO control. Data were tested by one-way ANOVA (followed by post-hoc t-test with Bonferroni correction). In this figure, the mean values from technical quadruplicates from two experiments are taken. Data points are represented as mean +/- SEM. Analysis was carried out using Prism version 9.1 (GraphPad Inc., San Diego, CA, USA).

The bar graph figure 22 results shows that at a concentration of 100 µM the TRPM2 inhibitors did not show significant impact on the rate of proliferation of MIA PaCa-2 cells but two of the six TRPM2 inhibitors have shown a small impact on the rate of proliferation but is not statistically significant so could be due to variation.

So far, for exploring the role of TRPM2 in case of pancreatic cancer, researchers have used pancreatic cancer cell models by overexpressing hTRPM2. Development of cell models was done by using different pancreatic cancer cells overexpressing hTRPM2 like PANC-1 (Lin et al., 2018) and BxPC-3 (Lin et al., 2021). Hence, for this experiment after using MIA PaCa-2 cells, TRPM2 overexpressing HEK293 #24 cells were used. And the same experiment was performed using the same experimental conditions but just with half the concentration (50 µM) of the TRPM2 inhibitors using TRPM2 overexpressing HEK293 cells. The result for the proliferation assays studying the impact of TRPM2 inhibitors on TRPM2 overexpressing HEK293 cells is shown in figure 23.

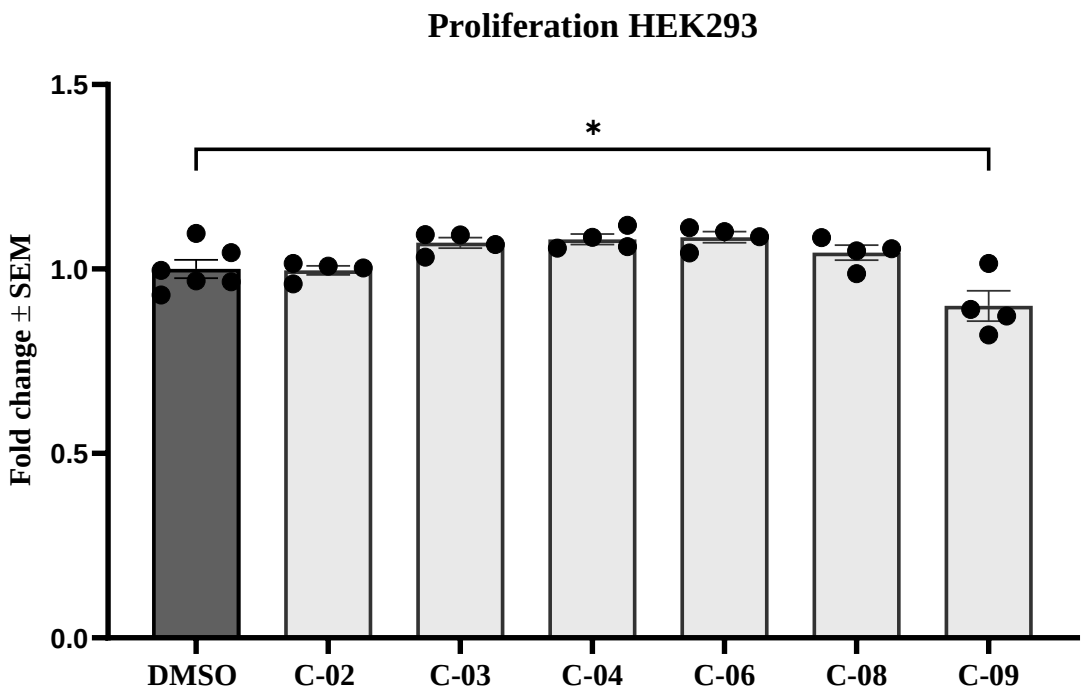

Figure 23: Bar graph showing impact of TRPM2 inhibitors on TRPM2 overexpressing HEK293 cell proliferation rate

The figure shows the bar graph showing the impact of TRPM2 inhibitors on TRPM2 overexpressing HEK293 cells. For the experiment the cells were seeded in quadruplicates in a density of 2000 cells per well in a 96-well plate a day before. Then on the experiment day, the TRPM2 inhibitors in a final concentration of 50 μM were added into each well except the control wells. Then plate was transferred into the IncuCyte® Zoom Live Cell Analysis System and cell confluence was measured every two hours. The analysis of data was performed same as before. In this figure, the mean values from technical quadruplicates from one experiment are shown. Data points are represented as mean +/- SEM. Statistical significance was analyzed with a one-way ANOVA. Asterisk indicate *p value < 0.05 and in comparison to the control well sample containing 0.4% dimethyl sulfoxide (DMSO) in culture media. Statistical analysis was carried out using Prism version 9.1 (GraphPad Inc., San Diego, CA, USA).

The bar graph figure 23 results shows that at a concentration of 50 μM (half of the concentration used for MIA PaCa-2) out of the six TRPM2 inhibitors compound 09 showed a small but significant impact on the rate of proliferation. There has been 10% reduction in rate of proliferation of HEK293 cells treated with compound 09 compared to the DMSO control at the time point of 32hrs. This shows that compound 09 is the TRPM2 inhibitor, which could affect the rate of proliferation of cells overexpressing hTRPM2.

5 DISCUSSION

As being an important second messenger, Ca^{2+} is involved in numerous cellular processes and hence alterations in calcium signalling could lead to a number of pathological conditions including various human cancer types. Because of this reason Ca^{2+} transporting/regulating ion channels specifically TRP channels also have an important role in these pathological conditions and need to be investigated as cancer is one of the major causes of death and suffering in the western world (Gautier et al., 2019). The work in this thesis is focused on TRPM2 channel modulation because this channel has been reported to be highly expressed in various types of cancers including pancreatic ductal adenocarcinoma (PDAC). It is an especially hard to treat cancer and hence novel options are required for the treatment of PDAC. It has been shown that TRPM2 plays a role in proliferation and migration of PDAC cells (section 1.2.4).Hence it is an utmost important to develop TRPM2 inhibitors so that they could be used or at least facilitate the treatment of PDAC. So far, very little pharmacological modulators of TRPM2 are available with most of them showing poor selectivity. TRPM2 probably is the only ion channel regulated by ADPR. Hence, the studies performed in the thesis were aimed at developing novel TRPM2 inhibitors, which are ADPR antagonists in nature.

However, the major problem with developing the TRPM2 inhibitors was that the structure was not available. Just recently (in Sep 2019) the very first cryo-EM structures of human TRPM2 have been published by Juan Du *et al* (Huang et al., 2019). Before this, most of the investigations related to TRPM2 channel by Huang and co-workers were made using homology model based structures.

So far, in the absence of specific TRPM2 inhibitors, several attempts were made to use channel blockers (based on some prior screening assays) for the inhibition of TRPM2 channel but because they lack the specificity for TRPM2 channels, their use is avoided. Some of them are described as follows:

1. 2-aminoethyl-diphenylborate (2-APB): Togashi *et al* performed some patch clamp experiments using hTRPM2 transfected HEK293 cells. The channel activation was done by using either ADPR or cADPR and heat. Then upon infusing cells with 2-APB a dose dependent inhibition of TRPM2 currents with an IC_{50} of 1 μM was observed. Along with this inhibitory effect on TRPM2 channel, this 2-APB have also shown an inhibitory effect on a wide range of TRP channels and proteins. However, the effects observed with this compound are fast and revocable. So even though it is a very good compound but because of its rapid and reversible action as well as not being specific to TRPM2 it cannot be used as an TRPM2 inhibitor (Togashi et al., 2008, Xu et al., 2005).

2. Another example is N-(p-amylcinnamoyl) anthranilic acid (ACA): Actually this compound is a well-known phospholipase A2 blocker. But Harteneck *et al* also studied its effect on hTRPM2 transfected HEK293 cells using patch clamp recordings and channel activation was achieved by ADPR infusion. They also performed fluorometric imaging. Moreover, with these two techniques, they showed that ACA has inhibitory effect on TRPM2 channel. But not just TRPM2 this ACA also shows inhibitory effect on other TRP channels like TRPM8, TRPC6, TRPV1, TRPC3 and TRPV2 (for this channel it had shown the least effect). So overall ACA acts on other ion channels as well as have an inhibitory effect on phospholipase A_2. Which makes this compound also not specific to the TRPM2 channel (Harteneck et al., 2007, Chen et al., 1994).
3. Some other categories of compounds like some antifungal agents also have shown some inhibitory effects on TRPM2 channel activation but none of them are selective for TRPM2 channel. For instance clotrimazole and econazole: Hill *et al* performed patch clamp experiments using HEK293 cells expressing recombinant hTRPM2. Tested both the compounds at a concentration range from 3 to 30 μM and observed that at this concentration range these both compounds show full inhibition of ADPR-induced TRPM2 currents. But the problem was this inhibitory effect produced by these compounds was found to be happening in a delayed and irreversible manner (Hill et al., 2004b).
4. Then there is one more non-steroidal anti-inflammatory agent (NSAID), Flufenamic acid (FFA) which was also studied by Hill *et al* for its effect on TRPM2 channel. They performed patch clamp recordings using recombinant hTRPM2. In addition, they observed that the ADPR-induced TRPM2 current could be completely blocked upon infusion with this compound. However, this inhibition was facilitated by decrease in pH and the inhibition was found to be irreversible. Which showed that this compound inhibits the channel reversibly depending on the extracellular pH as well as in case of formulation strategy it is very difficult to formulate into high concentration preparations since it is not easily dissolved in aqueous solutions (Hill et al., 2004a, Shakeel and Alshehri, 2020).

   These both antifungal and NSAID class compounds have shown that TRPM2 inhibition by these two compounds (ACA and FFA) was improved at lower pH range, which could be because these both compounds are weak acids. Moreover, because of their weak acidic nature at lower pH values the number of uncharged molecules are increased.
5. Then Kheradpezhouh *et al* also checked curcumin for its effect on inhibition of TRPM2 channels. For this, they performed patch clamp and Fura-2 calcium imaging

experiments using HEK293 cells heterologously expressing TRPM2 channels. They checked effect of curcumin on increased Ca^{2+} influx due to paracetamol and H_2O_2 and observed that curcumin does inhibit the TRPM2 current (low nanomolar range) resulting from oxidative stress or because of accumulation of ADPR. However, it does not block directly the TRPM2 channel meaning it can only act in response to oxidative stress not directly onto the active channel. It also have shown inhibitory effect on number of other ion channels including CRAC channel, Kv11.1, Kv1.4 and Kv1.3. This shows that curcumin also lack the specificity for TRPM2. Curcumin is a known antioxidant so it could be that the inhibitory effect on TRPM2 channel is due to its antioxidant nature. Because antioxidants could decrease the mitochondrial and DNA damage resulting into stopping the production/accumulation of ADPR and thus inhibiting the ADPR-mediated TRPM2 activation (Kheradpezhouh et al., 2016).

6. Some novel bioactive metabolites were also tested for their inhibitory effect on TRPM2 channels. Starkus *et al* performed some screening assays for TRPM2 inhibitors in which they found a marine extract. They collected fractions of this extract by performing chromatographic separations and it has the scalardial as major component. This compound was tested using whole-cell patch clamp experiments as well as Fura-2 calcium measurements. And it did show inhibition of TRPM2 activation in nanomolar ranges. It was also checked for its specificity and it did not inhibit currents in other ion channels (TRPV1, TRPM4 and CRAC) so could not be considered as a general channel blocker like other compounds but it did show inhibitory effect on the TRPM7 channel making this scalardial also not specific to the TRPM2 channels (Starkus et al., 2017).
7. There was one attempt made to develop TRPM2 inhibitor, which was a cell membrane permeable peptide called tat-M2NX. This compound was developed to reduce TRPM2-induced stroke injury and when administered after 4 hours of onset of symptom it was found to be effective in decreasing the infarct volume. And for confirming if this compound offers protection against stroke injury, histological measurements of samples were taken. Hence, the problem with this peptide administration is that because of the need of histological measurements every time, it not a feasible option (Shimizu et al., 2016).
8. Some efforts were also made to develop TRPM2 inhibitors based on ADPR derivatives (7i and 8a) or some ADPR analogues (8 Br ADPR and 8-phenyl-2'-deoxy ADPR) themselves have been tried to use as a competitive antagonist for ADPR in case of its binding NudT9-H domain. But due to their nucleotide nature they were found to get degraded in serum easily so cannot be used as a TRPM2 inhibitors (Baszczyňski et al.,

2020). Luo *et al* synthesized two novel ADPR analogues namely 7i and 8a. These compounds did show moderate inhibition of TRPM2 channels upon intracellular application. They also proved to be TRPM2 specific, as when tested on the other TRP channels they did not show any inhibition of currents for those channels. However, the main problem with these compounds was with their potency and permeability. As when they were applied extracellularly, there was no inhibition of TRPM2 channel activity at all. Hence these compounds also cannot be used even though they are TRPM2 specific but are not membrane permeant so cannot reach the target (Luo et al., 2018).

9. There is a recent discovery of TRPM2 inhibitor called "JNJ-28583113" by Janssen research and development in 2019. They checked the effect of this compounds on cells expressing hTRPM2 using Ca^{2+} flux assays as well as patch clamp technique and shown the inhibition of TRPM2 at an IC_{50} of 126 nM. Then on further testing it has shown to be metabolised *in vivo* which made it unsuitable for systemic administration. So this compound still needs further optimization of its pharmacokinetic properties (Fourgeaud et al., 2019).

Therefore, in summary, following are the approaches so far which has been used to come up with the TRPM2 inhibitors but all were appear to be unsuccessful because of some reasons, which are:

a) Using channel blockers to inhibit TRPM2 channel: these compounds were unsuccessful because they lack the TRPM2 specificity (Togashi et al., 2008, Xu et al., 2005, Harteneck et al., 2007, Hill et al., 2004b, Hill et al., 2004a, Shakeel and Alshehri, 2020).
b) Using ADPR derivatives: as ADPR binding site is a unique feature of TRPM2 channel, using ADPR analogues was a good idea but because of the presence of the pyrophosphate bridge in ADPR made these compounds unstable in biological fluids hence unsuitable to be used as TRPM2 inhibitors (Baszczyňski et al., 2020). Luo *et al* tried synthesizing ADPR analogues by masking the pyrophosphate group but still ended up in having non-membrane permeant compounds (Luo et al., 2018).
c) Cell-based high throughput assays: this approach also led the compounds with poor membrane permeability issue (Song et al., 2008). Also Ca^{2+} flux screening assays resulted into some false positive compounds like PARP-1/PARG inhibitors as well as compounds with a need to optimize pharmacokinetic properties (Fourgeaud et al., 2019).

Therefore, after seeing all these attempts and their results it appears to be that there are no specific TRPM2 inhibitors available in the market and with these all problems leading into

suggestion of development of TRPM2 channel specific inhibitors as a promising therapeutic approach.

As the TRPM2 inhibitors are supposed to compete with the ADPR for the NudT9-H domain unique to TRPM2, the drug design for the development of TRPM2 inhibitors in the thesis was done aiming at compounds with structure/morphology, orientation, ligand interactions similar to ADPR but non-nucleotide in nature because nucleotides show limited membrane permeability and stability.

In this thesis structure-based drug design approach, using homology model structure and actual cryo-EM structure of hTRPM2 was used. Moreover, this decision was led by following reasons:

i. In general, the drug development could be done in two methods: high throughput screening (HTS) method or computer-aided drug design (CADD). As there were already some attempts made to screen the compounds using cell-based HTS method which resulted into compounds with poor membrane permeability (Song et al., 2008). Hence, in this thesis computer aided drug design approach was preferred.

ii. However, in CADD (section 1.3), there are two approaches structure-based drug design (SBDD) and ligand-based drug design (LBDD). Since for ligand-based drug design there was not enough structural information available as there are no TRPM2 inhibitors also not many ADPR analogues available and the ones available have very little quantitative data (because of time consuming patch clamp experiments). Also the fact that ADPR due to its large flexibility (more number of rotational bonds) is all but an ideal pharmacophore. Hence, SBDD approach was preferred over LBDD for the drug design.

iii. During this thesis work, two attempts were made for structure-based drug design, one was using homology model and the other one was using actual hTRPM2 cryo-EM structure.

iv. In the beginning, structure-based approach using homology model structure was used as there was no actual TRPM2 structure or even structure of isolated NudT9-H domain was available.

v. Then in late 2019, Juan du *et al* published an actual cryo-EM structure of hTRPM2. Hence another SBDD using this cryo-EM structure was performed. However, because of its not very well-resolved structure molecular dynamics (MD) simulation was performed to get a well-resolved structure for molecular docking.

Then compounds selected from both the drug design approaches were purchased from different suppliers. However, the compounds selected from drug design using homology model did not

show any significant pharmacological inhibition of activation of TRPM2 channel compared to the actual hTRPM2 cryo-EM structure. This could be because a homology model often nicely reflects the overall structure of the peptide backbone, but it is never nearly capable of showing the conformers of the amino acid side chains. Deceptively the side chains are placed in some conformation by the algorithms used. This hardly reflects the real conformers. Since the conformation of the side chains is essential for forming the binding pocket it is really hard to achieve a good docking result when starting from a homology model (Hillisch et al., 2004). This could be the reason why the compounds selected from drug design using homology model structure did not resulted into good compounds compared to the drug design performed using actual cryo-EM structure of hTRPM2.

Until recently, the NudT9-H domain was considered to be the only ADPR binding site of the TRPM2. And was called as a primary ADPR binding site as it was a well-known and unique nucleotide-binding site for the TRPM2 activation. Hence, for the structure-based drug design approach, the NudT9-H domain was targeted. However, in 2019 Huang *et al* discovered and proposed that there is one more nucleotide-binding site called MHR1/2 domain and that gives access to ADPR as well as 8-Br-cADPR for binding so it could activate the channel. However, apparently NudT9-H domain only allows ADPR to bind not the 8-Br-cADPR. The reason for the different selectivity could be the wider and more-relaxed shape of the binding cleft in the NudT9-H domain in comparison to the binding site in the MHR1/2 domain, allowing ADPR to sit in a more relaxed position. On the other hand, MHR1/2 domain is comparatively smaller in shape than that of NudT9-H domain. The two nucleotide-binding sites differ in not only shape but also serve different functions depending on the orthologue. For instance, MHR1/2 domain being a primary binding site is present in all the species while NudT9-H domain however is not required in the invertebrates (nvTRPM2). Nevertheless, a colleague in lab: Winnie Riekehr, has shown that at least in case of the hTRPM2 channel binding of two ligands to both of these binding sites is required for the full channel activation (Riekehr et al., 2022). Hence blocking one of these should be sufficient to produce inhibitory effect on human TRPM2 channels.

In the studies performed and explained in this thesis, the effects of the selected compounds were investigated using Fura-2 calcium measurements, onto the intact cells and then using patch clamp recordings, directly onto the target (TRPM2 channel).

The first 12 compounds selected from drug design using homology model did not show effect on TRPM2 inhibition. First, the compounds were tested directly on target using whole-cell patch clamp recordings. Moreover, most of them did not show any inhibition of ADPR-induced TRPM2 currents except compound A07 and compound B04. Only these two compounds

showed partial inhibition of ADPR-induced TRPM2 currents. Compound A07 showed 62% inhibition and compound B04 showed 69% inhibition of TRPM2 currents. Then in Fura-2 calcium measurements for all of these compounds, only one compound A08 did show concentration-dependent inhibition of TRPM2 activation-induced increase in the calcium signal. This compound did show a sigmoidal curve showing inhibition with an IC_{50} of around 6 μM. In conclusion, out of these 12 compounds two compounds (A08 and B04) showed partial inhibition of ADPR-induced TRPM2 currents in patch clamp experiments but did not show any concentration dependent inhibition of TRPM2 activation-induced increase in calcium signal. This could be because the compounds were not membrane-permeant hence could not even enter the cell to produce an effect on the channel activation-induced increase in calcium signal. Then only one compound A08 showed a good concentration dependent inhibition of TRPM2 activation-mediated increase in calcium signal. However, this compound A08 did not show any inhibition of ADPR-mediated TRPM2 currents. This could be because of its antioxidant nature that it produced an inhibition of TRPM2 activation because of oxidative stress but failed to inhibit the channel directly.

Then the compounds selected from the drug design based on actual cryo-EM structure of hTRPM2 were tested. Primary screening was performed using Fura-2 calcium measurements while only the compounds showing inhibition of increase in calcium signal due to activation of TRPM2 were further tested on target using whole-cell patch clamp technique. This was done to avoid unnecessary testing of non-membrane permeant compounds on target using time-consuming patch clamp experiments. As the NudT9-H binding (target) site is cytosolic, only the compounds, which are membrane-permeant, will reach the intracellular target and thereby act on it.

In Fura-2 calcium measurements, six of total 13 compounds selected from drug design using cryo-EM structure displayed potency with IC_{50}'s lower than 5 μM (results section. 4.2.2). Nevertheless, there were still some more compounds like compound 05, 10, 11 and especially compound 12 which showed inhibition of TRPM2 activation mediated increase in the $[Ca^{2+}]_i$. However, for constructing the concentration-response curves, the values from 3-4 individual experiments performed on different days over the period of several weeks were considered. And these compounds (compound 05, 10, 11 and 12) did not show any consistent results in case of the inhibition of TRPM2 activation mediated increase in the $[Ca^{2+}]_i$. As shown in the figure 24 in case of compound 05, 10, 11 and 12 in the first few days the compounds have shown a concentration dependent inhibition of TRPM2 activation mediated increase in the $[Ca^{2+}]_i$. However, after few weeks these compounds did not show any inhibition of $[Ca^{2+}]_i$ hence needed to check if they have been degraded over the period of time. This was checked

using RP-HPLC. Moreover, surprisingly, the compounds 05, 10 and 11 did not show any degradation with the chromatographic experiments but compound 12 did show degradation in the HPLC experiments (figure 25). After checking the structures of these compounds (section 3.2), it was noticed that compound 05, 10 and 11 have something in common and that was the sulfur dioxide which acts as an antioxidant as well as a reducing agent. Therefore, it could be plausible that because of this (presence of sulfur dioxide) in the beginning these compounds have shown some antioxidant property and have shown inhibition of increase in $[Ca^{2+}]_i$ due to activation of TRPM2 channel in response to oxidative stress caused due to application of H_2O_2. However, after few days/weeks they failed to show the same consistent effect even though they were not degraded. This could be a good sign indicating that the compounds that showed inhibition in Fura-2 calcium measurements have not shown any false positive results because if that had been the case, like these compounds those compounds would also have not been consistent with the results over the period. Which means it could be concluded that even though the compounds might not degrade but over the period of time it would lose its antioxidant property.

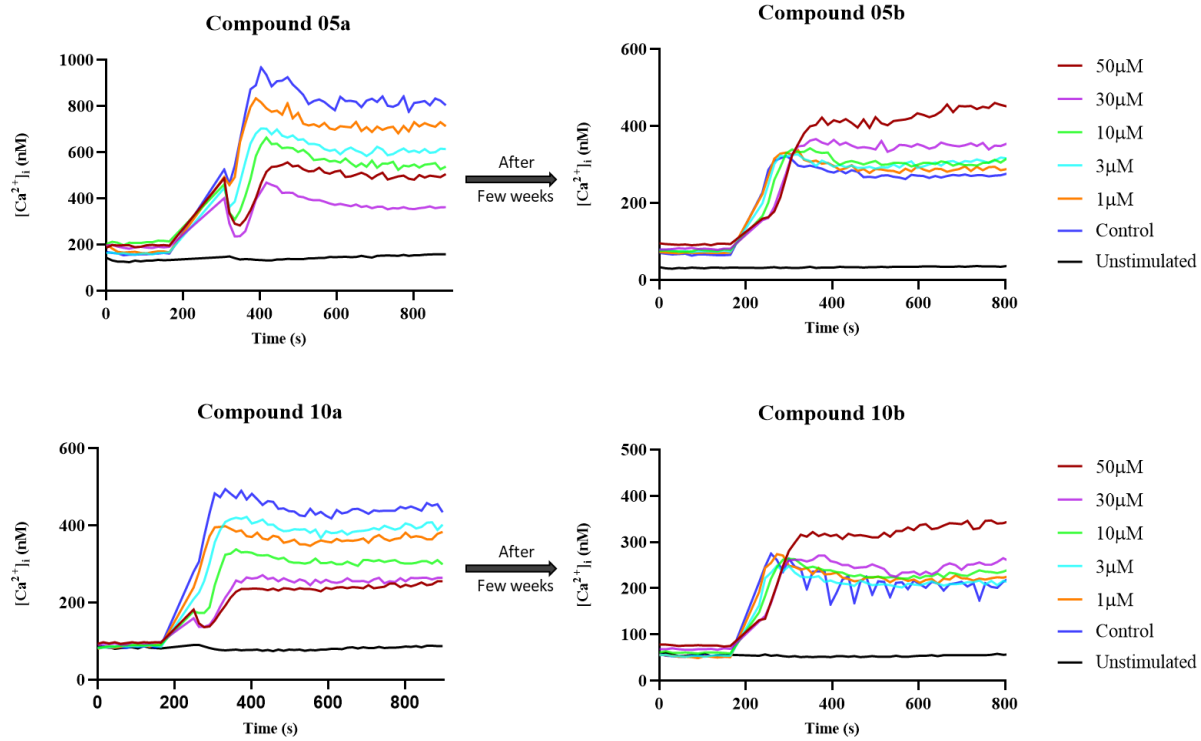

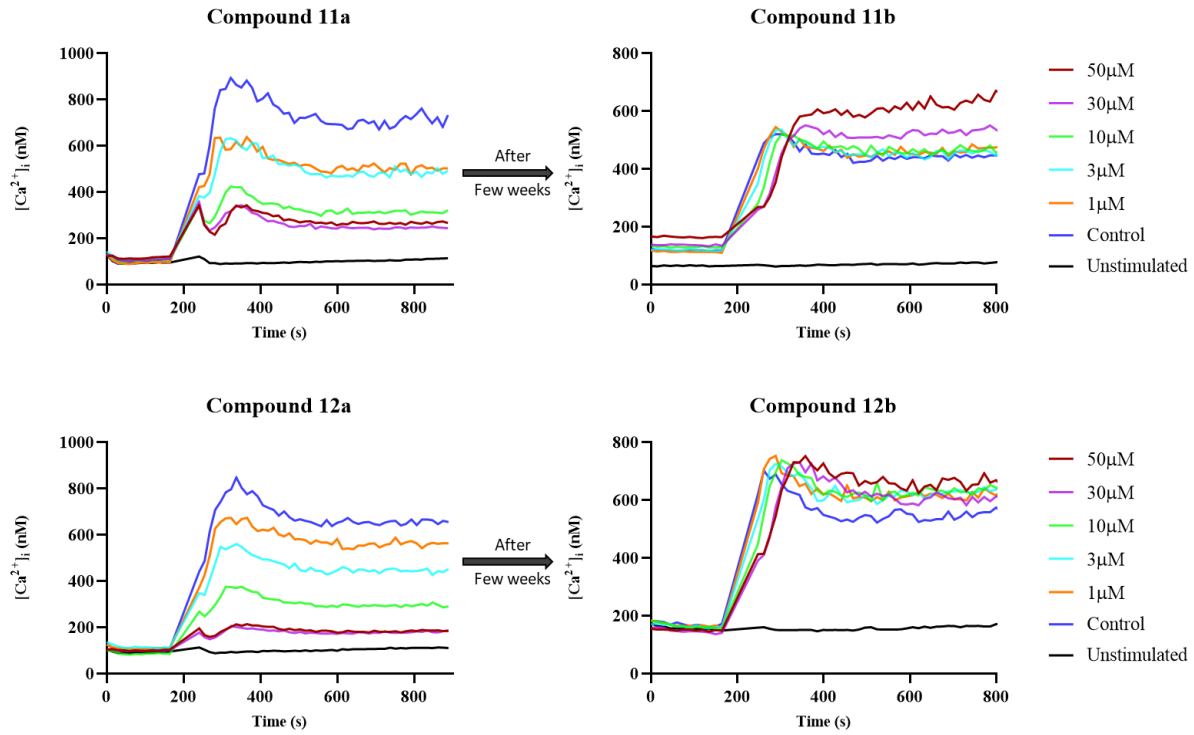

Figure 24: Fura-2 calcium measurement results for compound 05, 10, 11 and 12

The figure shows calcium tracings from the first few days of the Fura-2 experiments (5a, 10a, 11a and 12a) and then after few weeks (5b, 10b, 11b and 12b). It could be seen clearly that within the first few days the compounds did show inhibition of TRPM2 activation mediated increase in $[Ca^{2+}]_i$. Data points are represented as mean +/- SEM. Data analysis was performed in Microsoft Excel 2016 (Microsoft Corporation, Redmond, WA USA) as well as Prism version 8.4.3 (GraphPad Prism Software Inc., USA).

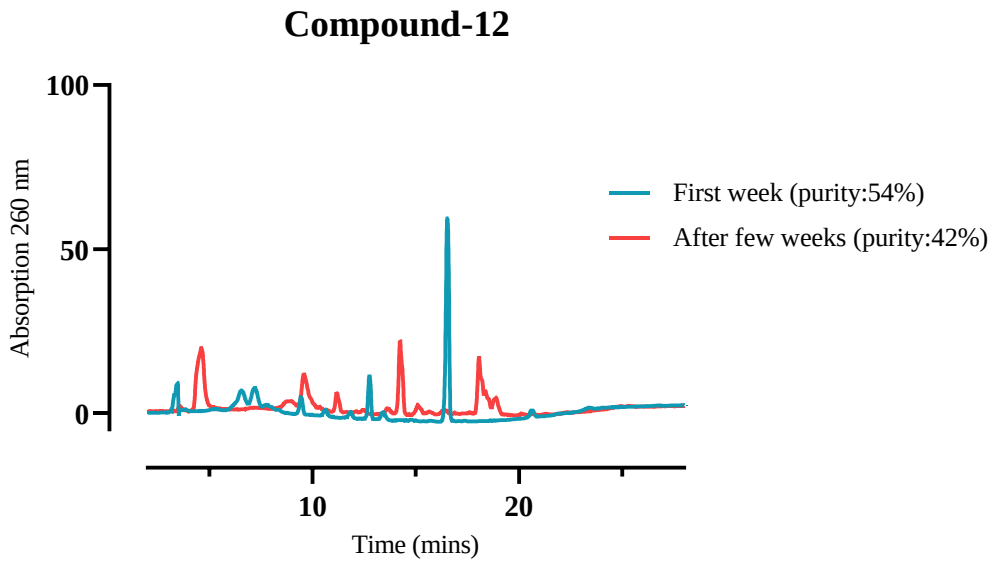

Figure 25: HPLC experiment results for compound 12 over the period

This figure demonstrates the RP-HPLC analysis results for the compound 12 performed to check the purity of the compound. Two experiments were performed 1) within the first week of dissolving the compound in DMSO and then 2) after few weeks of compound being in the DMSO solvent. Moreover, it could be seen that the compound got degraded showing different impurity peaks than the main peak as that of the first experiment. The data was analysed using Prism version 8.4.3 (GraphPad Prism Software Inc., USA).

The RP-HPLC results shows that the compound 12 has been degraded after few weeks forming different degradation byproducts at different retention times other than the retention time of the main peak of the compound. This could justify why even this compound has shown an

inhibition in the beginning but no inhibition in the later experiments. This was also visible in the concentration-response curves for compound 12 (figure 26). Hence, these all compounds were excluded from the further analysis/testing of compounds using patch clamp recordings as well as cancer cell proliferation assays.

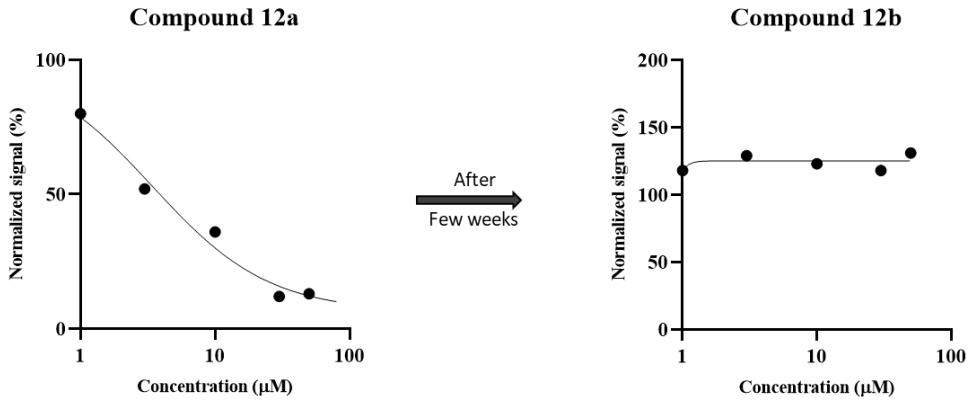

Figure 26: Concentration-response curve for compound 12

The figure shows the concentration-response curves constructed from Fura-2 calcium measurements for compound 12 in the first few weeks of measurement and after few weeks. Data analysis was performed in Microsoft Excel 2016 (Microsoft Corporation, Redmond, WA USA) as well as Prism version 8.4.3 (GraphPad Prism Software Inc., USA).

After the Fura-2 calcium measurements, the compounds were checked using patch clamp experiments. Moreover, these experiments showed that all six of them almost completely abolished ADPR-induced TRPM2 currents, confirming them as novel TRPM2 channel inhibitors (results in section 4.2.3).

Furthermore, these novel TRPM2 inhibitors were assessed for their impact on rate of proliferation of pancreatic cancer cells specifically MIA PaCa-2 and the TRPM2 inhibitors did not show impact on rate of proliferation of cancer cells (results in section 4.4). The summarized result for these all experiments is shown in the following figure 27.

As proliferation is not the only aspect of PDAC cells that could be affected by TRPM2 inhibition, hence it would be worthwhile to look into migration, clone formation and apoptosis in future. Additional experiments are prerequisite to determine whether this pharmacological inhibition of these novel inhibitors could also have a solid impact on pancreatic cancer cells or if combined synergistically with other known chemotherapeutic agent could result in potentiation of effect of those anticancer drugs.

Taken together, these results from the experiments performed identified six novel and structurally diverse TRPM2 channel inhibitors, which presumably work by antagonizing ADPR and therefore should be TRPM2 specific. None of them showed any impact on rate of proliferation of pancreatic cancer cells (MIA PaCa-2) but compound 09 showed significant impact on rate of proliferation of TRPM2 overexpressing HEK293 cells. Further studies are

required to determine their in depth impact on pancreatic cancer cells as well as determining PK properties required for confirming their metabolic stability.

Nevertheless, identification of such novel TRPM2 inhibitors could provide new tools to study and understand better the physiological and pathological functions of the human TRPM2 channels and develop therapeutics to treat diseases associated with expression of TRPM2 channels.

	Calcium measurement result		Patch clamp recording result
Compound 02	IC_{50}=3.6μM with 63% inhibition	➲	75% inhibition (@ 100μM)
Compound 03	IC_{50}=4.7μM with 60% inhibition		83% inhibition (@ 100μM)
Compound 04	IC_{50}=2.5μM with 89% inhibition		72% inhibition (@ 100μM)
Compound 06	IC_{50}=1.8μM with 85% inhibition		67% inhibition (@ 100μM)
Compound 08	IC_{50}=3.8μM with 81% inhibition		63% inhibition (@ 100μM)
Compound 09	IC_{50}=4.3μM with 82% inhibition		76% inhibition (@ 100μM)

Figure 27: Summary of results from calcium measurement and patch clamp experiments

This figure shows the summarized results for the calcium measurement and patch clamp experiments using these best six compounds selected from the computer-aided drug design using cryo-EM structure of hTRPM2.

6 LIST OF HAZARDOUS CHEMICALS

Name	H-Phrases	P-Phrases	GHS hazard
Adenosine diphosphate ribose (ADPR)	H315, H319, H335	P261, P264, P271, P280, P302 + P352, P305 + P351 + P338	GHS07
Calcium chloride ($CaCl_2$)	H319	P264, P280, P305 + P351 + P338, P337 + P313	GHS07
Ethanol	H225, H319	P210, P233, P240, P241, P242, P305 + P351 + P338	GHS02, GHS07
G-418	H317, H334	P261, P272, P280, P284, P302 + P352, P304 + P340 + P312	GHS08
Hydrochloric acid (HCl)	H290, H314, H335	P234, P261, P271, P280, P303 + P361 + P353, P305 + P351 + P338	GHS05, GHS07
Hydrogen peroxide (H_2O_2)	H318, H412	P273, P280, P305 + P351 + P338, P501	GHS05
Silver chloride (AgCl)	H290, H410	P234, P273, P390, P391, P501	GHS05, GHS09
Sodium hydroxide (NaOH)	H290, H314	P234, P260, P280, P303 + P361 + P353, P304 + P340 + P310, P305 + P351 + P338	GHS05
Penicillin-Streptomycin	H315, H317, H334, H335	P280, P261, P264, P284, P271, P302 + P352, P333 + P313, P304 + P340, P342 + P311, P312, P403 + P233, P501	GHS07
Methanol	H225, H301 + H311 + H331, H370	P210, P233, P280, P301 + P310, P303 + P361 + P353, P304 + P340 + P311	GHS02, GHS06, GHS08
Triton X-100	H302, H315, H318, H410	P264, P273, P280, P301 + P312, P302 + P352, P305 + P351 + P338	GHS05, GHS07, GHS09
TRIzol	H301 + H311 + H331, H314, H341, H373, H411	P202, P273, P280, P303 + P361 + P353,	GHS05, GHS06, GHS08, GHS09

		P304 + P340 + P310, P305 + P351 + P338	
Trypan blue	H350	P201, P202, P280, P308 + P313 - P405, P501	GHS08
Trypsin	H315, H319, H334, H335	P261, P280, P284, P304 + P340, P337 + P313, P342 + P311	GHS07, GHS08

H-Phrases:

1. Physical hazards-

   H225 Highly flammable liquid and vapor.

   H226 Flammable liquid and vapor.

   H228 Flammable solid.

   H229 Pressurized container: may burst if heated.

   H230 May react explosively even in the absence of air.

   H231 May react explosively even in the absence of air at elevated pressure and/or temperature.

   H232 May ignite spontaneously if exposed to air.

   H240 Heating may cause an explosion.

   H241 Heating may cause a fire or explosion.

   H242 Heating may cause a fire.

   H250 Catches fire spontaneously if exposed to air.

   H251 Self-heating; may catch fire.

   H252 Self-heating in large quantities; may catch fire.

   H260 In contact with water releases flammable gases, which may ignite spontaneously.

   H261 In contact with water releases flammable gas.

   H270 May cause or intensify fire; oxidizer.

   H271 May cause fire or explosion; strong oxidizer.

   H272 May intensify fire; oxidizer.

   H280 Contains gas under pressure; may explode if heated.

   H281 Contains refrigerated gas; may cause cryogenic burns or injury.

   H290 May be corrosive to metals.

2. Health hazards-

   H301 + H311 + H331 Toxic if swallowed, in contact with skin or if inhaled.

   H314 Causes severe skin burns and eye damage.

H315 Causes skin irritation.

H317 May cause an allergic skin reaction.

H318 Causes serious eye damage.

H319 Causes serious eye irritation.

H331 Toxic if inhaled.

H335 May cause respiratory irritation.

H370 Causes damage to organs.

H373 May cause damage to organs through prolonged or repeated exposure.

3. Environmental hazards-

H410 Very toxic to aquatic life with long lasting effects.

H411 Toxic to aquatic life with long lasting effects.

H412 Harmful to aquatic life with long lasting effects.

P-Phrases:

1. Prevention precautionary statements

P201 Obtain special instructions before use.

P202 Do not handle until all safety precautions have been read and understood.

P210 Keep away from heat/sparks/open flames/hot surfaces – No smoking.

P233 Keep container tightly closed.

P241 Use explosion-proof [electrical/ventilating/lighting/…] equipment.

P242 Use non-sparking tools.

P261 Avoid breathing dust/fume/gas/mist/vapours/spray.

P264 Wash … thoroughly after handling.

P271 Use only outdoors or in a well-ventilated area.

P273 Avoid release to the environment.

P280 Wear protective gloves/protective clothing/eye protection/face protection.

P284 Wear respiratory protection.

2. Response precautionary statements-

P301 + P310 IF SWALLOWED: Immediately call a POISON CENTER or doctor/physician.

P308 + P313 IF exposed or concerned: Get medical advice/attention.

P304 + P340 IF INHALED: Remove victim to fresh air and keep at rest in a position comfortable for breathing.

P303 + P361 + P353 IF ON SKIN (or hair): Take off immediately all contaminated clothing. Rinse skin with water [or shower].

P301 + P312 IF SWALLOWED: Call a POISON CENTRE/doctor/… if you feel unwell.

P302 + P352 IF ON SKIN: Wash with soap and water.

P337 + P313 If eye irritation persists get medical advice/attention.

P305 + P351 + P338 IF IN EYES: Rinse cautiously with water for several minutes. Remove contact lenses if present and easy to do. Continue rinsing.

3. Storage precautionary statements-

   P405 Store locked up.

   P501 Dispose of contents/container to …

7 REFERENCES

Adamska, A., Domenichini, A., Falasca, M., 2017. Pancreatic Ductal Adenocarcinoma: Current and Evolving Therapies. Int. J. Mol. Sci. 18, E1338.

Almasi, S., Kennedy, B.E., El-Aghil, M., Sterea, A.M., Gujar, S., Partida-Sánchez, S., El Hiani, Y., 2018. TRPM2 channel–mediated regulation of autophagy maintains mitochondrial function and promotes gastric cancer cell survival via the JNK-signaling pathway. J. Biol. Chem. 293, 3637–3650.

Artymovich, K., Patel, K., Szybut, C., Garay, P.M., O'Callaghan, T., Dale, T., Trezise, D., Appledorn, D.M., n.d. CellPlayer^{TM} Kinetic Proliferation Assay 6.

Bao, L., Chen, S.J., Conrad, K., Keefer, K., Abraham, T., Lee, J.P., Wang, J.F., Zhang, X.Q., Hirschler-Laszkiewicz, I., Wang, H.G., Dovat, S., Gans, B., Madesh, M., Cheung, J.Y., Miller, B.A., 2016. Depletion of the human ion channel TRPM2 in neuroblastoma demonstrates its key role in cell survival through modulation of mitochondrial reactive oxygen species and bioenergetics. J. Biol. Chem. 291, 24449–24464.

Barton, C., Staddon, S., Hughes, C., Hall, P., O'Sullivan, C., Klöppel, G., Theis, B., Russell, R., Neoptolemos, J., Williamson, R., 1991. Abnormalities of the p53 tumour suppressor gene in human pancreatic cancer. Br. J. Cancer 64, 1076–1082.

Baszczyňski, O., Watt, J.M., Rozewitz, M.D., Fliegert, R., Guse, A.H., Potter, B.V.L., 2020. Synthesis of phosphonoacetate analogues of the second messenger adenosine 5′-diphosphate ribose (ADPR). RSC Adv. 10, 1776–1785.

Bauer, I., Grozio, A., Lasiglie, D., Basile, G., Sturla, L., Magnone, M., Sociali, G., Soncini, D., Caffa, I., Poggi, A., Zoppoli, G., Cea, M., Feldmann, G., Mostoslavsky, R., Ballestrero, A., Patrone, F., Bruzzone, S., Nencioni, A., 2012. The NAD^+-dependent histone deacetylase SIRT6 promotes cytokine production and migration in pancreatic cancer cells by regulating Ca^{2+} responses. J. Biol. Chem. 287, 40924–40937.

Beck, A., Kolisek, M., Bagley, L.A., Fleig, A., Penner, R., 2006. Nicotinic acid adenine dinucleotide phosphate and cyclic ADP-ribose regulate TRPM2 channels in T lymphocytes. FASEB J. Off. Publ. Fed. Am. Soc. Exp. Biol. 20, 962–964.

Belrose, J.C., Jackson, M.F., 2018. TRPM2: a candidate therapeutic target for treating neurological diseases. Acta Pharmacol. Sin. 39, 722–732.

Berendsen, H.J.C., Postma, J.P.M., van Gunsteren, W.F., DiNola, A., Haak, J.R., 1984. Molecular dynamics with coupling to an external bath. J. Chem. Phys. 81, 3684–3690.

Buelow, B., Song, Y., Scharenberg, A.M., 2008. The Poly(ADP-ribose) polymerase PARP-1 is required for oxidative stress-induced TRPM2 activation in lymphocytes. J. Biol. Chem. 283, 24571–24583.

Chen, T.H., Lee, B., Hsu, W.H., 1994. Arginine vasopressin-stimulated insulin secretion and elevation of intracellular Ca^{++} concentration in rat insulinoma cells: influences of a phospholipase C inhibitor 1-[6-[[17 beta-methoxyestra-1,3,5(10)-trien- 17-yl]amino]hexyl]-1H-pyrrole-2,5-dione (U-73122) and a phospholipase A2 inhibitor N-(p-amylcinnamoyl)anthranilic acid. J. Pharmacol. Exp. Ther. 270, 900–904.

Clapham, D.E., 2003. TRP channels as cellular sensors. Nature 426, 517–524.

Cosens, D.J., Manning, A., 1969. Abnormal electroretinogram from a Drosophila mutant. Nature 224, 285–287.

Dölle, C., Rack, J.G.M., Ziegler, M., 2013. NAD and ADP-ribose metabolism in mitochondria. FEBS J. 280, 3530–3541.

Drucker, B.J., Marincola, F.M., Siao, D.Y., Donlon, T.A., Bangs, C.D., Holder, W.D., 1988. A new human pancreatic carcinoma cell line developed for adoptive immunotherapy studies with lymphokine-activated killer cells in nude mice. Vitro Cell. Dev. Biol. J. Tissue Cult. Assoc. 24, 1179–1187.

Exercise: Atomistic Simulation of Biomolecular function, Part 1, 2022. URL http://www2.mpibpc.mpg.de/groups/grubmueller/Lugano_Tutorial/part1/

Finkel, T., Holbrook, N.J., 2000. Oxidants, oxidative stress and the biology of ageing. Nature 408, 239–247.

Fliegert, R., Bauche, A., Wolf Pérez, A.-M., Watt, J.M., Rozewitz, M.D., Winzer, R., Janus, M., Gu, F., Rosche, A., Harneit, A., Flato, M., Moreau, C., Kirchberger, T., Wolters, V., Potter, B.V.L., Guse, A.H., 2017a. 2'-Deoxyadenosine 5' -diphosphoribose is an endogenous TRPM2 superagonist. Nat. Chem. Biol. 13, 1036–1044.

Fliegert, R., Glassmeier, G., Schmid, F., Cornils, K., Genisyuerek, S., Harneit, A., Schwarz, J.R., Guse, A.H., 2007. Modulation of Ca^{2+} entry and plasma membrane potential by human TRPM4b. FEBS J. 274, 704–713.

Fliegert, R., Watt, J.M., Schöbel, A., Rozewitz, M.D., Moreau, C., Kirchberger, T., Thomas, M.P., Sick, W., Araujo, A.C., Harneit, A., Potter, B.V.L., Guse, A.H., 2017b. Ligand-induced activation of human TRPM2 requires the terminal ribose of ADPR and involves Arg1433 and Tyr1349. Biochem. J. 474, 2159–2175.

Fonfria, E., Marshall, I.C.B., Boyfield, I., Skaper, S.D., Hughes, J.P., Owen, D.E., Zhang, W., Miller, B.A., Benham, C.D., McNulty, S., 2005. Amyloid β-peptide(1–42) and

hydrogen peroxide-induced toxicity are mediated by TRPM2 in rat primary striatal cultures. J. Neurochem. 95, 715–723.

Fonfria, E., Mattei, C., Hill, K., Brown, J.T., Randall, A., Benham, C.D., Skaper, S.D., Campbell, C.A., Crook, B., Murdock, P.R., Wilson, J.M., Maurio, F.P., Owen, D.E., Tilling, P.L., McNulty, S., 2006. TRPM2 is elevated in the tMCAO stroke model, transcriptionally regulated, and functionally expressed in C13 microglia. J. Recept. Signal Transduct. Res. 26, 179–198.

Fourgeaud, L., Dvorak, C., Faouzi, M., Starkus, J., Sahdeo, S., Wang, Q., Lord, B., Coate, H., Taylor, N., He, Y., Qin, N., Wickenden, A., Carruthers, N., Lovenberg, T.W., Penner, R., Bhattacharya, A., 2019. Pharmacology of JNJ-28583113: A novel TRPM2 antagonist. Eur. J. Pharmacol. 853, 299–307.

Gautier, M., Trebak, M., Fleig, A., Vandier, C., Ouadid-Ahidouch, H., 2019. Ca^{2+} channels in cancer. Cell Calcium 84, 102083.

Grynkiewicz, G., Poenie, M., Tsien, R.Y., 1985. A new generation of Ca^{2+} indicators with greatly improved fluorescence properties. J. Biol. Chem. 260, 3440–3450.

Hara, Y., Wakamori, M., Ishii, M., Maeno, E., Nishida, M., Yoshida, T., Yamada, H., Shimizu, S., Mori, E., Kudoh, J., Shimizu, N., Kurose, H., Okada, Y., Imoto, K., Mori, Y., 2002. LTRPC2 Ca^{2+}-permeable channel activated by changes in redox status confers susceptibility to cell death. Mol. Cell 9, 163–173.

Harteneck, C., Frenzel, H., Kraft, R., 2007. N-(p-amylcinnamoyl)anthranilic acid (ACA): a phospholipase A(2) inhibitor and TRP channel blocker. Cardiovasc. Drug Rev. 25, 61–75.

Hecquet, C.M., Ahmmed, G.U., Vogel, S.M., Malik, A.B., 2008. Role of TRPM2 channel in mediating H2O2-induced Ca^{2+} entry and endothelial hyperpermeability. Circ. Res. 102, 347–355.

Heiner, I., Eisfeld, J., Halaszovich, C.R., Wehage, E., Jüngling, E., Zitt, C., Lückhoff, A., 2003. Expression profile of the transient receptor potential (TRP) family in neutrophil granulocytes: evidence for currents through long TRP channel 2 induced by ADP-ribose and NAD. Biochem. J. 371, 1045–1053.

Hill, K., Benham, C.D., McNulty, S., Randall, A.D., 2004a. Flufenamic acid is a pH-dependent antagonist of TRPM2 channels. Neuropharmacology 47, 450–460.

Hill, K., McNulty, S., Randall, A.D., 2004b. Inhibition of TRPM2 channels by the antifungal agents clotrimazole and econazole. Naunyn. Schmiedebergs Arch. Pharmacol. 370, 227–237.

Hill, K., Tigue, N.J., Kelsell, R.E., Benham, C.D., McNulty, S., Schaefer, M., Randall, A.D., 2006. Characterisation of recombinant rat TRPM2 and a TRPM2-like conductance in cultured rat striatal neurones. Neuropharmacology 50, 89–97.

Hillisch, A., Pineda, L.F., Hilgenfeld, R., 2004. Utility of homology models in the drug discovery process. Drug Discov. Today 9, 659–669.

Hopkins, M.M., Feng, X., Liu, M., Parker, L., Koh, D., 2015. Inhibition of the transient receptor potential melastatin-2 channel causes increased DNA damage and decreased proliferation in breast adenocarcinoma cells. Int. J. Oncol.

Huang, C., Qin, Y., Liu, H., Liang, N., Chen, Y., Ma, D., Han, Z., Xu, X., Zhou, X., He, J., Li, S., 2017. Downregulation of a novel long noncoding RNA TRPM2-AS promotes apoptosis in non–small cell lung cancer. Tumor Biol. 39, 1010428317691191.

Huang, Y., Roth, B., Lü, W., Du, J., 2019. Ligand recognition and gating mechanism through three ligand-binding sites of human TRPM2 channel. eLife 8, e50175.

Jorgensen, W.L., Chandrasekhar, J., Madura, J.D., Impey, R.W., Klein, M.L., 1983. Comparison of simple potential functions for simulating liquid water. J. Chem. Phys. 79, 926–935.

Jorgensen, W.L., Tirado-Rives, J., n.d. The OPLS Potential Functions for Proteins. Energy Minimizations for Crystals of Cyclic Peptides and Crambin 10.

Kashio, M., Sokabe, T., Shintaku, K., Uematsu, T., Fukuta, N., Kobayashi, N., Mori, Y., Tominaga, M., 2012. Redox signal-mediated sensitization of transient receptor potential melastatin 2 (TRPM2) to temperature affects macrophage functions. Proc. Natl. Acad. Sci. U. S. A. 109, 6745–6750.

Katsila, T., Spyroulias, G.A., Patrinos, G.P., Matsoukas, M.-T., 2016. Computational approaches in target identification and drug discovery. Comput. Struct. Biotechnol. J. 14, 177–184.

Kheradpezhouh, E., Barritt, G.J., Rychkov, G.Y., 2016. Curcumin inhibits activation of TRPM2 channels in rat hepatocytes. Redox Biol. 7, 1–7.

Klumpp, D., Mišović, M., Szteyn, K., Shumilina, E., Rudner, J., Huber, S., 2016. Targeting TRPM2 Channels Impairs Radiation-Induced Cell Cycle Arrest and Fosters Cell Death of T Cell Leukemia Cells in a Bcl-2-Dependent Manner. Oxid. Med. Cell. Longev.

Koh, D., Powell, D.P., Blake, S., Hoffman, J.L., Hopkins, M.M., Feng, X., 2015. Enhanced cytotoxicity in triple-negative and estrogen receptor-positive breast adenocarcinoma cells due to inhibition of the transient receptor potential melastatin-2 channel. Oncol. Rep.

Kolisek, M., Beck, A., Fleig, A., Penner, R., 2005. Cyclic ADP-ribose and hydrogen peroxide synergize with ADP-ribose in the activation of TRPM2 channels. Mol. Cell 18, 61–69.

Kraft, R., Grimm, C., Grosse, K., Hoffmann, A., Sauerbruch, S., Kettenmann, H., Schultz, G., Harteneck, C., 2004. Hydrogen peroxide and ADP-ribose induce TRPM2-mediated calcium influx and cation currents in microglia. Am. J. Physiol. Cell Physiol. 286, C129-137.

Lange, I., Penner, R., Fleig, A., Beck, A., 2008. Synergistic regulation of endogenous TRPM2 channels by adenine dinucleotides in primary human neutrophils. Cell Calcium 44, 604–615.

Lieber, M., Mazzetta, J., Nelson-Rees, W., Kaplan, M., Todaro, G., 1975. Establishment of a continuous tumor-cell line (panc-1) from a human carcinoma of the exocrine pancreas. Int. J. Cancer 15, 741–747.

Lin, R., Bao, X., Wang, H., Zhu, S., Liu, Z., Chen, Q., Ai, K., Shi, B., 2021. TRPM2 promotes pancreatic cancer by PKC/MAPK pathway. Cell Death Dis. 12, 585.

Lin, R., Wang, Y., Chen, Q., Liu, Z., Xiao, S., Wang, B., Shi, B., 2018. TRPM2 promotes the proliferation and invasion of pancreatic ductal adenocarcinoma. Mol. Med. Rep. 17, 7537–7544.

Lipinski, C.A., 2004. Lead- and drug-like compounds: the rule-of-five revolution. Drug Discov. Today Technol. 1, 337–341.

Lipski, J., Park, T.I.H., Li, D., Lee, S.C.W., Trevarton, A.J., Chung, K.K.H., Freestone, P.S., Bai, J.-Z., 2006. Involvement of TRP-like channels in the acute ischemic response of hippocampal CA1 neurons in brain slices. Brain Res. 1077, 187–199.

Liu, X., Cotrim, A., Teos, L., Zheng, C., Swaim, W., Mitchell, J., Mori, Y., Ambudkar, I., 2013. Loss of TRPM2 function protects against irradiation-induced salivary gland dysfunction. Nat. Commun. 4, 1515.

Luo, X., Li, M., Zhan, K., Yang, W., Zhang, Lihe, Wang, K., Yu, P., Zhang, Liangren, 2018. Selective inhibition of TRPM2 channel by two novel synthesized ADPR analogues. Chem. Biol. Drug Des. 91, 552–566.

McHugh, D., Flemming, R., Xu, S.-Z., Perraud, A.-L., Beech, D.J., 2003. Critical intracellular Ca^{2+} dependence of transient receptor potential melastatin 2 (TRPM2) cation channel activation. J. Biol. Chem. 278, 11002–11006.

Mcule [WWW Document], URL https://mcule.com/ (accessed 11.08.22).

Miller, B.A., 2019. TRPM2 in Cancer. Cell Calcium 80, 8–17.

MODELLER, URL https://salilab.org/modeller/

Molport-Compound Sourcing, Selling and Purchasing Platform [WWW Document], Molport. URL https://www.molport.com/shop/index?version=2 (accessed 11.08.22).

Montell, C., Rubin, G.M., 1989. Molecular characterization of the Drosophila trp locus: a putative integral membrane protein required for phototransduction. Neuron 2, 1313–1323.

Nagamine, K., Kudoh, J., Minoshima, S., Kawasaki, K., Asakawa, S., Ito, F., Shimizu, N., 1998. Molecular Cloning of a Novel Putative Ca^{2+} Channel Protein (TRPC7) Highly Expressed in Brain. Genomics 54, 124–131.

Nazıroğlu, M., Özgül, C., Çelik, Ö., Çiğ, B., Sözbir, E., 2011. Aminoethoxydiphenyl borate and flufenamic acid inhibit Ca^{2+} influx through TRPM2 channels in rat dorsal root ganglion neurons activated by ADP-ribose and rotenone. J. Membr. Biol. 241, 69–75.

Nilius, B., Owsianik, G., 2011. The transient receptor potential family of ion channels. Genome Biol. 12, 218.

Okabe, T., Yamaguchi, N., Ohsawa, N., 1983. Establishment and characterization of a carcinoembryonic antigen (CEA)-producing cell line from a human carcinoma of the exocrine pancreas. Cancer 51, 662–668.

Okada, Y., Nonaka, S., Tanaka, Y., Saijoh, Y., Hamada, H., Hirokawa, N., 1999. Abnormal Nodal Flow Precedes Situs Inversus in iv and inv mice. Mol. Cell 4, 459–468.

Olah, M.E., Jackson, M.F., Li, H., Perez, Y., Sun, H.-S., Kiyonaka, S., Mori, Y., Tymianski, M., MacDonald, J.F., 2009. Ca^{2+}-dependent induction of TRPM2 currents in hippocampal neurons. J. Physiol. 587, 965–979.

Perraud, A.-L., Fleig, A., Dunn, C.A., Bagley, L.A., Launay, P., Schmitz, C., Stokes, A.J., Zhu, Q., Bessman, M.J., Penner, R., Kinet, J.-P., Scharenberg, A.M., 2001. ADP-ribose gating of the calcium-permeable LTRPC2 channel revealed by Nudix motif homology. Nature 411, 595–599.

Perraud, A.-L., Takanishi, C.L., Shen, B., Kang, S., Smith, M.K., Schmitz, C., Knowles, H.M., Ferraris, D., Li, W., Zhang, J., Stoddard, B.L., Scharenberg, A.M., 2005. Accumulation of free ADP-ribose from mitochondria mediates oxidative stress-induced gating of TRPM2 cation channels. J. Biol. Chem. 280, 6138–6148.

Renaud, J.-P., Chari, A., Ciferri, C., Liu, W., Rémigy, H.-W., Stark, H., Wiesmann, C., 2018. Cryo-EM in drug discovery: achievements, limitations and prospects. Nat. Rev. Drug Discov. 17, 471–492.

Riekehr, W.M., Sander, S., Pick, J., Tidow, H., Bauche, A., Guse, A., Fliegert, R., 2022. cADPR Does Not Activate TRPM2.

Schrödinger maestro, Schrödinger Maest. URL https://www.schrodinger.com/products/maestro

Shakeel, F., Alshehri, S., 2020. Solubilization, Hansen Solubility Parameters, Solution Thermodynamics and Solvation Behavior of Flufenamic Acid in (Carbitol + Water) Mixtures. Processes 8, 1204.

Shen, B.W., Perraud, A.L., Scharenberg, A., Stoddard, B.L., 2003. The crystal structure and mutational analysis of human NUDT9. J. Mol. Biol. 332, 385–398.

Shimizu, T., Dietz, R.M., Cruz-Torres, I., Strnad, F., Garske, A.K., Moreno, M., Venna, V.R., Quillinan, N., Herson, P.S., 2016. Extended therapeutic window of a novel peptide inhibitor of TRPM2 channels following focal cerebral ischemia. Exp. Neurol. 283, 151–156.

Song, Y., Buelow, B., Perraud, A.-L., Scharenberg, A.M., 2008. Development and Validation of a Cell-Based High-Throughput Screening Assay for TRPM2 Channel Modulators. SLAS Discov. 13, 54–61.

Starkus, J.G., Poerzgen, P., Layugan, K., Kawabata, K.G., Goto, J.-I., Suzuki, S., Myers, G., Kelly, M., Penner, R., Fleig, A., Horgen, F.D., 2017. Scalaradial Is a Potent Inhibitor of Transient Receptor Potential Melastatin 2 (TRPM2) Ion Channels. J. Nat. Prod. 80, 2741–2750.

Sumoza-Toledo, A., Lange, I., Cortado, H., Bhagat, H., Mori, Y., Fleig, A., Penner, R., Partida-Sánchez, S., 2011. Dendritic cell maturation and chemotaxis is regulated by TRPM2-mediated lysosomal Ca^{2+} release. FASEB J. Off. Publ. Fed. Am. Soc. Exp. Biol. 25, 3529–3542.

Sumoza-Toledo, A., Penner, R., 2011. TRPM2: a multifunctional ion channel for calcium signalling. J. Physiol. 589, 1515–1525.

Tan, M.H., Nowak, N.J., Loor, R., Ochi, H., Sandberg, A.A., Lopez, C., Pickren, J.W., Berjian, R., Douglass, H.O., Chu, T.M., 1986. Characterization of a new primary human pancreatic tumor line. Cancer Invest. 4, 15–23.

Togashi, K., Hara, Y., Tominaga, T., Higashi, T., Konishi, Y., Mori, Y., Tominaga, M., 2006. TRPM2 activation by cyclic ADP-ribose at body temperature is involved in insulin secretion. EMBO J. 25, 1804–1815.

Togashi, K., Inada, H., Tominaga, M., 2008. Inhibition of the transient receptor potential cation channel TRPM2 by 2-aminoethoxydiphenyl borate (2-APB). Br. J. Pharmacol. 153, 1324–1330.

Tong, Q., Zhang, W., Conrad, K., Mostoller, K., Cheung, J., Peterson, B., Miller, B., 2006. Regulation of the Transient Receptor Potential Channel TRPM2 by the Ca^{2+} Sensor Calmodulin. J. Biol. Chem. 281, 9076–85.

Tóth, B., Csanády, L., 2010. Identification of direct and indirect effectors of the transient receptor potential melastatin 2 (TRPM2) cation channel. J. Biol. Chem. 285, 30091–30102.

Trott, O., Olson, A.J., 2010. AutoDock Vina: improving the speed and accuracy of docking with a new scoring function, efficient optimization, and multithreading. J. Comput. Chem. 31, 455–461.

Uchida, K., Tominaga, M., 2011. The role of thermosensitive TRP (transient receptor potential) channels in insulin secretion. Endocr. J. 58, 1021–1028.

Uemura, T., Kudoh, J., Noda, S., Kanba, S., Shimizu, N., 2005. Characterization of human and mouse TRPM2 genes: identification of a novel N-terminal truncated protein specifically expressed in human striatum. Biochem. Biophys. Res. Commun. 328, 1232–1243.

Voets, T., Talavera, K., Owsianik, G., Nilius, B., 2005. Sensing with TRP channels. Nat. Chem. Biol. 1, 85–92.

Wang, L., Fu, T.-M., Zhou, Y., Xia, S., Greka, A., Wu, H., 2018. Structures and gating mechanism of human TRPM2. Science 362, eaav4809.

Webb, B., Sali, A., 2016. Comparative Protein Structure Modeling Using MODELLER. Curr. Protoc. Bioinforma. 54, 5.6.1-5.6.37.

Xu, S.-Z., Zeng, F., Boulay, G., Grimm, C., Harteneck, C., Beech, D.J., 2005. Block of TRPC5 channels by 2-aminoethoxydiphenyl borate: a differential, extracellular and voltage-dependent effect. Br. J. Pharmacol. 145, 405–414.

Yamamoto, S., Shimizu, S., Kiyonaka, S., Takahashi, N., Wajima, T., Hara, Y., Negoro, T., Hiroi, T., Kiuchi, Y., Okada, T., Kaneko, S., Lange, I., Fleig, A., Penner, R., Nishi, M., Takeshima, H., Mori, Y., 2008. TRPM2-mediated Ca^{2+} influx induces chemokine production in monocytes that aggravates inflammatory neutrophil infiltration. Nat. Med. 14, 738–747.

Yin, Y., Wu, M., Hsu, A.L., Borschel, W.F., Borgnia, M.J., Lander, G.C., Lee, S.-Y., 2019. Visualizing structural transitions of ligand-dependent gating of the TRPM2 channel. Nat. Commun. 10, 1–14.

Zeng, X., Sikka, S.C., Huang, L., Sun, C., Xu, C., Jia, D., Abdel-Mageed, A.B., Pottle, J.E., Taylor, J.T., Li, M., 2010. Novel role for the transient receptor potential channel

TRPM2 in prostate cancer cell proliferation. Prostate Cancer Prostatic Dis. 13, 195–201.

Zhang, Z., Tóth, B., Szollosi, A., Chen, J., Csanády, L., 2018. Structure of a TRPM2 channel in complex with Ca^{2+} explains unique gating regulation. eLife 7, e36409.

Zhao, L.-Y., Xu, W.-L., Xu, Z.-Q., Qi, C., Li, Y., Cheng, J., Liu, L.-K., Wu, Y.-N., Gao, J., Ye, J.-H., 2016. The overexpressed functional transient receptor potential channel TRPM2 in oral squamous cell carcinoma. Sci. Rep. 6, 38471.

Zhou, K., Liu, B., 2022. Chapter 3 - Control techniques of molecular dynamics simulation, in: Zhou, K., Liu, B. (Eds.), Molecular Dynamics Simulation. Elsevier, pp. 67–96.

DECLARATION ON OATH

Surname: Ohol Name: Swati Balasaheb

"I hereby declare on oath that this doctoral dissertation is written independently and solely by my own based on the original work of my PhD and has not been used other than the acknowledged resources and aids. The submitted written version corresponds to the version on the electronic storage medium. I declare that the present dissertation was prepared maintaining the Rules of Good Scientific Practice of the German Research Foundation and it has never been submitted in the present form or similar to any other University or board of examiners…"

Hamburg, 22/09/2022

Place, Date Signature

ACKNOWLEDGEMENT

First, I would like to thank Prof. Dr. Dr. Andreas H. Guse, Head of the Institute of Biochemistry and Molecular Cell biology, who gave me the chance to work on this PhD thesis and provided his supervision and immense support. Then I would like to express my gratitude to Dr. Ralf Fliegert for his constant guidance and support throughout the 3 years of my PhD tenure.

This project was funded by the European Union's Horizon 2020 research and innovation programme under grant agreement No 81328 (INTEGRATA). Hence, I would also like to appreciate the support from the INTEGRATA consortium throughout.

Further, I would like to thank Prof. Dr. Chris Meier for agreeing to evaluate this thesis as well as being part of my defense committee. I am also very grateful to all the members of my defense committee.

I would also wish to express my gratitude to the following people who have played a very important role in completion of this thesis by providing their support:

- A very special thanks to our INTEGRATA colleagues Dr. Alberto Del Rio and Jorge Franco, from Innovamol Srl, Italy for their constantly big support with the computer aided drug design and with the selection of novel TRPM2 inhibitors. Without them, it would not have been possible.
- Dr. med Louisa Stern and Lukas Fabian-Bohme from the Department of General, visceral and thoracic surgery, University Medical Center Hamburg-Eppendorf (UKE) for providing the pancreatic cancer cell lines.
- PD. Dr. George Feldmann and Mochammad Ichsan from University Hospital Bonn (UKB) for providing the pancreatic cancer cell lines (MIA PaCa-2 and PANC-1).
- Prof. Dr. Manfred Jücker and Dr. Daniel J. Smit from the Institute of Biochemistry and Signal Transduction, UKE, for providing access to the IncuCyte instrument to perform the proliferation assays as well as Daniel for helping me with the analysis of the IncuCyte data.
- Birgit Henkel from the Institute of Biochemistry and Molecular Cell Biology, UKE, for helping with the RT-qPCR experiments.
- Andreas Bauche from the Calcium signalling group for his support with all the HPLC analysis for this project.

I would like to appreciate all my colleagues of the calcium signalling group especially, Imrankhan Khansahib, Feng Gu, Frederike Kulow, Stefanie Etzold, Winnie Riekehr and Jelena Pick for their constant support throughout.

Then I would like to convey my thanks and best wishes for their future endeavour to all my INTEGRATA colleagues who became friends along the way: Elena, Jorge, Ben, Irene, Agata, Moustafa, Pablo, Ichsan, Simone, Paulina, Burak, Melanie, and Elise for making all the secondments so much fun.

Last but not the least I would like to thank my parents and my family members for all their constant emotional support and love without which nothing would have been possible. Also I would like to thank Ganpati Bappa for his blessings.